

# NASA

Technical Memorandum **80569**

## On the Physical Environment in Galactic Nuclei

**J. H. Beall**

(NASA-TM-80569) ON THE PHYSICAL ENVIRONMENT  
IN THE GALACTIC NUCLEI Ph.D. Thesis -  
Maryland Univ. (NASA) 190 p HC A09/MF A01

N80-17939

CSCL 03B

G3/90

Unclas  
12893

**SEPTEMBER 1979**

National Aeronautics and  
Space Administration

**Goddard Space Flight Center**  
Greenbelt, Maryland 20771



ON THE PHYSICAL ENVIRONMENT IN GALACTIC NUCLEI\*

by  
James Howard Beall

DISSERTATION SUBMITTED TO THE FACULTY OF THE GRADUATE SCHOOL  
OF THE UNIVERSITY OF MARYLAND IN PARTIAL FULFILLMENT  
OF THE REQUIREMENTS FOR THE DEGREE OF  
DOCTOR OF PHILOSOPHY

1979

\*Work supported by NASA Grant NGR 21-002-316

ABSTRACT

On the Physical Environment in Galactic Nuclei

James Howard Beall, Doctor of Philosophy, 1979

Dissertation directed by : W.K. Rose

Professor

Department of Physics and Astronomy

Galactic nuclei and quasars emit radiation over the entire electromagnetic spectrum. There is considerable interest in the nature of the emission mechanisms which may be responsible for the observed radiation. The possibility that a single mechanism is responsible for a wide frequency range of the electromagnetic flux suggests that multiple frequency observations of galactic nuclei and quasars can be used to place constraints on models for the source mechanisms involved.

In conjunction with observations by the High Energy X-ray Spectrometer on OSO-8, four sources have been investigated in this manner:

- (i) the nucleus of the elliptical galaxy, Centaurus A (NGC 5128);
- (ii) the quasar, 3C273;
- (iii) the nucleus of the Seyfert galaxy, NGC 4151; and
- (iv) the nucleus of the Milky Way galaxy.

Concurrent observations have been taken for Cen A at radio and X-ray frequencies, and for NGC 4151 at radio, infrared,

optical, and X-ray frequencies. The data from these observations and from other work are used to construct composite spectra (radio to gamma-ray) for the sources. Additionally, a computer program has been developed to obtain source strengths from regions of the sky where more than one source is in the OSO-8 Spectrometer field of view. Using this program, we have analyzed the OSO-8 data for the galactic center region of the Milky Way. The OSO-8 data are consistent with the presence of a high-energy X-ray source at the position of the center of the Milky Way as determined from radio and infrared measurements. We note that this region has been previously observed to harbor many discrete, variable soft X-ray sources. The source associated with the galactic nucleus is commonly called GCX. Composite spectra for 3C273 and GCX have been constructed using the OSO-8 data and data from other observers.

The nucleus of Centaurus A is observed to vary on timescales from days to years at radio and X-ray frequencies. The pattern of variability of the radiation of the nucleus of Centaurus A is suggestive of a thermal-Compton model wherein relativistic synchrotron electrons inverse Compton scatter blackbody radiation from a dense, hot plasma to produce the observed X-rays. The composite spectra of the sources and the observed variability are interpreted in light of this model. We also use the model to establish up-

per limits to the total energy in relativistic electrons which suggest that there is sufficient energy in the nucleus of Centaurus A to form a pair of radio lobes similar to the two already present.

A comparison of the composite spectra of each of the four sources shows similarities between the spectra of the nucleus of the Seyfert galaxy, NGC 4151, and the nucleus of the Milky Way, and between the spectra of the nucleus of the elliptical galaxy, Centaurus A, and the quasar, 3C273. Based on these similarities, it is possible that the nucleus of the Milky Way has a physical environment similar to that of the Seyfert galaxy, NGC 4151. We also note that the distinction between radio-bright and radio-quiet quasars may be that they represent emission from the nuclei of galaxies with elliptical and Seyfert morphologies, respectively. This is contrary to the customary association between Seyfert galaxies and quasars.

## CURRICULUM VITAE

Name: James Howard Beall.

Permanent address: [REDACTED]  
[REDACTED]

Degree and date to be conferred: Ph.D., 1979.

Date of birth: [REDACTED]

Place of birth: [REDACTED]

Secondary education: Calhoun High School, Grantsville, W.Va., 1963.

Collegiate institutions attended	Dates	Degree	Date of Degree
Univ. of Colorado	1969-1972	B.A.	June 1972
Univ. of Maryland	1972-1975	M.S.	June 1975
Univ. of Maryland	1975-1979	Ph.D.	June 1979

Majors: Physics & Astronomy.

Professional publications:

"On the Physical Environment in the Nucleus of Centaurus A (NGC 5128),  
J.H. Beall, and W.K. Rose, 1978, submitted to Ap.J.

"An Upper Limit to the Total Energy Contained in Relativistic  
Particles in the Early Stages of Supernova Explosions", J.H. Beall,  
Ap.J., 15 June 1979.

"Radio and X-ray Variability of the Nucleus of Centaurus A (NGC 5128)",  
J.H. Beall, W.K. Rose, W. Graf, K.M. Price, W.A. Dent, R.W. Hobbs,  
E.K. Conklin, B.L. Ulich, B.R. Dennis, C.J. Crannell, J.F. Dolan,  
K.J. Frost, and L.E. Orwig, 1978, Ap.J., 219, 836.

"Concurrent Radio, Infrared, Optical and X-ray Observations of the Nucleus of NGC 4151", J.H. Beall, W.K. Rose, B.R. Dennis, C.J. Crannell, J.F. Dolan, K.J. Frost, and L.E. Orwig, 1978, Bulletin of A.A.S., vol.9,#4, part II, p558.

"On the long-term variability of Centaurus A", P. Kaufmann and J.H. Beall, 1979, preprint.

"Observations of Celestial X-ray sources above 20 keV with the High-Energy Scintillation Spectrometer on board OSO-8", C.J. Crannell, B.R. Dennis, J.F. Dolan, K.J. Frost, L.E. Orwig, J.H. Beall, and G.S. Maurer, 1977, Proc. 12th ESLAB Symp., Frascati, Italy.

"Energy", M. Wolfson, R. Speed, J.H. Beall, L. Kontnick, R. Ross, D. Williamson, P. White, S. Hatch, U. of Colo. and The Environmental Action Committee of Colorado, Jan. 1972.

Professional positions held: Congressional Fellow  
Office of Technology Assessment  
Congress of the United States  
Washington, D.C.

Graduate Research Assistant at  
Department of Physics and Astronomy  
University of Maryland, College Park,  
Maryland.

DEDICATION

-for Tara Siobhan Beall

PRECEDING PAGE BLANK NOT FILMED

## ACKNOWLEDGEMENTS

I take this opportunity to thank my thesis advisor, Professor W.K. Rose, for his guidance during the past three years in the theoretical work which is well represented in this dissertation. I also thank professor Rose for helpful discussions of the data.

I thank Dr. B.R. Dennis for his patient assistance with the analysis of the data from the OSC-8 High-Energy X-ray Spectrometer, and for his helpful discussions of the theoretical work. I am also indebted to Dr. Dennis for discussions on the imperatives of form and content. I thank Dr. J.F. Dolan for his considerable insight into aspects of the theoretical work.

During the past three years, I have been of two houses: the University of Maryland Department of Physics and Astronomy, and the Laboratory for Astronomy and Solar Physics at Goddard Space Flight Center. Without the helpful interactions I have had with scientists in both organizations, this dissertation would not have been possible. I am especially grateful to Dr. R.W. Hobbs of LASP for his assistance with aspects of the radio observations, and to Dr. J. Scott of the Maryland Astronomy Program for helpful discussions.

I also thank Dr. J. Condon for his help with reduction of the NGC 4151 data, and Dr. J. Felten for his discussions on aspects of the theoretical work.

I thank T.S. Beall and D.K. Wright for their human perspective, and Mrs. Mary Dobbins for her continuing moral support.

Jim Beall

College Park

January 1979

## TABLE OF CONTENTS

Chapter	Page
Dedication.....	i
Acknowledgments.....	ii
Table of Contents.....	iv
List of Tables.....	viii
Figure Captions.....	ix
Chapter 1: Introduction.....	1
Chapter 2: The Experiment.....	10
2.1: General Description of the Satellite (OSO-8) .....	10
2.2: The High Energy X-ray Spectrometer.....	11
2.3: Collection of Data.....	14
2.4: Skymaps.....	15
2.4.1: Constructing a Local Map of the Sky.....	17
2.4.2: Expressing the Detector Axis in Terms of the Local Coordinate System.....	18
2.5: Analysis of the Skymap.....	20
2.5.1: Constructing a Map of Count Rates and Uncertainties.....	20
2.5.2: Analysis of a Skymap.....	22
2.5.3: Least-squares Fitting to a Skymap.....	23
2.5.4: Determining the Spectrum of the X-ray Photons Incident on the Detector.....	24
2.6: Test Cases for the Skymap.....	25
2.6.1: A Strong, Isolated Source of Constant Intensity.....	25
2.6.2: Cygnus X-1 and X-3: A Confused Source Region with one strong and one weak source.....	25
Chapter 3: Observations of Centaurus A (NGC 5128).....	27

3.1: Introduction.....	27
3.2: Radio Observations.....	29
3.3: X-ray Observations.....	30
3.4: Discussion.....	31
3.5: Recapitulation of the Available Data.....	32
3.6: Interpretation of the Radio and X-ray Temporal Variability.....	33
Chapter 4: Observations of 3C273.....	37
4.1: Introduction.....	37
4.2: Discussion.....	40
Chapter 5: Observations of NGC 4151.....	43
5.1: Introduction.....	43
5.2: Observations.....	46
5.3: Discussion.....	47
Chapter 6: The Galactic Center (GCX).....	49
6.1: Introduction.....	49
6.2: Observations.....	50
6.3: Discussion.....	57
Chapter 7: Theory.....	59
7.1: Centaurus A (NGC 5128).....	59
7.1.1: Models for the Spectral Features of Cen A.....	59
7.1.1.1: The Blackbody-Compton Model.....	59
7.1.1.2: Consequences of the Blackbody-Compton Model.....	63
7.1.1.3: An Upper Limit for the Energy Contained in Relativistic Electrons in the Nucleus of Cen A.....	67
7.1.2: A Detailed Model for the Temporal Variability of the Nucleus of Centaurus A.....	70

7.1.2.1: Introduction.....	70
7.1.2.2: Determination of the Dominant Radiation Field which Contributes to the Inverse Compton Production of X-rays.....	72
7.1.2.3: Possible Models for Source Variability.....	74
7.1.2.4: Radio and X-ray Radiation from a Dense, Hot Plasma...	77
7.1.2.5: Radio and X-ray Radiation from an Optically Thin Plasma within a Dense Association of Stars.....	84
7.1.3: Discussion.....	86
7.1.4: Conclusions.....	89
7.2: 3C 273.....	89
7.2.1: General Discussion.....	89
7.2.2: A Model for the Radio and X-ray Flux from 3C 273.....	92
7.2.3: The Energy Contained in Relativistic Particles in 3C 273.....	94
7.2.4: A Discussion of the Optical and Ultraviolet Continuum...	94
7.3: NGC 4151.....	98
7.3.1: General Discussion.....	98
7.3.2: A Model for the X-ray Flux from NGC 4151.....	101
7.4: The Galactic Center (GCX).....	102
7.4.1: General Discussion.....	102
7.4.2: A Model for the X-ray Emission from GCX.....	103
Chapter 8: Discussion.....	104
8.1: The Thermal Source in a Galactic Nucleus.....	104
8.2: The Composite Spectra of the Sources Observed.....	106
8.3: General Remarks.....	107
8.4: Possible Sources of Relativistic Particles Produced	

in a Galactic Nucleus.....	109
<b>E.5: A Possible Distinction Between the Physical Environments</b>	
in Radio-Bright and Radio-Quiet Galactic Nuclei....	109
<b>Conclusions.....</b>	<b>111</b>
<b>Appendix A.....</b>	<b>114</b>
<b>Appendix B.....</b>	<b>119</b>
<b>Appendix C.....</b>	<b>121</b>
<b>Bibliography.....</b>	<b>126</b>
<b>Tables.....</b>	<b>134</b>
<b>Figures.....</b>	<b>136</b>

LIST OF TABLES

Table	Page
3.1 Radio Observations of Centaurus A (NGC 5128).....	134
5.1 Radio Observations of NGC 4151.....	135

FIGURE CAPTIONS

Figure	Page
Figure 2.1: The OSO-8 Spacecraft. The drawing shows the various axes of interest and the orientation of the High-Energy X-ray Spectrometer in the wheel section. Note the 5° offset of the detector axis from the anti-spin axis of the spacecraft.....	136
Figure 2.2: Cross-sectional view of the High-Energy X-ray Spectrometer onboard OSO-8.....	137
Figure 2.3: The arbitrary positions of a source and the origin of the local coordinate system on the celestial sphere. The right ascension and declination of the origin of the local coordinate system are given by $\alpha_\ell$ and $\delta_\ell$ , respectively. The axes for the local coordinate system are defined so that $x_\ell$ is pointing due east, $y_\ell$ is pointing due north, and $z_\ell$ is defined perpendicular to the plane that is tangent to the celestial sphere at the origin of the local coordinate system. A similar convention is used to define the coordinate system for any source of interest.....	138
Figure 2.4: A view of the local coordinate system (x-y plane) from outside the celestial sphere. The spacecraft anti-spin axis intersects the celestial sphere at the center	

of the circle with a  $5^\circ$  radius. Acceptable events (see chapter 2) occurring when the wheel azimuth angle (WAZ)=0 are assumed to originate from the point on the celestial sphere indicated as the location of the detector axis. The finite angular resolution of the detector causes a point source to appear as a cone of enhanced counting rate centered on the location of the source in the local coordinate system. The location of the detector axis when the spacecraft WAZ= $270^\circ$  is also marked. As the spacecraft spin-axis drifts through a region of the sky, the skymap of counts as a function of local X and Y positions is gradually filled in..... 139

Figure 2.5: An example of a mathematical function (or template) showing the counting rate as a function of location of the detector axis in a region in the sky which contains three detectable sources. Note that two of the three sources, S1 and S2, are within  $10^\circ$  of one another and, thus, their cones overlap. The values of the counting rates at the peak of the source cones S1, S2, S3, and the background B are parameters which are determined by a least-squares fit of the template to the skymap of count rates and corresponding uncertainties..... 139

Figure 2.6: The spectrum of the Taurus X-1 determined by a least-squares fit of one source to the skymap of the region

near the Crab Nebula. The source spectrum derived from the skymap is fit by a power-law  $dN/dE=A(E/E_0)^{-\alpha}$  photons  $\text{cm}^{-2}\text{s}^{-1}\text{keV}^{-1}$ , where  $A=(6.29\pm 0.16)\times 10^{-4}$ ,  $E_0=100$  keV, and  $\alpha=2.01\pm 0.03$ . This is in agreement with the spectrum proposed by Toor and Seward (1974) of  $\alpha=2.08\pm 0.05$ , and with the spectrum obtained by Dolan et al. (1977) (with  $\alpha=2.00\pm 0.06$ ) from the OSO-8 High-Energy X-ray Spectrometer using other techniques for data reduction. The spectral fits taken from Clark et al. (1973) and Dolan et al. are extrapolated beyond the energy ranges of the experiments to show the difference between the two results..... 140

Figure 2.7: The X-ray spectrum of Cygnus X-1 from a skymap of the Cygnus region taken during November 1975. The energy spectrum of Cygnus X-1 is fit by a power-law with parameters  $A=(3.87\pm 0.17)\times 10^{-4}$ ,  $E_0=100$  keV, and  $\alpha=2.11\pm 0.07$ . Dolan et al. (1977) report a spectral index  $\alpha=1.87\pm 0.17$  averaged over the 1975 observations. The typical range of variation measured by Dolan et al. is shown by "low state" and "high state" power-law spectra plotted in the figure..... 141

Figure 2.8: The X-ray spectrum of Cygnus X-3 obtained from the same skymap run used to determine the Cygnus X-1 spectrum. The spectrum for Cygnus X-3 is fit by a power-law with parameters  $A=(1.68\pm 1.57)\times 10^{-5}$  and  $\alpha=3.62\pm 0.76$ . The data may also be fit by a thermal spectrum of the form  $dN/dE=(A/E)\exp((E-E_0)/kT)$ , where

$A=1.89 \times 10^{-2} \pm 1.89$ ,  $kT=17.0 \pm 6.0$ , and  $E_0=43 \pm 1171$ ..... 142

Figure 3.1: Radio emission from the nucleus of Cen A. Data are taken from Price and Stull 1973, Stull and Price 1975, Dent and Hobbs 1973, Kellerman 1974, and Beall et al 1978. 143

Figure 3.2: History of Cen A 2-6 keV X-ray Flux: Data taken from Lampton et al. 1972, Tucker et al. 1973, Winkler and White 1975, Davison et al. 1975, Stark et al. 1976, Grindlay et al. 1975b, Serlemitsos et al. 1975, and Lawrence et al. 1977..... 144

Figure 3.3: History of Cen A 100 keV X-ray Intensity. Data are taken from Hayes et al. 1969, Lampton et al. 1972, Mushotzky et al. 1976, Hall et al. 1976, Stark et al. 1976, and Beall et al 1978..... 145

Figure 3.4: History of Cen A X-ray Power-law Spectral Index. Data are taken from Lampton et al. 1972, Tucker et al. 1973, Winkler and White 1975, Mushotzky et al. 1976, Hall et al. 1976, Stark et al. 1976, and Mushotzky et al. 1978..... 146

Figure 3.5: The Spectrum of Centaurus A as derived from the skymap using observations taken by OSO-8 in July and August

1975. The spectrum is fit by a power-law with parameters  $A = (2.26 \pm 0.54) \times 10^{-4}$ ,  $E_0 = 70 \text{ keV}$ , and  $\alpha = 1.13 \pm 0.33$ . The spectrum is consistent with an extrapolation of the Cen A spectrum measured simultaneously by Mushotzky et al (1978) ..... 147

Figure 3.6: The Spectrum of Cen A obtained from the sky map for observations taken during July and August 1976. The spectrum is fit by a power-law with parameters  $A = (1.16 \pm 0.42) \times 10^{-4}$ ,  $E_0 = 70 \text{ keV}$ , and  $\alpha = 2.05 \pm 0.39$ . The spectrum is consistent with an extrapolation of the 1976 spectrum of Mushotzky et al. (1978) ..... 148

Figure 3.7: The Composite Spectrum of Centaurus A. Data are represented as solid lines, upper limits, or individual points. The data are taken from the references cited in chapter 3. The dashed lines are possible theoretical models for emission from the source, and are discussed in chapter 7. The infrared data point is from Harper (1978). The integral data point is from Grindlay et al. (1975a). The upper limits at  $10^{22}$  to  $10^{23}$  Hz are from Fichtel et al. 1978 ..... 149

Figure 4.1: Radio Observations of 3C273 are taken from:  
Andrew et al. (1978),  
    at 6.7 GHz and 10.7 GHz,  
Dent and Kapitzky (1976),  
    at 7.9 GHz

Hobbs (1976),  
 at 31.4 GHz and 90 GHz,  
 Waak and Hobbs (1977),  
 at 18.2 GHz and 31.4 GHz..... 150

Figure 4.2: Upper limits for the X-ray Flux from 3C273  
 obtained with the skymap. The solid line is from data  
 reported by Sanford  
 (1977)..... 151

Figure 4.3: The Composite Spectrum of 3C273. The data are  
 taken from the references cited in the text, and are plotted  
 as solid lines. The two Gamma-ray points are from  
 Swanenburg et al (1978). Possible theoretical spectra are  
 drawn as dashed lines, and  
 are discussed in the text..... 152

Figure 5.1: Radio Observations of the Seyfert Galaxy, NGC  
 4151. The slightly larger flux values evident in the data  
 obtained by Crane (1977), de Bruyn and Wills (1974), and  
 Condon and Dressel (1977) are likely to be the result of  
 contributions to the nuclear flux from a more extended  
 region. However, the data do not rule out the possibility of  
 a slowly varying, extended source in the Seyfert nucleus.  
 The total flux of the nucleus of NGC 4151 during the Sept  
 1974 observations of Crane (1977) comes  
 from a region with dimensions of 1x2 arcseconds at 8.1 GHz.

.....153

Figure 5.2: Infrared and Optical Observations of NGC 4151. The data are taken from the works indicated (see references in text). The data are generally in the form of a power-law. The photon energy spectrum  $dP/d\nu$  in ergs  $\text{cm}^{-2}\text{s}^{-1}\text{Hz}^{-1}$  is given in the figure. We note that a turnover in the infrared spectrum at a wavelength of approximately  $1.5 \times 10^{12}$  Hz is likely in view of the 34 micron point taken by Rieke and Low (1972)..... 154

Figure 5.3: The X-ray spectrum of NGC 4151 derived using the skymap. The observations were taken during May and June 1977. An extrapolation of the low-energy data (Mushotzky et al. 1976) is plotted for comparison. The Ariel V spectrum is taken from Dyer et al. (1978). The skymap spectrum from OSO-6 is not adequately fit by either a single power-law or a thermal spectrum (see text). The spectrum is, however, in general agreement with the data of Mushotzky et al. (1978), and Dyer et al. (1978)..... 155

Figure 5.4: The variability of the nucleus of NGC 4151 at radio, optical, and X-ray frequencies during the concurrent observations of the source. Data are taken from: Mushotzky et al. 1976, Tapia and Wizniewski 1977, and current observations. 156

Figure 5.5: Concurrent radio, optical, and X-ray observations of the nucleus of NGC 4151. The data are shown as solid lines, and are taken from the references cited in the text. The gamma-ray data are taken from Schoenfelder et al. (1978)..... 157

Figure 6.1: The X-ray spectrum of GX3+1. The data represent a single 2-sigma detection between 33 and 43 keV during the September 1975 observations of the galactic center by OSO-8..... 158

Figure 6.2: The X-ray spectrum of GX 3+1 derived from observations of the galactic center region by OSO-8 during 1976..... 159

Figure 6.3: The X-ray spectrum in 1975 of the source at the radio and infrared position of the galactic center. The spectrum is derived from the same skymap used to produce the spectrum in figure 6.1 (Sept. 1975). The data are fit by a power-law spectrum with parameters of  $A=(6.76\pm 6.13)\times 10^{-5}$ ,  $E_0=70$  keV, and  $\alpha=3.28\pm 1.03$  .....160

Figure 6.4: The X-ray spectrum in 1976 of the source at the radio and infrared position of the galactic center derived from the same skymap as the spectrum in figure 6.2 (Sept-Oct 1976). The data are fit by a power-law with parameters  $A=(4.08\pm 1.09)\times 10^{-4}$ ,

$E_0=70$  keV, and  $\alpha=2.28\pm 0.35$ ..... 161

Figure 6.5: The composite spectrum of the nuclear region of the Milky Way galaxy. The solid lines are taken from the data as discussed in chapter 6. Dashed lines are possible models for the observed radiation. The radio flux decreases with decreasing angular size of the source. The near-infrared data (at approximately  $10^{12}$ Hz) are taken from Becklin et al. 1978. The far-infrared data ( $10^{12}$  to  $10^{13}$  Hz) are taken from Gatley et al. (1977), and represent the total emission from Sgr A west. The 1971 X-ray data are taken from Kellogg et al. (1971).

The 1974 data at  $10^{16}$  to  $10^{20}$  Hz are from Haynes et al. (1975) and are an integrated flux from a circle with a diameter of  $13''$  centered on the position of GX1+4. The 1975 and 1976 X-ray data are taken from the OSO-8 skymap. The gamma-ray upper limit taken in 1972 is due to Bennett et al. (1972)..... 162

Figure 7.1: Radio flux from an optically thick plasma as a function of the expansion of the spherical plasma from an initial radius  $R_0$ .

Solid line:  $\tau_0=5$ ,  $\xi=5\times 10^{-2}$ ,  $a=R_0/2$

Dashed line:  $\tau_0=5$ ,  $\xi=1\times 10^{-3}$ ,  $a=R_0/2$

Dotted line:  $\tau_0=2$ ,  $\xi=1\times 10^{-3}$ ,  $a=R_0/2$ ..... 163

Figure 7.2: A comparison of the observations of Cen A and calculated radio and X-ray fluxes from an adiabatically expanding plasma. Radio data taken from Dent and Hobbs 1973, Kellermann 1974, and Beall et al. 1978; X-ray data taken from Winkler and White 1975, Davison et al. 1975, Stark et al. 1976, Grindlay et al. 1975b, Serlemitsos et al. 1975, and Sanford 1976. The starting time for the expansion of the plasma was chosen to be early 1974... 164

## CHAPTER 1: INTRODUCTION

In 1925, Hubble used observations of Cepheid variables in the "spiral nebula" in Andromeda to demonstrate that the nebula was actually a spiral galaxy at an immense distance. Other observations have shown that these vast distributions of stars generally possess some degree of symmetry about a central region, or nucleus, which typically has a high surface brightness. Dynamical studies suggest that all galaxies which are relatively symmetric will have concentrations of mass toward their centers. The nuclei of active galaxies are likely to represent extreme examples of this general trend.

The nucleus of a galaxy is more luminous than any other region of the same angular size within the galaxy. We have known for some time that certain galactic nuclei are much brighter when compared to their parent galaxies than is normal. Seyfert (1943) originally studied 12 such spiral galaxies whose bright nuclei had a star-like appearance and broadened emission lines. Current estimates (see e.g., Weedman 1977) are that approximately one percent of all spiral galaxies are of the Seyfert type.

Seyfert galaxies are not the only examples of galaxies with bright, or active, nuclei. The N-galaxy classification originated by Morgan (1958) is used to denote galaxies with brilliant, star-like nuclei associated with faint nebulosities. Most N-galaxies show similar emission-line spectra to those found in Seyfert nuclei. From the definition of N-galaxies, it is clear that Seyfert galaxies could be classified as N-galaxies if they were so distant that their spiral could not be resolved. However, the majority of N-galaxies contain strong, compact radio sources, while most Seyfert galaxies have relative weak, extended sources at radio frequencies.

Relatively high surface brightness is one indication of activity in a galactic nucleus. Non-thermal radio emission is another. In fact, the detection of radio galaxies was the first indication of violent, non-thermal processes in extragalactic objects (Burbidge, Burbidge, and Sandage 1963).

The association of some N-galaxies with bright, compact radio sources suggests a possible connection (at least observationally) between the nuclear regions of radio galaxies and the nuclear regions of Seyferts. Weedman (1977) also makes the point that in a redshift-vs-luminosity plot for Seyfert galaxies and quasi-stellar objects (QSO's),

there is an overlap between the Seyfert and quasar luminosities. A similar redshift-luminosity plot has been constructed for radio galaxies, QSO's, and Seyfert galaxies (Sandage 1971). In this case, also, the distribution of radio galaxies and QSO's overlap. Quasars also exhibit the strong, broadened emission lines found in Seyfert and N-galaxies (cf. Burbidge 1970, Weedman 1977).

The comparison between active galactic nuclei and quasars prompted Burbidge (1970) to investigate possible similarities between the nucleus of the Milky Way and Seyfert galaxies. On the basis of published observations at that time, Burbidge concluded that the nucleus of the Milky Way is a miniature Seyfert galaxy radiating with 100 to 1000 times less power than a classical Seyfert. At the time of Burbidge's article, there was no evidence for X-ray or gamma-ray emission from the nucleus of our galaxy.

The existence of active galactic nuclei and their possible association with quasars has led to considerable speculation on the nature of the physical environment which produces the observed radiation. The basic mechanisms first suggested have remained topics of discussion to the present day. Jeans (1929) conjectured that the nuclei of galaxies may be "singularities" from which matter is poured into our universe from some other. The more conventional view (Jeans

1902) is that galaxies are formed by dynamical collapse from clouds of dust and gas. The formation of galactic nuclei may represent a continuation of this process.

The continued collapse of the dense associations of dust and stars in galactic nuclei may trigger the violent non-thermal activity which is observed. Three possible mechanisms for the energy production in QSOs and active galactic nuclei have been proposed:

- (i) multiple supernova explosions,
- (ii) accretion onto a massive black hole, or
- (iii) particle acceleration by means of a supermassive star or "spinar".

All of these possible sources may be associated with very dense clusters of stars.

Woltjer (1964) has suggested that galactic nuclei may become so dense that collisions between stars can produce quasar-like luminosities. Alternatively, Colgate (1967) proposed that in such a dense distribution of stars, star-star collisions will lead to the formation of supermassive stars. The rapid evolution of these stars produces supernova explosions which Colgate uses to explain the observed quasar luminosities. Subsequent versions of this idea (Petschek, Colgate, and Colvin 1976 and the references cited therein) use the interaction of the

supernova explosions with an ambient medium to produce the observed radiation. The possibility that supermassive stars contribute directly to the observed luminosities has also been suggested by Hoyle and Fowler (1963).

The physical environment in galactic nuclei may also readily lead from the evolution of massive stars to the formation of black holes. Salpeter (1964) and Zel'Dovich (1964) first suggested that accretion onto a black hole might produce a continuous energy source. More recently, Fabian et al. (1976) have suggested that a massive black hole (approximately  $10^6 M_{\odot}$ ) undergoing quasi-spherical accretion may be responsible for the energy source in the nucleus of the elliptical galaxy, Centaurus A.

The third possible consequence of a dense star cluster is the formation of a supermassive star or spinar which accelerates particles by some process which involves the star's magnetic field. The theory of supermassive stars has been developed from the original suggestion of Hoyle and Fowler (1963). Though there are calculations suggesting that non-rotating, supermassive stars may be subject to fragmentation or collapse (see, e.g. Fowler 1964, Chandrasekhar 1964, and Zel'dovich and Novikov 1971), Ozerney (1966) suggests that a supermassive star (called a "magnetoid") may be supported in equilibrium by some

combination of rotation, a magnetic field, and radiation pressure, and may be stable against collapse. Ozernoy (1972) makes the important point that we may not be able to distinguish observationally between the radiation associated with accretion onto a massive black hole and that coming from a supermassive "magnetoid", since the physical environments in both may be quite similar. Morrison (1969) has also suggested the possibility of pulsar-like action in quasars.

Galactic nuclei and quasars emit radiation over the entire electromagnetic spectrum. The traditional method of studying extragalactic objects is to observe a large number in one frequency range (for example, with UV photometry). This technique has the disadvantage of viewing the sources over a relatively small portion of the electromagnetic spectrum in which the objects may be radiating. We take the somewhat different approach of investigating a few extragalactic objects at many different frequencies spread over as broad a range of the electromagnetic spectrum as possible. This composite-spectrum technique provides a powerful tool for placing constraints on the possible models for production of electromagnetic radiation in the sources observed.

To the extent that emission in one frequency range is related to the emission in another, it is necessary to take the multiple-frequency observations concurrently. We mean by "concurrent" that the observations at different frequencies are conducted within an interval of time short compared to the expected timescale of the variability of the object. The lack of a concurrent, composite (multiple-frequency) spectrum for a source increases the uncertainty of the parameters derived when we apply a particular model to the source.

For this dissertation, four sources have been investigated in this way:

- (i) the nucleus of the radio galaxy, Centaurus A (NGC 5128);
- (ii) the quasar, 3C273;
- (iii) the nucleus of the Seyfert galaxy, NGC 4151; and
- (iii) the nucleus of the Milky Way galaxy.

The observations at radio, infrared, and optical frequencies were arranged to be concurrent with the observations of the sources by the High-Energy X-ray Spectrometer onboard the OSO-8 spacecraft. This instrument is described in Chapter 2.

To obtain an X-ray spectrum of the nuclear region of the Milky Way galaxy, a program was developed to analyze regions of the sky where more than one source is in the X-ray

spectrometer field of view. This method of analysis of the X-ray data is also presented in Chapter 2.

Observations of the radio and X-ray variability of Centaurus A are discussed in Chapter 3. Chapter 4 presents a summary of the radio, infrared, optical, and X-ray observations of the quasar 3C273. Due to the relatively weak X-ray flux of 3C273, no attempt was made to arrange concurrent observations at other frequencies during the X-ray observing period. The Seyfert galaxy, NGC 4151, was observed concurrently at radio, infrared, optical, and X-ray frequencies. These results are presented in chapter 5. The X-ray observations of the nucleus of the Milky Way presented in chapter 6 are not concurrent with the observations at other frequency ranges. In this regard, it should be noted that the electromagnetic radiation from galactic nuclei is often observed to vary by factors of roughly two. The relative magnitudes of the components of the composite spectrum presented are, thus, uncertain at least by that amount.

A model for the temporal variability and composite spectra of the sources observed is presented in chapter 7. In the model, thermal photons from an optically thick plasma are inverse-Compton scattered by relativistic synchrotron electrons to produce the observed X-ray radiation. In

chapter 6, we conclude by noting the implications of the proposed model for the physical environment in the nuclei of galaxies.

## CHAPTER 2-THE EXPERIMENT

### 2.1: General description of the satellite (OSO-8)

Orbiting Solar Observatory 8 was launched on June 21, 1975 from Cape Canaveral by a Delta launch vehicle into a circular orbit 550 km above the earth. The angle of inclination of the plane of the orbit with respect to the equator is  $33^{\circ}$ .

The satellite consists of a wheel section (see figure 2.1), which rotates at 6 rpm for gyroscopic stability, and a sail section containing photocells and the solar instruments. The sail section is maintained perpendicular to a line joining the spacecraft and the sun (the solar vector) to within  $\pm 3^{\circ}$ . As the position of the sun changes seasonally with respect to the background stars, the orientation of the sail section also must change to maintain the alignment of the solar instruments which point at the solar disk. Thus, the spin-axis of the spacecraft can project onto the celestial sphere in a great circle perpendicular to the solar vector. For our purposes, this limit is the significant observational constraint of the spacecraft.

The wheel section is divided into nine pie-shaped sections, each containing a separate experiment. The High Energy X-ray Spectrometer (Dennis et al. 1977) is located in bay II, where the bays are numbered clockwise as one looks along the spacecraft spin axis. The detector is mounted so

that it "looks" at a position on the sky opposite the center line of the bay and  $5^\circ$  from the projection of the antispin axis onto the celestial sphere (see figure 2.1). As the wheel section rotates, the detector axis sweeps out a circle on the celestial sphere with a radius of  $5^\circ$ . It is possible for the High-Energy X-ray Spectrometer to observe a source located in the ecliptic plane for a maximum of approximately 18 days as the anti-spin axis drifts through a region. Longer observation times are possible for sources which do not lie in the ecliptic plane.

The orientation of the spacecraft is controlled by a magnetic torquing system and nitrogen gas jets. The gas jets also maintain the spin rate of the spacecraft at  $6 \pm 1$  rpm. Magnetic torquing can move the spin axis of the spacecraft a maximum of  $3^\circ$  each day, while the gas jets can move the spin axis as much as  $15^\circ$  per minute.

## 2.2: The High Energy X-ray Spectrometer

The OSO-8 satellite moves in and out of the inner van Allen radiation belt in the region of the South Atlantic Anomaly as the spacecraft orbits the earth. The high energy protons magnetically trapped in the radiation belt interact with the detector crystals and produce many radioactive spallation products. This induced radioactivity in the shield and central crystals exponentially decays after the spacecraft leaves the van Allen belt. Typically, OSO-8

passes through the South Atlantic Anomaly on 6 or 7 orbits in a 24 hour period. Consequently, the background radiation in the detector crystals varies by a factor of at least two during the course of each day.

The off-axis orientation of the detector axis was chosen to allow the detector to sweep on and off a source during the observation so the varying background could be continually sampled.

The CSO-8 High-Energy X-ray detector (Dennis et al. 1977) consists of two separate, optically isolated central crystals (CsI(Na)) surrounded by shield crystals of the same material (see figure 2.2). There are 17 parallel holes drilled through the top shield crystal which expose 27.5 cm<sup>2</sup> of the "open central crystal" to the X-ray sky. The "shielded central crystal" serves to monitor the internal detector background in the continuously changing particle environment of the spacecraft orbit.

The shield crystals consist of 5 optically isolated sections viewed by a total of 12 photomultiplier tubes. The shield crystals are arranged so that a minimum of 5 cm of CsI shields the central crystals. This thickness attenuates 99 percent of the X-rays incident at energies less than 250 keV. When a pulse is detected simultaneously in both the central crystal and a shield crystal, an anticoincidence circuit prevents the event from being pulse-height analyzed. A pulse in one of the central crystals is considered an

"acceptable event" only when it is not accompanied by a coincident pulse in one of the shield crystals. When this condition is met, the acceptable event is analyzed by the 256-channel pulse-height analyzer.

The dimensions of the collimation holes give the instrument a circular aperture with a full-width at half maximum (FWHM) of 5° for X-rays of less than 100 keV. At higher energies, the FWHM increases slightly because of the increased ability of the off-axis X-rays to penetrate a significant thickness of the shield crystals.

The detector aperture is covered with a 0.635-cm thick plastic scintillator (Nuclear Enterprises NE102), which is used in anticoincidence with the central crystals to reject events produced by charged particles entering through the collimation holes.

Two charged-particle monitors in the X-ray detector compartment automatically turn off the high voltage to the photomultiplier tubes when the spacecraft enters the van Allen belts. This automatic system acts as a back up to the normal high voltage turn off by timed command from the ground.

The output of the central and shield crystals can be calibrated in orbit. The central crystals have a single  $\text{Am}^{241}$  source placed immediately below them (see figure 2.2). The 5 Mev alpha particles from this source are detected by one of two solid-state detectors sandwiching the source. At

the same time, the coincident 59.6keV X-rays have a certain probability of stopping in one of the two central crystals. A central crystal X-ray event coincident with the detection of an alpha particle is tagged electronically as a calibration pulse. The shield crystals are calibrated in flight by using seven  $\text{Am}^{241}$  sources placed in four of the 5 shield crystals.

### 2.3: Collection of the Data:

As previously mentioned, a pulse in the open or shielded central crystal in anticoincidence with the output of the shield crystals and the plastic scintillator over the detector aperture is considered an "acceptable event", and is pulse-height analyzed. The data for such an event consist of the amplitude of the pulse from the central crystal and the time of occurrence of the event. The data for up to eight events together with the instrument livetime are stored in 17 eight-bit words in each minor frame covering 160 milliseconds. Sixteen of these words are arranged in eight equally spaced pairs. Each word pair carries the pulse amplitude and the time of occurrence of the first event in the previous 20 milliseconds, a bit to indicate in which of the two central crystals the event occurred, and a bit which tells if the data is a calibration event. A maximum of 50 events each second can thus be analyzed. From this minor frame data, the 256-channel

energy-loss spectrum of the central crystals can be determined.

In addition to the amplitude and time information, spacecraft data on the rotation of the wheel section with respect to the sail section, and data from star sensors and magnetometers are transmitted. The angle of rotation of the wheel with respect to the sail is determined to within  $0.04^\circ$  each 160 milliseconds. From this information, the orientation of the spacecraft and hence the detector axis can be determined at any given time. The maximum uncertainty of the attitude solutions for the spacecraft is customarily better than  $0.1^\circ$  during satellite night when good star tracking data are available. The accuracy of position determination can deteriorate to as much as  $1^\circ$  during satellite day, especially after a large gas maneuver.

#### 2.4: Skymaps:

The satellite data as recorded for each minor frame consists of counts from the open and shielded central crystals as a function of the energy deposited in the crystal, and of the wheel azimuth angle of the spacecraft. The wheel azimuth angle (WAZ) is the angle between the zero mark on the wheel encoder shaft and the partition between bay I and bay IX. For the data analyzed, the zero of the wheel azimuth encoder and the spacecraft roll-axis vector are colinear to  $\pm 1^\circ$ . To analyze the data, these

distributions are transformed into a  $20^\circ \times 20^\circ$  local coordinate system tangent to the celestial sphere at some reference point. Each acceptable event in the wheel azimuth distribution is put in the appropriate  $1^\circ \times 1^\circ$  box in the local coordinate system. Each acceptable event is assumed to be the result of an X-ray photon incident on the detector in a direction parallel to the axis of the collimation holes. The  $5^\circ$  circular field of view of the detector is not taken into account at this stage, but is incorporated into the least-squares fitting of the X-ray source strengths as discussed in section 2.5.3.

There are only a few regions in the X-ray sky which contain close-lying hard X-ray sources, among them the region in Cygnus and that part of the sky near the center of the Milky Way. Thus, even for the High Energy X-ray Spectrometer on OSO-8, which has a  $5^\circ$  FWHM, there are few regions in the sky where the confusion of close-lying sources is likely. For these regions, a source-by-source analysis of the data must exclude the region of the sky containing the adjacent sources. This exclusion of certain parts of the data may decrease the accuracy with which the source strength and the background can be determined. In these regions, skymaps are especially useful, since the maps can extract information about several sources simultaneously. The details of this procedure will be discussed in part 2.3.2 of this chapter.

It should be noted that the skymaps are accumulated as the anti-spin axis drifts through a particular region of the sky. They therefore represent an average spectrum of the sources observed, and are not appropriate for analysis of time-dependent behavior of sources on timescales short compared to the coverage time, which can be as long as two weeks for a single source.

#### 2.4.1: Constructing a local map of the sky:

The position of a celestial source is customarily given in terms of Right Ascension (RA) and Declination (Dec) with respect to a celestial coordinate system defined for a particular epoch (year). For a particular year, the X-axis is defined by the first point in Aires, and the Z-axis is defined by the position of the North Celestial Pole (see figure 2.3). For the OSO-8 experiment, the coordinate system is defined for the epoch 1950. If we choose some RA and Dec on the celestial sphere, we may define a coordinate system with an origin at the point where the position vector defined by RA and Dec intersects the celestial sphere. For this local coordinate system, the local Z-axis is co-linear with the position vector, while the local X-axis and Y-axis are local north and local east, respectively. If we choose the origin of this local coordinate system close to a source of interest, we may express the position of the source as a vector in the local coordinate system. The technique we

have used to express a position on the celestial sphere as a vector in the local coordinate system is discussed in appendix B.

#### 2.4.2: Expressing the detector axis in terms of the local coordinate system:

We must also express the detector axis in terms of the local coordinate system. To do this, two methods are available. First, we may perform the rotations for each wheel azimuth angle (WAZ) through the spacecraft primary coordinate system into celestial coordinates. From celestial coordinates, we may proceed in a fashion similar to the rotations described in appendix B to the local coordinate system.

Alternatively, we may transform the spacecraft anti-spin axis vector and the position vector of the spacecraft roll axis onto the local coordinate system (see figure 2.4). Both the spacecraft spin axis and roll axis can be obtained from the star tracker data and are available on the data tapes provided by the Information Processing Division at Goddard Space Flight Center. The spacecraft roll axis is normally within  $\pm 3^\circ$  of the position vector of the sun. The zero of the wheel azimuth angle is in the same direction as the projection of the spacecraft roll axis onto the local coordinate system to within  $\pm 1^\circ$  for data used to construct the skymap from the local coordinate system. The detector

look axis (at  $WAZ=0$ ) lags the zero mark of the wheel azimuth counter by  $120^\circ$  as the spacecraft rotates. Thus, an acceptable event associated with a  $WAZ=0$  would be assigned to the location  $5^\circ$  away from the anti-spin axis vector and in the direction of the zero of the wheel azimuth angle minus  $120^\circ$ .

In practice, it is not necessary to compute the position of the detector axis for every count and livetime in terms of the local coordinate system. Since the spin axis drifts at most approximately  $3^\circ$  each day for magnetic torquing, distributions of counts and livetime as a function of the  $WAZ$  can be accumulated for each orbit around the earth. The  $WAZ$  distributions can then be transformed onto the local coordinate system. As the anti-spin axis drifts through a source region, a time-averaged "picture" of the X-ray sky is gradually filled in.

Distributions of three sets of data are accumulated in the local coordinate system for any region of the sky:

- (i) counts from the open central crystal,
- (ii) counts from the shielded central crystal, and
- (iii) the detector livetime.

This data is accumulated in the  $10 \times 10$  bins in the local coordinate system to produce a skymap. We will discuss in some detail the manner in which the maps are used to extract information about X-ray sources within the mapped region.

## 2.5.: Analysis of skymaps:

### 2.5.1: Constructing a Map of Count Rates and Uncertainties.

Due to the inclination of the spacecraft's orbit, the internal detector background varies as a function of time. To reduce this effect, the difference in counting rate between the open and the shielded central crystals is used in each  $10 \times 10$  bin of the skymap. This technique will not completely correct for the gain changes of the photomultiplier tubes (Dennis et al. 1978) since the gain changes are not identical for the two crystals. However, the effect for the stronger sources of interest here is small. We note that the difference in counting rates between the open and central crystals should average to zero in all regions of a skymap except those where sources are present. The difference in the rates,  $R$ , of the two central crystals is given by the relation

$$2.1 \quad R_{ij} = \frac{O_{ij} - C_{ij}}{t_{ij}}$$

where  $O_{ij}$  and  $C_{ij}$  are the numbers of counts from the open and shielded central crystals, respectively,  $t_{ij}$  is the livetime, and  $i$  and  $j$  identify the X and Y coordinates for a particular  $10 \times 10$  bin in the local coordinate system.

In general, the uncertainty for any count rate in a local coordinate bin is equal to the uncertainty in the expected rate for that bin. The best estimate available for the expected rate is the average count rate,  $\bar{R}$ , for all the  $10 \times 10$  bins at the same energy. Thus,

2.2

$$\bar{R} = \frac{\sum c_{ij}}{\sum t_{ij}}$$

where  $c_{ij}$  and  $t_{ij}$  are the counts and livetimes for each bin and the indices represent a summation over all the values for a particular energy range. We multiply this average rate by the livetime,  $t_{ij}$ , for the  $ij$ th bin to get the expected counts for that bin. The standard deviation on those counts is the usual  $\sqrt{N}$ , assuming Poisson statistics. Therefore, the standard deviation in the rate of the  $ij$ th value is

2.3

$$\sigma_{R_{ij}} = \frac{\sqrt{\bar{R}} t_{ij}}{t_{ij}} = \sqrt{\frac{\bar{R}}{t_{ij}}}$$

In practice, since we are drawing from two populations, the open and the shielded central crystals are treated separately. Thus, the uncertainty on the difference between the rates of the open and shielded crystals for the skymap is

$$2.8 \quad \sigma_{R_{ij}} = \sqrt{(\sigma_{ij}(\text{open}))^2 + (\sigma_{ij}(\text{shielded}))^2}$$

### 2.5.2: Analysis of the skymap

Given a map of the X-ray sky in count rates and uncertainties, sufficiently strong sources will show up as enhanced regions above the background. However, maps showing contours of equal rates may be difficult to interpret because of the large statistical fluctuations in the rate in each  $10 \times 10$  bin or because of the unequal coverage in each bin. The unequal coverage is due to the fact that, as the anti-spin axis drifts through a region of interest, the detector look axis spends unequal amounts of livetime sweeping through each  $10 \times 10$  bin. If the statistics are poor, a single bin can have large deviations from the mean rate of that region even though these deviations are not statistically significant. Contour maps of the counting rate of the region can present apparently significant sources which do not exist, and can disguise weaker sources which are present.

If one attempts to plot a map of the source region in "sigma space" ( $R_{ij}/\sigma_{R_{ij}}$ ), the map is still sensitive to the unequal coverage. In this case, large uncertainties can still produce anomalously low or high regions. Combining adjacent bins can help smooth the contours, but this may

also hide close lying-sources which would otherwise be resolved. For instance, GX3+1 and GCX in the galactic center region are approximately  $3^\circ$  apart. One must look both at the count rate and at the sigma plots, and determine regions of significantly enhanced rates by taking both maps into account.

### 2.5.3: Least-squares fitting to a skymap:

These difficulties may be overcome if we know the location of the high energy X-ray sources. Given the location of the sources within the  $20^\circ \times 20^\circ$  region covered by the skymap, we construct a template (see figure 2.5) which represents the ideal detector response to point sources at the positions assumed. The detector's response to a point source results in a region of excess counting rate which approximates a cone in the skymap. The radius of the cone at the base is energy dependent, and is  $5^\circ$  for energies less than 100 keV. The counts from sources closer than  $10^\circ$  to one another will add together. This template is then fitted to the data by the method of least squares, allowing the source strengths and the background level to vary while keeping the source positions fixed. The source strengths and the background level are obtained for each energy bin. The count rates for the sources and background are then divided by the width of the energy bin in which they occur. The result is a spectrum of counting rate as a function of

the energy loss in the central crystal in units of counts  $s^{-1}keV^{-1}$  together with the corresponding uncertainties. To compare these results with data from other observers, it is necessary to convert this counting rate spectrum into the intensity spectrum of the X-ray photons incident on the detector.

#### 2.5.4: Determining the Spectrum of the X-ray Photons Incident on the Detector

The interaction of an incident X-ray photon with the detector crystal does not always result in the total energy of the X-ray photon being deposited in the crystal (see appendix A or Birks 1957). The effects of the variability in the energy loss in the crystal and of the amplitude of the signal detected from the crystal are removed from the data using the matrix inversion method (Dolan 1972). This process first removes the effect of the detector's finite energy resolution by apodization. Then, effects of the detector quantum efficiency, the fluorescent escape photons, and the attenuation of overlying material are removed by inverting the attenuation matrices which are obtained through laboratory calibration (Dolan et al. 1977). The process thus transforms the spectrum of counts  $s^{-1}keV^{-1}$  into the incident spectrum in photons  $cm^{-2}s^{-1}keV^{-1}$ .

## 2.6: Test cases for the skymap:

We have conducted test cases for the skymap analysis to demonstrate the applicability of the skymap technique to obtaining source spectra for both confused and isolated regions of the X-ray sky.

### 2.6.1: A strong, isolated source of constant intensity

The obvious candidate for this source is the Crab Nebula (Taurus XR-1). It is an extremely bright X-ray source with a constant, well-studied spectrum. Spectra obtained with the skymap analysis technique can be compared not only to the results in the literature, but also to spectra obtained with the distance-from-source analysis method currently in use to analyze OSO-8 data for isolated X-ray sources (Dolan et al. 1977).

A spectrum derived from the skymap for the Crab Nebula is plotted in figure 2.6 along with the spectrum for the Crab taken from Clark et al. (1973) and Dolan et al. (1977). The two spectra are in agreement within the limits of statistical uncertainties, lending credence to the skymap analysis technique.

### 2.6.2: Cygnus X-1 and Cygnus X-3: A confused source region with one strong and one weak source.

The situation for the Cygnus region is complicated by the fact that both sources are variable. The spectra yielded by

the skymap are average spectra, and must be compared with average spectra for the sources. The spectra for Cygnus X-1 and Cygnus X-3 derived from the skymap are shown in figures 2.7 and 2.8, respectively, along with data from other observers. The spectrum of Cygnus X-1 derived from the skymap is within the limits of statistical uncertainty for the source, and falls between the "low" and "high" state values reported by Dolan et al (1977). The skymap spectrum for Cygnus X-3 is also in general agreement with previously reported results (Ulmer 1972 and Ulmer et al. 1975).

## CHAPTER 3: OBSERVATIONS OF CENTAURUS A (NGC 5128)

### 3.1: Introduction

Centaurus A (NGC 5128) is a radio galaxy with an active nucleus that emits radiation over the entire electromagnetic spectrum. At radio frequencies, Cen A consists of two separate sets of radio lobes (Wade et al. 1971) centered on the nuclear component. The outer radio lobes are approximately 5 degrees apart and the inner lobes are separated by 3.5 arc minutes. Since the distance to Cen A is approximately 5 Mpc, the linear separations of the outer and inner lobes are 400 kpc and 5 kpc, respectively. Both sets of radio lobes lie along what appears to be the rotation axis of the galaxy, although some asymmetry is observed. The angular size of the nucleus is smaller than  $10^{-3}$  arcseconds at 7.85 GHz (Kellermann 1975). Kellermann (1974) reported evidence for variability of the nucleus of Cen A at 90 GHz (3mm) on a timescale of days (see Figure 3.1). Fogarty and Schuch (1975) observed Cen A from April through December 1974 and found no significant variability at 22 GHz (13.5mm). Price and Stull (1973), and Stull and Price (1975) observed fluctuations in the 10.7 GHz (2.8cm) flux of the nucleus of Cen A from 1973 to 1975 though no day-to-day variability was detected.

Optically, Cen A is an E0 type galaxy with an obscuring dust lane girdling the equator. Rodgers (1978) reports that

the dust lane is rapidly rotating and may have originated with the same event that produced the nearer radio lobes approximately  $2.5 \times 10^7$  years ago. A near infrared ( $< 1$  micron) "hot spot" with an angular size of approximately 5 arc seconds (linear dimension of 120 pc) has been observed at the center of the galaxy by Kunkel and Bradt (1971). A source with an angular size of less than 7 arc seconds was also detected by Becklin et al. (1971) at 1.6 and 10 microns. They showed that the intensity of the radiation at 2.2 microns is more than 10 times the surface brightness of our galaxy. Kleinmann and Wright (1974) measured the flux from the nucleus at 10 microns in June 1973, two years after the Becklin observation, and found that the flux had decreased by a factor of three to  $1.0 \pm 0.1$  Jy ( $1 \text{ Jy} = 10^{-23} \text{ ergs cm}^{-2} \text{ s}^{-1} \text{ Hz}^{-1}$ ). Grasdalen and Joyce (1976) observed the nucleus at 10 microns in August 1975 and obtained the same intensity as that reported by Becklin et al. (1971). They further note that the significance of the previously reported decrease may have been overestimated due to a systematic error.

Cen A has been observed at X-ray wavelengths intermittently since 1971 (see Figures 3.2 and 3.3). These observations provide evidence for marked variability in the intensity and also suggest changes in the spectral index (see Figure 3.4). An increase of the X-ray flux in

the energy range 2-60 keV over an interval of six days has been observed by Winkler and White (1975). The additional longer timescale variability is evident in Figure 3. 2. Mushotzky et al. (1978) have observed concurrent variability between their 2-6 keV data and the 10.7 GHz flux reported by Beall et al. (1978). At 100 keV, the photon flux is sufficiently low that day-to-day variations are difficult to measure and none has been observed. However, a significant increase did occur in the interval between 1971 and 1973, followed by a decrease between 1975 and 1976. At gamma-ray energies, an upper limit of  $10^{-32}$  ergs  $\text{cm}^{-2}$   $\text{s}^{-1}$   $\text{Hz}^{-1}$  at approximately 250 MeV has been obtained by Fichtel et al. (1976). An integral flux of  $(4.4 \pm 1) \times 10^{-11}$  photons  $\text{cm}^{-2}\text{s}^{-1}$  at energies greater than  $3 \times 10^{11}$  eV has been reported by Grindlay et al. (1975a).

### 3.2: Radio Observations

The radio observations presented in table 3.1 and in Figure 3.1 are taken from Beall et al. (1978). All radio observations were centered on the nuclear component of Cen A and the contribution from the inner radio lobes is negligible at all frequencies. The observations of Cen A were particularly difficult because they were all made from sites in North America, where the source was never more than 15 degrees above the horizon. An important confirmation of the overall variability of the source between 1974 and 1976

has come from observations taken in Brazil (Kaufmann and Beall 1979).

### 3.3: X-ray Observations

Cen A was observed with the high energy X-ray detector (Dennis et al. 1977) on board OSO-8 during July and August of 1975, 1976, and 1978. The 1978 data are unavailable at this writing. The data were reduced using the skymap technique described in Chapter 2 for an isolated source, and deconvolved through the detector response function (Dolan et al. 1977). A power-law least-squares fit to the spectrum is obtained and the intensity at 100 keV plotted in figure 3.3 along with similar values obtained by other workers. In figure 3.4, the X-ray power-law spectral index as determined from the available data is shown as a function of time. The spectra of Cen A for July-August 1975 and July-August 1976 are plotted in figures 3.5 and 3.6, respectively. The spectrum for the 1975 OSO-8 observations of Cen A is best-fit by a power-law  $dN/dE=A(E/E_0)^{-\alpha}$ , with  $A=(2.26\pm 0.54)\times 10^{-4}$ ,  $E_0=70\text{keV}$ , and  $\alpha=1.13\pm 0.33$ . The best-fit parameters for the 1976 observations are  $A=(1.18\pm 0.42)\times 10^{-4}$ ,  $E_0=70\text{keV}$ , and  $\alpha=2.05\pm 0.39$ .

### 3.4: Discussion

The data shown in figure 3.1-3.4 provide information on the variability of Cen A over an extremely wide range of frequencies. We will discuss the nature of this variability in detail in the next sections (3.5 and 3.6). Using the available data, we may construct a composite spectrum of the nucleus of Centaurus A (see figure 3.7). These observations, together with the infrared data discussed in section 3.1, are consistent with a single injection of a cloud of relativistic electrons which evolves by adiabatic expansion and turbulent acceleration. The observed fluctuations in both the radio and the X-ray spectra imply that the energy emitted as electromagnetic radiation may not represent the total energy available in the nucleus. In Chapter 4, previously proposed models will be discussed in which the radio radiation is produced by the synchrotron process and the X-rays are produced by inverse Compton scattering of the synchrotron photons. An alternative model (Beall et al. 1978) is proposed in which the X-rays are produced by inverse Compton scattering of photons with a blackbody distribution. This model is used to determine the magnetic field strength and the physical size of the emitting region, and the radiation temperature of the blackbody photon distribution in the nucleus. Upper limits on the energy in the nucleus will also be calculated, and we will show that there may be sufficient energy available to

form another pair of radio lobes similar to the two already present.

### 3.5: Recapitulation of the available observations

The available radio and X-ray data have been accumulated from many observers and do not have uniform time coverage. However, it is interesting to note the concurrences and differences between the fluctuations at various frequencies which can be seen by examination of figures 3.1, 3.2, and 3.3. The 10.7 GHz measurements show that the flux density increased by approximately a factor of 1.5 between September 1973 and March 1974. The flux went through an apparent minimum in July 1975, followed by a second increase in the fall of 1975 and subsequent decrease during the spring and summer of 1976. During this period there is evidence for day-to-day variability, which may confuse these long term trends. Kellermann's 1974 data at 31.5 and 89 GHz, coupled with the observations by Beall, et al. (1978) at 31.4, 85.2 and 90 GHz show a similar pattern of temporal variability. The 2-6 keV X-ray flux observations can be interpreted as a single, long-term increase in 1972 and 1973 followed by a decrease in 1975 and 1976 (Lawrence, et al. 1978) with short-term variability (Winkler and White 1975, Lawrence et al. 1978) superimposed on this general trend. The increase by a factor of 1.5 occurred approximately one year before the first observed

increase in the 10.7 GHz flux. The X-ray intensity at 100 keV seems to have followed the same general trend as the 2-6 keV flux, although there is some evidence that the initial brightening at 100 keV may have taken place approximately six months before the increase at 2-6 keV. The magnitude of the total increase at 100 keV was also apparently a factor of 2 larger.

### 3.6: Interpretation of the Radio and X-ray Temporal Variations.

The radio and X-ray spectra can be determined as a function of time from the data discussed in the previous section. The radio spectrum is consistent with a self-absorbed synchrotron source in which the 10.7 GHz flux density remains in the self-absorbed region, and the 30 and 90 GHz data lie along the power-law portion. The power-law index for the photon energy spectrum obtained in this way is approximately 0.6 in late 1975, and 0.4 in late 1976. For the 1974 data, the spectral index is 0.5 if we use the low value of the 89 GHz data and 0.1 if we choose the high number (Kellermann 1974). The flux density in July 1976 has apparently decreased at all measured frequencies from the values measured during December 1975. Between May and August 1976, the radio measurements at 10.7 GHz and 90 GHz show approximately the same rate of decline. These data demonstrate clearly that significant variability can arise

over timescales that are on the order of a month. Daily variability is apparent in the 10.7 GHz data, and is corroborated by concurrent variability with the 2-6 keV X-ray data (Mushotzky et al. 1978). Kaufmann and Beall (1978) have observed the source at 22 GHz during 1974 and 1976 from the Southern Hemisphere. The flux reported and the day-to-day temporal variability are in general agreement with the synchrotron spectrum constructed from the data presented by Beall et al. (1978)

The X-ray power-law spectral index as determined from the available data is shown as a function of time in Figure 3.6. In view of the importance of the possible temporal changes in this spectral index for models of Cen A (see Chapter 4), it is of interest to determine the probability that the observations do indicate a statistically significant variation. The hypothesis of a constant spectral index,  $\alpha$ , gives a chi-squared value of 65.4 for 10 degrees of freedom. Thus, the probability that the fluctuations of the data are random variations about a constant value of  $\alpha$  is less than  $10^{-6}$ . The two data points reported by Mushotzky et al. (1976) are usually thought to be the most telling evidence for the variability of the spectral index. Even if we exclude these two data points, the remaining data indicate the observations of the spectral index have less than a 2 percent probability of being drawn

from a constant value. We have neglected the influence of possible systematic errors in calculating these probabilities; the effect of these errors would be to lower the confidence levels in a varying spectral index which we have derived.

There are several plausible models for the radio and X-ray radiation produced by the nucleus of Cen A. These models will be discussed in detail in Chapter 7. However, several general comments can be made in view of the concurrent radio and X-ray observations discussed above.

The observed variations of the X-ray and radio radiation are consistent with the injection of a single burst of relativistic electrons in the galactic nucleus sometime during 1971 or early 1972. These electrons produce the synchrotron radio radiation and the inverse Compton X-ray spectrum. A delay between the rise in the X-ray flux and the 10.7GHz flux density is to be expected because the electrons responsible for the burst are initially opaque to their own synchrotron radiation (van der Laan 1966), though transparent to X-rays. Such a delay cannot be confirmed due to lack of data at 10.7 GHz prior to 1973. This interpretation of the data is, however, supported by the high flux values that were measured at 89 and 31.5 GHz during 1974 (Figure 3.1). The short-term variability might

not be expected with the van der Laan interpretation which invokes adiabatic expansion, but may be adequately explained by turbulence in the source (Pacholczyk and Scott 1976).

## CHAPTER 4: OBSERVATIONS OF 3C273

### 4.1: Introduction

3C273 is one of the nearest and brightest quasars ( $z=0.156$ , or 876 Mpc), with an absolute visual magnitude of  $M=-22$ . The quasar is also apparently associated with an optical jet.

At radio frequencies, 3C273 has been the subject of two long-term observing programs. Hobbs and Dent (1977) and Hobbs (1978) have observed 3C273 intermittently from 1970 through 1977 at 90 GHz, and report significant variability on a timescale of years. Shorter timescale variability may also be present in the data. Andrew et al. (1978) have also developed an extensive record of observations from 1970 to 1978 at 2.8 cm (10.7 GHz) and 4.5 cm (6.7 GHz) which shows variability on the same timescale and of the same general character as the work of Dent and Hobbs. However, there appears to be an anticorrelation between the low and high frequency fluxes. Finally, Waak and Hobbs (1978) have reported observations of 3C273 at 1.65 cm (18.2 GHz) and 0.95 cm (31.6 GHz) which extend the frequency range of the observations, and, in general, confirm the aforementioned variability. The radio spectrum assembled from various observations is plotted in figure 4.1. Recent observations by O'Dell et al. (1978) produce a spectrum for the source from  $10^{10}$  to  $10^{11}$  Hz consistent with the plotted data.

At infrared frequencies, 3C273 has been observed extensively due to its high luminosity and intrinsic interest as a source. Rieke and Low (1972) report a 0.3 Jy variable flux. For a source at a distance of 876 Mpc, this implies a luminosity of  $4.0 \times 10^{45}$  ergs  $s^{-1}$  between 7.9 and 13.3 microns. O'Dell et al. (1978) have reported an infrared spectrum between  $10^{14}$  and  $10^{15}$  Hz observed concurrently with the radio data mentioned above. Their infrared data are in general agreement with other observations. Measurements by Kemp et al. (1977) in the range of 1-8 microns indicate that the polarization of the nuclear source is surprisingly low ( $0.13 \pm 0.06$  percent). Schmidt and Peterson (1978) have obtained measurements of the jet associated with 3C273 which show that the jet is also unpolarized ( $3.7 \pm 4.1$  percent).

Spectra of 3C273 have been obtained by Oke and Shields (1976) from 3300 to 10500 Angstroms which show broadened emission lines of FeII and OI. Sandage (1964) reports optical variability of approximately 0.1 magnitudes. Davidson et al. (1977) have observed the source with an instrument flown by rocket, and have obtained the optical and ultraviolet spectrum of the source. The data show an optical and ultraviolet continuum with broadened emission line features. The power-law spectral index,  $\alpha$ , of the non-thermal continuum from  $1 \times 10^{14}$  to  $4 \times 10^{14}$  Hz obtained by

comparing these observations with the work of Grasdalen (1975) and Oke and Shields (1976) is  $\alpha=1.0$ . The spectrum between  $4 \times 10^{14}$  (the frequency of the hydrogen alpha line) and  $2.5 \times 10^{15}$  is significantly flatter with  $\alpha=0.6$ . Davidson et al. note that the spectral index must increase beyond the Lyman-alpha line ( $2.5 \times 10^{15}$ ), since the extrapolation of their data to X-ray frequencies would be greater than the X-ray flux observed. On the basis of these observations, they conclude that the optical and ultraviolet spectrum of 3C273 cannot be adequately described by a single power-law. Their conclusion has been confirmed by other workers. Wu (1977), using observations taken by the ANS satellite, derives a "de-reddened" ultraviolet spectrum. The corrected spectrum was reported to be  $F(\nu) = 1.10 \nu^{-2.1}$  ergs  $\text{cm}^{-2} \text{s}^{-1} \text{Hz}^{-1}$ , where  $F(\nu)$  is the flux density at a frequency  $\nu$ . This spectrum is in agreement with that of Davidsen et al. (1977). Boksenburg et al. (1978) obtain similar results with  $\alpha=1.0$  from the IUE data.

The first X-ray detection of 3C273 (Boyer et al. 1970) came from a rocket flight on 14 June 1969. The flux obtained from that observation was  $3 \times 10^{-10}$  ergs  $\text{cm}^{-2} \text{s}^{-1}$  from 1 to 10 keV, which implies a flux density of  $(1.17 \pm 0.40) \times 10^{-28}$  ergs  $\text{cm}^{-2} \text{s}^{-1} \text{Hz}^{-1}$  at  $10^{18}$  Hz. Using data from the UHURU satellite, Kellogg et al. (1971) obtained a flux of  $(6.6 \pm 1.0) \times 10^{-11}$  ergs  $\text{cm}^{-2} \text{s}^{-1}$  in an energy range from

2.4 to 6.9 keV. 3C273 was also observed by Ariel V in December 1975 and 1976 (Sanford 1977). The measured spectrum over the UHURU energy band agrees with the previous results and shows no variability. Pounds (1977) has obtained evidence for variability in the X-ray data from 2-10 keV using the Ariel V data from the Sky Survey instrument. In that work, he notes a possible correlation between the low energy X-ray flux and the flux density at 2.8 cm taken by Andrew et al. (1978).

The 2-sigma upper limits obtained using the skymap analysis (see Chapter 2) are plotted in figure 4.2 for the 1976 OSO-8 observations. An extrapolation of the spectrum reported by Sanford (1977) is shown for comparison. The upper limits from the OSO-8 data are in agreement with the Ariel V data.

#### 4.2: Discussion

The radio observations previously reported can be used to construct a radio spectrum for 3C273. As previously mentioned, these data are plotted in figure 4.1. Possible spectra are drawn through the data points which are concurrent. The spectrum is consistent with radiation from a synchrotron source with a maximum flux at 8 to 15 GHz. The low frequency decrease in the radio flux is suggestive of a low-energy cutoff to the distribution of relativistic electrons, since the value of the power-law spectral index,

$\alpha$ , in the radio at  $<10^{10}$  Hz is  $-0.3$ . At higher frequencies, the synchrotron spectrum can also deviate from a straight power-law. Relativistic electrons can lose energy by synchrotron radiation. The more energetic electrons lose energy more rapidly than less energetic electrons. This preferential energy loss causes a break in the electron spectrum and consequently, a break in the spectrum of the synchrotron radiation. If there is a change in  $\alpha$  due to synchrotron losses, we would expect the value of  $\alpha$  to change from  $0.5$  observed between  $10^{10}$  and  $10^{11}$  Hz to approximately  $1$  at higher frequencies. The infrared data do have a spectrum with  $\alpha=1$ . This suggests that the radio and far infrared spectrum of 3C273 may be produced by a single synchrotron source. The spectrum flattens in the optical range, and then steepens again to  $\alpha > 1.2$  beyond the Lyman-alpha line frequency.

The composite spectrum of 3C273 as taken from published data is plotted in figure 4.3. It should be noted that the observations for 3C273 are not for the most part taken concurrently. The suggestion of concurrent variability between the  $10.7$  GHz flux density and the  $2-10$  keV X-ray flux (Founds 1977) is reminiscent of the concurrent variability at  $10.7$  GHz and  $2-6$  keV reported by Mushotzky et al. (1978) for Centaurus A. If this pattern of variability also occurs for 3C273, it implies that the morphologies of the emitting regions of the quasar, 3C273, and the

elliptical galaxy, Cen A, may be similar. In this regard, it may be noted that Stockton (1978) has discovered a galaxy associated with 3C273.

## CHAPTER 5: OBSERVATIONS OF NGC 4151:

### 5.1: Introduction

The Seyfert galaxy NGC 4151 is a highly inclined spiral at a distance of 19 Mpc. Like Centaurus A it has been observed at frequencies extending from radio to X-ray. It is important to consider these results in modelling the emission mechanisms in the source.

At radio frequencies, NGC 4151 is a relatively weak and constant source, and has consequently not been extensively observed. De Bruyn and Willis (1974) measured the total flux of the nucleus to be  $135(\pm 10)$  Jy at 6 cm (4.996 GHz) using the Westerbork aperture synthesis telescope. Colla et al. (1973) have reported that the power-law spectral index,  $\alpha$ , from 6 to 73 cm has a value of  $0.74 \pm 0.05$ . On 31 Oct 76, Condon and Dressel (1978) observed NGC 4151 using the NRAO 3-element Interferometer and reported the flux to be  $188 \pm 10$  mJy at 2.695 GHz and  $89 \pm 10$  mJy at 8.085 GHz.

At infrared frequencies, Seyfert galaxies in general, and NGC 4151 in particular, have been observed extensively. Considerable controversy exists over the nature and degree of the apparent variability. Penston et al. (1971, 1974) have detected variability in the infrared at 1.6 and 2.2 microns using a 15 arcsecond aperture. They also report variability at 3.4 microns using a 10 arcsecond aperture. No attempt was made to determine the statistical

significance of this reported infrared variability. Rieke and Low (1972) obtained values of  $4.3 \pm 0.7$  Jy at 33.5 microns for observations taken on 18-19 Feb 75 using an 8.5 arcsecond aperture, and 1.2 Jy at 10 microns with no evidence for variability at either frequency. Kemp et al. (1977) note very small ( $0.13 \pm 0.06$ ) percent polarization of NGC 4151 at 10 microns.

At optical frequencies, Penston et al. (1971, 1974) have observed variability in the UV fluxes from the nucleus of NGC 4151. The observations showing this variability were made with a 25-arcsecond aperture and were conducted concurrently with their infrared observations mentioned above. Lyuty and Pronik (1975) on the basis of a compilation of their own and previous results, state that the U magnitude of the nucleus of NGC 4151 varies by 1 magnitude over periods of several years, and also exhibits short flares of 0.5 to 0.8 magnitude on timescales of 20 to 100 days. Ultraviolet observations by Wu and Weedman (1978) from the ANS satellite also suggest variability at wavelengths shorter than the U band.

NGC 4151 is a relatively weak X-ray source at low energies. Gursky et al. (1971) report a 3.8-sigma detection of a flux in the direction of NGC 4151 using the UHURU satellite. The spectrum of NGC 4151 has, however, been

determined to be very hard. An X-ray flux from 7 to 110 keV has been detected by Baity et al. (1975) with a spectrum of  $1.2 \times 10^{-2} E^{-1.4 \pm 0.2}$  photons  $\text{cm}^{-2} \text{s}^{-1} \text{keV}^{-1}$ . Ives et al. (1976) suggest, on the basis of a disagreement between their Ariel V value and the UHURU flux measured in 1970-71, that absorption of the low-energy X-rays may have changed. However, they find no evidence for variability of the power-law portion of the spectrum in their data, taken in Nov 1974 and Jan 1976. Ulmer (1977) shows a range of flux levels from UHURU (2 to 6 keV) of 4.8 to  $12.7 \times 10^{-11}$  ergs  $\text{cm}^{-2} \text{s}^{-1}$  on timescales less than a week, while Tananbaum et al. (1978) report variability on extremely short timescales (10 minutes or less) by a factor of  $6(\pm 2, -2.2)$  over the average rate. Mushotzky et al. (1978) have shown that the flux from the nucleus at 2-6 keV varies in intensity by a factor of 2 on timescales of days. However, they do not find evidence of significant changes in the absorption coefficient or the power-law spectral index of  $1.42 \pm 0.06$  used to fit their spectra. Recently, Auriemma et al. (1978) and Schenfelder et al. (1978) reported the detection of gamma-rays at  $>1$  MeV from the direction of NGC 4151. Their data are plotted in the composite spectrum of NGC 4151 in figure 5.5.

## 5.2: Observations

NGC 4151 was observed at radio, infrared, optical, and X-ray frequencies during the interval from 18 May through 12 June 1977. The radio observations at 2.695 and 8.085 GHz were taken by the author using the NRAO 3-element Greenbank Interferometer on 31 May 77 and 3 June 77. The data were reduced using the standard NRAO programs (Hjellming 1973), and are listed in table 5.1 and plotted in figure 5.1 along with radio measurements by other observers.

Infrared measurements were taken by Rieke (1977) and Pipher (1977), and optical (UBV photometry) measurements of the source were taken by Wisniewski and Tapia (Tapia 1977). These data are plotted as an infrared to ultraviolet spectrum in figure 5.2. The optical data for 30 May 1977 is normalized to an aperture of 10 arcseconds.

High energy X-ray observations of the nucleus were reduced by the author using the standard skymap routine (see Chapter 2). These data are compared to the data obtained by other X-ray observers in figure 5.3. Radio, optical, and X-ray flux densities are shown as a function of time in figure 5.4.

No evidence is found for variability at radio frequencies during the observing period. It seems likely that the slight decrease in flux suggested by figure 5.1 for longer timescales is an aperture effect, since the higher fluxes are those from detections of the total flux without

resolution of the nuclear component. The lower flux at each frequency is believed to come from the nuclear component.

There is also no evidence for variability in the infrared portion of the spectrum at wavelengths greater than 2.2 microns. There is apparent variability at 1.25 and 1.65 microns, but it is possible that the variability may result from instrumental effects in the two different systems involved in the observations.

In contrast with the radio and infrared observations, the UV photometry does show significant variability during the observing period. This data is plotted in figure 5.4 with the 2-6 keV X-ray data of Mushotzky et al. (1978) which also shows significant variability. The source is sufficiently weak that daily variability at energies above 20 keV cannot be detected with the current X-ray spectrometer.

### 5.3: Discussion

The composite spectrum from radio to X-ray is plotted in figure 5.5 for NGC 4151 during the observing period. The radio spectrum is relatively weak compared to Cen A and 3C273. A straight-line extrapolation of it falls below the observed X-ray spectrum. On the basis of this fact, and the lack of variability of the radio data, it is unlikely that synchrotron photons responsible for the radio observations are inverse Compton scattered to produce all of the observed X-ray flux.

The infrared spectrum at wavelengths less than 3.4 microns is reasonably well fit by a power-law ( $\alpha=1.26$ ). The infrared spectrum may be synchrotron radiation, or it may be caused by the summed emission of a number of thermal sources (stars and dust) with varying temperatures (Rieke 1977). In the latter view, the thermal emission may be excited by the non-thermal source, ultraviolet light, or particle interactions. The apparent lack of variability of the infrared data suggests that the mechanism associated with the infrared flux is not directly related to the variable, non-thermal source as evidenced by the X-ray data.

We are left with a possible association between the variable optical and the variable X-ray sources. Unfortunately, due to lack of coverage, we have evidence only that the optical and X-ray fluxes varied during the observing period. We do not know if they varied simultaneously.

It is possible that a power-law spectrum contributes to the UV photometry observations. Wu and Weedman (1978) find that the corrected spectrum for the ultraviolet continuum can be fit by a power-law with a spectral index of  $1.13 \pm 0.1$ . Boksenburg et al. (1978) report that the spectrum from optical to ultraviolet may be fit by a power-law with a spectral index of 1.0. They note, however, that the spectrum tends to flatten toward longer wavelengths.

## CHAPTER 6: OBSERVATIONS OF THE GALACTIC CENTER (GCX)

### 6.1: Introduction

Closest to home of all galactic nuclei (which is where, according to David Stern (1975), Astrophysics and Charity begin) is the nuclear region of the Milky Way. Partly because of its proximity, and partly because it is obscured from our optical view, the galactic nucleus has been intensively studied at radio, infrared, X-ray, and gamma-ray frequencies.

#### 6.1.1: Radio Observations of the Galactic Center Region

Balick and Brown (1974), using the NRAO 4-element interferometer, have observed an intense, unresolved (less than 0.1 arcsecond) source within the inner 1 parsec of the galactic nucleus. The measurements were taken at frequencies of 2.695 GHz (2.8 cm), and the brightness temperature reported for the source is greater than  $10^7$  K. Balick and Sanders (1974) present synthesis maps of the Galactic Center at 2.7 and 8.1 GHz using the 3-element NRAO interferometer. Their data show three principal sources of radio emission. Further investigation of one of these sources (called Sagittarius A) at 8.1 GHz shows a highly resolved structure. Using a 2 arcsecond beam, this region has a typical scale size of 10 arcseconds. If we assume the region is at a distance of 10 kpc, the corresponding linear

dimension is 0.5 pc. The flux density of the source is  $25 \pm 5$  Jy at 2.7 GHz. Balick and Sanders also report a weaker, unresolved ( $< 2$  arcseconds) structure within the northern complex of Sagittarius A. The galactic center is customarily identified with this compact radio source and with the extended infrared source at the same location (see next section).

The possible detection of a radio flare at an angular separation of 5 arcseconds from the galactic center has been reported by Davies et al. (1976). The data consist of a single detection on 30.2 March 1975, sandwiched between preceding and subsequent observing runs which produced only upper limits. This radio detection followed an X-ray flare (Eyles et al. 1978) from the same general region (within 7 arcminutes) by approximately one month. The temporal and spatial proximity of the radio and X-ray flares may imply some common origin but the connection remains uncertain.

#### 6.1.2: Infrared Observations of the Galactic Center

Infrared observations of the galactic center by Becklin and Neugebauer (1968 and 1969), and Low et al. (1969) have shown the region to be an intense infrared source. Rieke and Low (1973) produced infrared maps of the galactic center with 5 arcsecond resolution. Some structure is evident in these maps, taken at wavelengths of 3.5, 5.0, 10.0, and 20.0 microns. Becklin and Neugebauer (1975) observed the region

at 2.2 microns with an angular resolution of 2 arcseconds. Their data show considerable structure to the infrared emission from the galactic center, including an extended source coincident with the compact radio source reported by Balick and Brown (1974). Becklin et al. (1978) have obtained maps of the galactic center region in the near infrared. From an analysis of these maps, they conclude that the infrared source is likely to be a star cluster with a density greater than  $10^6 M_{\odot} \text{pc}^{-3}$ .

### 6.1.3: X-ray and Gamma-ray Observations of the Galactic Center

The literature on X-ray observations of the Galactic Center is both extensive and confused. Initial observations suggested a possible hard X-ray source near the galactic center (Friedman et al. 1967, Boldt et al. 1967). After that, the specificity of the galactic center observations rapidly deteriorated due to more sensitive instruments and somewhat better angular resolution. Due to this wealth of information, we will confine our discussion only to those sources likely to be associated (or confused) with the radio and infrared source at the galactic nucleus.

Buselli et al. (1968) reported a significant hard X-ray flux from the galactic center extending as a power law with a spectral index of 2.0 to almost 200 keV. The conical

field of view of the balloon-borne detector was 8 degrees FWHM. In a more extensive analysis of the Buselli et al. data, Thomas et al. (1975) conclude that the source of hard X-rays was GX1+4. Bradt et al. (1968) using data from a 2.1 x 20 degree rocket-flown X-ray detector with an energy range of 2 to 6 keV compared their data with count rates obtained by Gursky et al. (1967) to attempt to locate the positions of the sources present near the center of the galaxy. We should note that this is a reliable method only if the data are taken between intervals short compared to the timescale of variability of the source. Their work found no source at the position of the galactic center. Fischer et al. (1968) detected possible multiple sources near the galactic center. According to their data, the sources remained at the same intensity between two rocket flights conducted in 1964 and 1965. Lewin et al. (1969) reported the detection of high energy X-rays from four separate galactic center sources, but did not concur with Buselli that the source nearest the galactic center was GX3+1. Lewin et al. concluded that the dominant source of high-energy X-rays in the region was GX1+4. Schnopper et al. (1970) determined the positions of the sources GX3+1 and GX5-1 to within 1 or 2 arcminutes using a rocket flown rotation modulation collimator. Mayer et al. (1970) refined Bradt's X-ray positions using data taken from rocket flights. As their detector scanned across the galactic center, the data showed an increase in count

rate, which they associated with the source GX-2.5. Lewin et al. (1971), during observations of the galactic center region, reported flux changes by factors of 2 to 4 during an interval of 40 minutes with rise times and decay times of about 1 minute for observations of GX1+4 at energies from 18 to 50 keV. One of their scans through the region also shows an increase in count rate from the vicinity of the galactic center by an amount equal to that produced by GX1+4. Some variability may also be present in the data. Lewin et al. choose to associate the second hard X-ray detection with GX3+1. The detector had a field of view of  $1.5 \times 13$  degrees FWHM. Ricker et al. (1973) present relatively hard spectra of GX1+4 and GX3+1 using balloon data from a similar detector to Lewin et al. Coe (1978) also reports the detection of a hard X-ray source in the vicinity of the galactic nucleus. The UHURU satellite (Kellogg et al. 1971) showed an extended region of emission (approximately 2 degrees) near Sagittarius A at 2-10 keV. We conclude the discussion of these observations by noting that the data are consistent only if we assume that the sources which produce the observed X-ray flux from the vicinity of the galactic center vary in intensity.

The first report of variability from a source associated with the galactic center region was made by Eyles et al. (1977) using the Ariel V rotation modulation

collimator (RMC) experiment. The X-ray flux for the source A1742-294 increased by a factor of two over a 3 to 4 day interval, and then declined over a period of approximately 12 days. Wilson et al. (1977) note that the RMC data also show GX3+1 and GX5-1, as well as the X-ray transient source previously mentioned. Cruddace et al. (1978) have demonstrated that there are several 2-10 keV X-ray sources within 2 degrees the galactic center, but suggest that the major source of X-rays is the transient source A1742-294 detected with the RMC on Ariel V. Jernigan et al. (1978) have observed a flux of  $1.28 \times 10^{-10}$  ergs  $\text{cm}^{-2}\text{s}^{-1}$  from 2-11 keV in May-June 1977 from the position of the transient source.

At higher energies, Kniffen and Fichtel (1970) report the detection of gamma radiation at energies greater than 100 MeV. Haynes et al. (1975) report balloon measurements of a gamma-ray spectrum from 0.02-12.27 MeV using an instrument with an angular resolution of 13 degrees FWHM. At the time of the observations, the instrument was pointed in the vicinity of GX1+4. Haynes et al. also report a 3-sigma detection of line emission from the galactic center region at an energy of 0.5 MeV. This result is corroborated by a recent detection of line emission at 511 keV by an instrument with a field of view of 15 degrees FWHM has been reported by Leventhal et al. (1978) from the direction of the galactic center.

## 6.2: Observations

The High Energy Spectrometer on OSO-8 has mapped the galactic center region as the anti-spin axis of the spacecraft drifted through the region in August and September 1975, 1976, and 1978. The data for the 1975 and 1976 observations are available and are presented here. The data are analyzed using the skymap technique as described in Chapter 2. The positions of the known sources GX5-1, GX3+1, and GX1+4, and the radio/infrared position of the galactic center are used to fit four sources to the data available in the skymap. The spectra of GX3+1 and GCX (the X-ray source at the infrared/radio position of the galactic center) are shown in figures 6.1 through 6.4, respectively.

We note that the low-energy X-ray data for the 1975 observations of GX3+1 represent a 2-sigma detection of the source between 23 and 33 keV. The 1976 data for GX3+1 are at the 1-sigma level from 23 to 33 keV. In contrast to the relatively weak source at the position of GX3+1, the X-ray source at the radio and infrared position of the galactic center (GCX) emits a strong, hard flux during both observing periods. For the 1975 observation, the data are fit by a power-law spectrum with parameters of  $A=(6.76\pm 6.13)\times 10^{-5}$ ,  $E_0=70\text{keV}$ , and  $\alpha=3.38\pm 1.03$ . For the 1976 observations, the data are fit by a power-law with parameters of  $A=(4.08\pm 1.09)\times 10^{-4}$ ,  $E_0=70\text{keV}$ , and  $\alpha=2.28\pm 0.35$ . This

suggests the possibility that the power-law portion of the X-ray spectrum from the galactic center may be variable. The results from other sources represent marginal detections or upper limits.

The coverage of GX1+4 for the 1975 observation (the only time the source was in the detector's field of view) would allow only a marginal detection if the source were at the intensity reported by Ricker et al. (1973). The measured flux is consistent with data obtained with other instruments. It is important to note that the observations taken by OSO-8 in July and August 1975 do not rule out the possibility that GX1+4 has a hard X-ray spectrum. However, the 3 days of observation by OSO-8 in 1975 were sufficient only to produce upper limits for the X-ray flux. The skymaps are produced as the spacecraft drifts through a particular region of the sky. The time the detector spends exposed to any area varies greatly. Thus, for the 1975 observations of the galactic center, the observations of GX1+4 represent an exposure to the source of approximately 3 days, while the observations of the galactic center source represent an exposure of approximately 9 days to that source. For the 3 days of observation time on GX1+4, the flux detected from 43-63 keV was  $(2.05 \pm 1.57) \times 10^{-6}$  photons  $\text{cm}^{-2}\text{s}^{-1}$ .

On the basis of the observations of the galactic center, we conclude that the dominant hard X-ray source in the galactic center region is at a position coincident with the radio and infrared position of the nucleus of the Milky Way galaxy. In view of the flaring in the low-energy X-ray range that has been associated with this source, the suggestion of variability which is present in the OSO-8 data may not be unreasonable.

### 6.3: Discussion

The radio, infrared, and X-ray fluxes taken from the literature and from the OSO-8 data are shown in figure 6.5 as a composite spectrum. We should note that the observations have not been taken concurrently.

The location of the compact radio and infrared source effectively defines the position of the nucleus of the Milky Way galaxy. The hard X-ray source which we have detected is within approximately  $2^\circ$  of that position. It is unlikely that GX3+1 contributed a significant, time-averaged, hard X-ray spectrum during the OSO-8 observations of the region.

There is considerable evidence that the nuclear region of the galaxy contains a dense cluster of stars (Becklin et al. 1978). The apparently variable nature of the complex association of low energy X-ray sources in the region is

consistent with our understanding of evolved binary systems. However, the association of a hard X-ray source with this complex region represents a significant advance in our knowledge of the physical environment in the nucleus of the galaxy.

## CHAPTER 7: THEORY

### 7.1: Centaurus A (NGC 5128)

There is much more data available for Centaurus A than for any other galactic nucleus observed. Consequently, we will construct a detailed model of the nucleus of Cen A and address the other galactic nuclei only as the data permit. First, we will develop a model which can reproduce the spectral features of Cen A, and then we will analyze the observed temporal variability in light of this model.

#### 7.1.1: Models for the Spectral Features of Cen A

##### 7.1.1.1: The Blackbody-Compton Model

The radio radiation from Cen A's nucleus is almost certainly synchrotron in nature. The X-ray radiation is most likely to be photons inverse Compton scattered by the relativistic synchrotron electrons. Previous models are based on the assumption that the photons scattered in this way are the synchrotron radiation from the relativistic electrons moving in the magnetic field, the so-called synchrotron-Compton models. If these models are correct, and the low energy cutoff in the radio data is caused by synchrotron self-absorption, then both the magnetic field and the angular diameter of the source can be calculated from the measured synchrotron and inverse Compton fluxes (see e.g., Kellermann and Pauliny-Toth 1968). Grindlay (1975) has proposed such a model in which the high energy

X-rays are produced as synchro-Compton radiation from the source responsible for the centimeter and millimeter radio data. In this model, the low energy X-rays are mainly the synchrotron emission from a second more extended radio source. Mushotzky (1977) has proposed a similar model which uses only one source of synchrotron and synchro-Compton radiation. This model accounts for the spectral variability of the X-rays by adiabatic expansion (after van der Laan 1966) and by synchrotron losses. Both of these theories require that the spectrum of the microwave source extend into the infrared. At present, the simultaneous observations in the radio and infrared which may corroborate this assumption are unavailable. Tucker et al. (1973) suggested that the X-ray radiation might be produced by inverse Compton scattering of the infrared photons. This radiation is emitted by dust grains heated by electromagnetic radiation from the non-thermal source.

We propose here (as in Beall et al. 1978) a model for the nucleus of Cen A in which X-rays are produced by inverse Compton scattering of a blackbody radiation field located in a small ( $\leq 10$  pc) region of the nucleus near the center, where the blackbody temperature is much greater than the temperature suggested by the infrared measurements of Kunkel and Bradt (1971). Because of dust extinction, the optical luminosity of the nucleus is greater than that actually

observed. Thus, even for starlight, the blackbody photon distribution may have an energy density much greater than the energy density of the 3K background radiation. We must calculate the energy density of the radiation field to determine whether synchrotron radiation, the 3K microwave background, starlight, or a distribution of photons from some other source has the greatest energy density. The energy density of a distribution of thermal photons is proportional to a dilution factor which we call  $\Omega$ . For photons coming from a distribution of stars, the value of  $\Omega$  is calculated in Appendix C. For a plasma, the factor is simply the greybody approximation for the energy density of the radiation in the plasma. For a distribution of stars, a dilution factor of less than unity is equivalent to saying that the sky in a galactic nucleus is not completely covered by the discs of stars. For radiation from an optically thick, thermal plasma, the dilution factor is equal to one. Such an environment has been proposed by Fabian et al. (1976), who suggest that a massive ( $10^6 M_{\odot}$ ) black hole undergoing quasi-spherical accretion will have an effective photosphere with a temperature of  $10^4$ K and a radius of approximately  $5 \times 10^{15}$  cm.

The suggestion of such thermal photon distributions in the nucleus of Cen A is supported by both the infrared measurements of Kunkel and Bradt (1971) and by the optical

measurements of van den Bergh (1976). The angular diameter of 5 arc seconds and the temperature of 250K obtained for the infrared source can be used to place an upper limit on the energy in the relativistic electrons in the emitting region. The 10<sup>4</sup>K blackbody photon distribution will be used in calculating the magnetic field and linear dimension of the source.

It is relevant to note here that the observed radio and X-ray flux densities do not track one another throughout the plotted interval (see chapter 3). The 2-6 keV flux apparently does not share the fluctuation that occurs at 10.7 and 31.4 GHz from July 1975 to July 1976, but continues to decline. The 100 keV intensity decreases during this period by a factor of approximately 3. Synchrotron-Compton models for Centaurus A cannot naturally account for this lack of concurrent variability, since the synchrotron photons are always in the same volume as the emitting electrons. However, this lack of concurrent variability between the radio and X-ray data can be interpreted within the blackbody-Compton model as being the result of an expanding cloud of relativistic synchrotron electrons leaving the region in which the density of the blackbody photons is high. In such a case, the synchrotron emission may stay constant or even increase as the X-ray flux decreases. Some part of the decrease in the 2-6 keV flux

may be caused by increased absorption of the low energy X-rays in an ionized intervening medium that is beginning to recombine. An intervening medium is suggested by Davison et al. (1975) and Serlemitsos et al. (1975) who observe X-ray absorption consistent with  $1.6 \times 10^{23}$  atoms of hydrogen  $\text{cm}^{-2}$  along the line of sight. Van den Bergh (1975) notes that these observations are consistent with optical data which suggest an extinction of 100 magnitudes. An initial burst of X-ray radiation associated with the injection of relativistic electrons might ionize the intervening medium. If the decrease in the 2-6 keV flux during 1975 were due solely to recombination, the value implied for the density of hydrogen atoms is  $10^4 \text{ cm}^{-3}$ . Using the X-ray absorption, and Munkel and Bradt's infrared hot spot as a linear dimension, the density of hydrogen atoms becomes  $10^4 \text{ cm}^{-3}$ . The values are not inconsistent. However, increased absorption does not account for the decrease in the 100 keV flux.

#### 7.1.1.2: Consequences of the Blackbody-Compton Model

We assume that the ambient radiation field in the nucleus is principally that of a blackbody. The cloud of relativistic electrons, the magnetic field, and the blackbody photon field may not be distributed uniformly throughout the nucleus. If the relativistic electrons, the blackbody photons, and the magnetic field occupy the same

region of space, then we can calculate the relationship between the magnetic field and the photon temperature in the source from the ratio of the X-ray flux density,  $F(\nu_c)$ , to the synchrotron flux density,  $F(\nu_s)$ . The frequencies are chosen such that  $\nu_c$  and  $\nu_s$  are in the power-law (unabsorbed) portions of the radio and X-ray spectra, respectively. We also assume that the relativistic electrons have a power-law spectrum of the form  $N(\gamma) = A\gamma^{-n}$ , where  $N(\gamma)$  is the electron number density in electrons  $\text{cm}^{-3}$  at a particular value of  $\gamma$ , the ratio of an electron's total energy to its rest mass energy ( $m_e c^2$ ), and  $n$  is the power-law spectral index of the electron number spectrum. To account for the possibility that the energy density of the thermal photons is not equal to that of a blackbody, we modify equation 4-53 of Tucker (1976) by inserting the dilution factor,  $\Omega$ . Combining equations 4-53 and 4-54 then yields:

$$7.1 \quad \frac{F(\nu_c)}{F(\nu_s)} = 2.47 \times 10^{-19} (5.25 \times 10^3)^q \cdot \Omega \cdot \frac{b(n)}{a(n)} T^{3+q} B^{-(q+1)} \left(\frac{\nu_c}{\nu_s}\right)^{-q}$$

where  $B$  is the magnetic field in gauss;  $\Omega$  is the dilution factor which accounts for the greybody approximation;  $a(n)$  and  $b(n)$  are determined from the synchrotron spectrum and depend only on the electron power law index,  $n$ ;  $T$  is the temperature of the thermal photon

distribution in degrees K; and  $q$  is the power-law spectral index of the X-ray energy spectrum. Note that  $q=(n-1)/2$ . We choose  $\nu_c=2.4 \times 10^{18}$  Hz (100 keV) and  $\nu_s=5 \times 10^{10}$  Hz. Substituting these values and  $q=0.5$  (which implies  $n=2$ ,  $b(2)=5.25$ , and  $a(2)=0.103$ ) from X-ray observations into equation 7.1 yields:

$$7.2 \quad \frac{F(\nu_c)}{F(\nu_s)} = 4.16 \times 10^{-20} \Omega T^{3.5} B^{-1.5}$$

In the 1974 observations, the ratio of  $F(\nu_c)/F(\nu_s)$  at the chosen frequencies was found to be  $8.4 \times 10^{-7}$ . Thus, from Equation 7.2,

$$7.3 \quad \Omega T^{3.5} B^{-1.5} = 2.02 \times 10^{13}$$

If we use the temperature suggested by Fabian et al. (1977) of  $10^4$  K, and a dilution factor of  $\Omega=1$ , equation 7.3 yields a value for the magnetic field  $B=2.9$  gauss. This is considerably greater than a typical galactic magnetic field, which is on the order of microgauss, but may be reasonable for the dense plasma suggested by Fabian et al. Alternatively, we may allow the source to be optically thin ( $\Omega < 1$ ), and assume that the photons come from O or B-type stars in the galactic nucleus (see Appendix C), or from an optically thin plasma. For these cases, also, we let  $T=10^4$  K. Consequently, the value of the magnetic field is

considerably lower. The exact value depends, obviously, on  $\Omega$ . For  $\Omega=10^{-5}$ , the magnetic field becomes  $1.4 \times 10^{-3}$  gauss.

For a self-absorbed synchrotron source, the magnetic field,  $B$  (in gauss), is given by the relation

$$7.4 \quad B = 2.2 \times 10^7 F(\nu_m)^{-2} \nu_m^5 \theta^4$$

where  $F(\nu_m)$  is the maximum synchrotron flux density in Jy,  $\nu_m$  is the frequency in GHz at which the flux density is a maximum, and  $\theta$  is the angular size of the source in arcseconds (Sligh 1963 and Williams 1963). For  $B=2.9$  gauss ( $\Omega=1$ ), and the frequency at which the observed radio flux density is maximum ( $\nu_m=25$  GHz), we obtain from Equation 7.4,  $\theta=1.7 \times 10^{-3}$  arcseconds. This corresponds to a linear diameter of 50 light days. If we choose  $T=10^3$ K, then the values of  $B$  and  $\theta$  are  $1.4 \times 10^{-2}$  gauss and  $4.5 \times 10^{-4}$  arcseconds (12.6 lt. days), respectively. From the example cited in the previous paragraph, we take  $\Omega=10^{-5}$  and  $T=10^4$ K. Then  $B=1.4 \times 10^{-3}$  g, and  $\theta$  is  $2.5 \times 10^{-4}$  arcseconds (7.3 lt. days).

### 7.1.1.3: An Upper Limit for the Energy Contained in Relativistic Electrons in the Nucleus of Cen A.

The change in the X-ray spectral index as a function of time, if it is real, has important physical consequences (see section 7.3 for a discussion). The apparent tendency of the spectral index to harden with time during the initial X-ray brightening indicates that particle acceleration may be taking place during that period of time. Particle acceleration or some repopulation of the emitting relativistic electrons is also suggested by the fluctuations in the radio spectrum throughout the observing period. This evidence for continuing particle acceleration suggests that only a small fraction of the total energy in the nucleus of Cen A is emitted in the form of X-ray and radio radiation, the remaining being contained in kinetic energy of the ejecta, thermal energy, magnetic field energy, etc. It follows that the energy release which was observed in the nucleus of Cen A may be sufficient to lead to the eventual formation of a pair of radio lobes similar to those that are already present. We pursue this line of reasoning in some detail.

The energy density of the relativistic electrons,  $\epsilon_e$ , can be expressed as (Tucker 1976)

7.5

$$\epsilon_e = \bar{\gamma} m_e c^2 N_e$$

where  $m_e c^2$  is the "average" total electron energy and  $N_e$  is the average density of electrons in some emitting region.  $N_e$  may be expressed as

$$7.6 \quad N_e = \int_{\gamma_0}^{\gamma_1} N(\gamma) d\gamma$$

for the power-law distribution of electrons,  $N(\gamma) = A\gamma^{-n}$ , between the values of  $\gamma$  from  $\gamma_0$  to  $\gamma_1$ . Assuming that the power-law portion of the synchrotron spectrum extends from 25 to 90 GHz,  $\gamma_0$  and  $\gamma_1$  are approximately  $10^3$  and  $10^4$ , respectively, the exact values depending on the magnetic field (Ginzberg and Syrovatskii 1965). The flux density of the inverse Compton X-ray radiation,  $F(\nu_c)$ , caused by inverse Compton scattering from a thermal photon field with energy density  $u = \Omega a T^4$  (where  $a$  is the first radiation constant,  $T$  is the effective temperature, and  $\Omega$  is the factor to account for the greybody approximation) is, following Tucker (1976):

$$7.7 \quad F_{\nu_c} = \frac{L(\nu_c)}{4\pi D^2} = \frac{4.2 \times 10^{-40} R^3}{3D^2} \Omega A T^{3+q} b(n) \left( \frac{2.1 \times 10^{10}}{\nu_c} \right)^q$$

Here,  $D$  is the distance to Cen A in cm ( $1.55 \times 10^{25}$  cm = 5 Mpc),  $R$  is the radius of the emitting region in cm, and  $L(\nu_c)$  in ergs  $s^{-1} Hz^{-1}$  is the luminosity at a frequency  $\nu_c$ . The X-ray and radio spectra are consistent with  $n=2$  ( $q=0.5$ ), which gives  $b(2)=5.25$ .

The blackbody-Compton radiation mechanism is relatively sensitive to the effective temperature of the blackbody photons. By choosing a lower limit for the temperature, we can find an upper limit to the total energy in relativistic electrons. The 250K value obtained for the infrared source is certainly a lower limit for the effective temperature, and suggests a dilution factor of unity since the infrared source certainly contains the galactic nucleus. Substituting  $T=250\text{K}$  and  $R=5$  light days into equation 7.4, we find that the normalization constant  $A$  becomes  $1.7 \times 10^9 \text{ cm}^{-3}$ , corresponding to an electron density,  $N_e$ , of  $7 \times 10^5$  electrons  $\text{cm}^{-3}$  for the observed value of  $F(\nu)$ . Substituting this value into equation 7.4 yields  $\epsilon_e = 6 \times 10^3 \text{ ergs cm}^{-3}$  as a maximum energy density for the relativistic particles. For  $T=10^3$  and  $10^4\text{K}$ ,  $A$  becomes 2 and  $10^{-4}$  ergs  $\text{cm}^{-3}$ , respectively, assuming  $\Omega=1$ . If the emitting region is the only region in the nucleus that contains these relativistic particles, then the maximum energy of the source for the observed outburst is  $6 \times 10^{51}$  ergs. This is comparable to the energy release in a supernova.

It is possible, however, that the radiation we see may come from regions of enhanced magnetic field strength or blackbody photon energy density, or both. If this is true, there may be non-emitting regions within the nucleus that contain energetic particles. We can calculate an upper

limit for the total energy in relativistic electrons in the nucleus by assuming that the electron density throughout the nucleus is the same as that calculated for the emitting region. Using a blackbody photon temperature of  $10^3$  K and the infrared nuclear dimension of 120 pc, and setting  $\Omega=1$ , we obtain  $5 \times 10^{61}$  ergs as the maximum energy of relativistic electrons in the nucleus. For a  $10^4$  K blackbody photon temperature, the maximum energy is  $5 \times 10^{57}$  ergs. These energies are sufficient to form a pair of radio lobes similar to the two sets already present.

#### 7.1.2: A Detailed Model for the Temporal Variability of the Nucleus of Centaurus A

##### 7.1.2.1: Introduction

The actual physical environment of the nucleus of Cen A is undoubtedly quite complex. We wish to determine what constraints can be placed on models of the radio and X-ray production mechanisms. The radio radiation is most likely to be produced by the synchrotron mechanism. It is probable that the X-ray radiation is inverse Compton scattering of an ambient distribution of photons.

The exact character of the X-ray radiation, and the dominant source of the scattered photons depend on the nature of the power law distribution of relativistic electrons. In general, however, the the source of ambient

photons which most contributes to the inverse Compton scattered X-ray flux will be that distribution with the greatest energy density. We must, therefore, compare the energy densities of the various radiation fields in a galactic nucleus.

The radiation field in a galactic nucleus can come from a combination of the following:

- (i) synchrotron radiation from a non-thermal source,
- (ii) starlight,
- (iii) the 3K background radiation,
- (iv) thermal radiation from dust, and
- (v) thermal radiation from an optically thick plasma.

In order to compare the energy densities of the radiation, we must be able to calculate the energy density of starlight in a dense distribution of stars. This calculation (see appendix C) produces a dilution factor which "dilutes" the energy density of the starlight. Obviously, the 3K background radiation, being isotropic, does not require this treatment. We note, however, that the contribution of the 3K blackbody radiation is not significant when compared to  $10^4$ K starlight radiation unless the dilution factor for the stellar distribution is  $<10^{-12}$ . Therefore, we do not consider the 3K background radiation further in calculating the energy density of electromagnetic radiation in this environment.

7.1.2.2: Determination of the Dominant Radiation Field  
Which Contributes to Inverse Compton Production  
of X-rays

The rate at which energy is lost by a single relativistic particle moving in an ambient radiation field is (Felten and Morrison 1963 and 1966)

$$7.8 \quad P = \frac{4}{3} \sigma_t \gamma^2 u$$

where  $P$  is the total radiated power,  $\sigma_t$  is the Thomson cross-section,  $\gamma$  is the ratio of the total electron energy to its rest mass ( $E/m_e c^2$ ), and  $u$  is the energy density of any ambient radiation field.

The dominant energy loss will be through scattering by the radiation field whose energy density is greatest. If we are interested in comparing the relative contributions to the electron energy loss by inverse Compton scattering of synchrotron and thermal photons, we may construct the ratio  $R$  of the energy density of synchrotron photons ( $u_s$ ) and of the thermal photons ( $u_t$ ) as

$$7.9 \quad R = \frac{u_t}{u_s} = \frac{\Omega_s T^4}{u_s}$$

We should note, however, that the relative contributions to the inverse Compton flux from synchrotron or thermal

scattering at a particular frequency are not unequivocally determined by this ratio. It is possible that thermal photons (which often have higher frequencies on the average than the synchrotron radiation) will be the dominant source of inverse Compton scattered X-ray and gamma-ray photons. The actual contributions at a particular frequency of the inverse Compton flux from thermal and synchrotron photons depends on the energy distribution of the relativistic electrons, when the energy density of the synchrotron radiation is greater than the energy density of the thermal radiation. If the energy density of the thermal photons is greater than that of the synchrotron photons, however, the thermal photons dominate the inverse Compton emission for any distribution of relativistic electron energies.

The energy density of synchrotron radiation can be determined from the measured flux. If we observe a spectrum of the form

$$7.10 \quad F(\nu) = A \nu^{-q}$$

where  $F(\nu)$ ,  $A$ , and  $q$  are empirically determined from the power law portion of the synchrotron spectrum, and the radiation comes from a source of radius  $R$  at a distance  $D$ , then the energy density  $U_s$  is given by the equation

$$7.11 \quad u_s = \frac{1}{c} \left( \frac{D}{R} \right)^2 \int_{\nu_1}^{\nu_2} F_\nu \, d\nu$$

C-2

where  $c$  is the velocity of light, and the synchrotron spectrum extends from  $\nu_1$  to  $\nu_2$ .

For Cen A's nucleus, the measured value of the radio radiation yields  $u_B = 3.37 \times 10^{-17} \frac{1}{c} \left(\frac{D}{R}\right)^2 \int_{\nu_1}^{\nu_2} \nu^{-.5} d\nu$ . The power law portion of the radio spectrum extends from 22 to 90 GHz.

Then

$$7.12 \quad R = 1.31 \times 10^{-11} \Omega T^4$$

If we assume that  $T=10^4 K$ , the ratio becomes  $1.3 \times 10^5 \Omega$ . Thus, in order for the thermal photon energy density to dominate over the synchrotron energy density by an order of magnitude, we require  $\Omega > 10^{-4}$ . For an expanding sphere of material of sufficient density, the dilution factor will be 1, and the blackbody energy will dominate over the synchrotron radiation. For greybody radiation from a distribution of stars in a galactic nucleus,  $\Omega > 10^{-4}$  will occur only for an extremely dense distribution of stars.

#### 7.1.2.3: Possible Models for Source Variability

It is interesting to note that the minimum values of the X-ray spectral index shown in figure 3.4 occur in late 1972 and early 1973. This time interval shows an increasing flux at 2-6 and 100 keV (see figures 3.2 and 3.3). If the X-ray radiation is the result of inverse Compton scattering of an

ambient source of photons, then the X-ray power-law spectral index is directly related to the number spectrum of the relativistic electrons. It follows that the variability of the spectral index (if real) between 1972 and 1973 indicates a change in the slope of the number spectrum of the relativistic electrons, and that the increase in X-ray flux suggests a corresponding increase in the number of relativistic electrons radiating at a given energy. This is usually evidence for either particle acceleration or the injection of new high-energy particles into the source region.

Facholczyk and Scott (1977) have suggested that the variability associated with the compact radio sources in active galactic nuclei can be explained by turbulent acceleration and adiabatic expansion of a plasma containing relativistic electrons. The acceleration is caused in this view by turbulence associated with the movement of the plasma through an ambient medium.

If the apparent variation of the X-ray power-law spectral index is real, then it is likely that the initial brightening of Cen A which occurred from 1972 through 1973 was the result of some undetermined mechanism which accelerated particles to relativistic energies. The evidence for continued particle acceleration after early

1974 is less convincing. This suggests the possibility that the relativistic particles are accelerated within a plasma sufficiently dense in its interior to suppress synchrotron radiation either by the Razin-Tsytoich effect (Razin 1960) or by free-free absorption. The long-term variability at radio frequencies would then be the result of expansion of the plasma and consequent decrease in the suppression or absorption of the radiation produced in the plasma's interior. In this situation, flares in the radio are possible even though the inverse Compton X-ray flux decreases. Eventually, the volume in which the suppression or absorption occurs will go to zero. Thereafter, the source is modelled by van der Laan (1966) expansion.

We assume, as before, that the major source of thermal radiation in Cen A's nucleus is either blackbody radiation from an optically thick plasma, or starlight radiation from a centrally condensed distribution of stars. Thermal radiation from a plasma and from a distribution of stars suggest rather different physical environments for the source. We will discuss each of these possibilities in turn.

#### 7.1.2.4: Radio and X-ray Radiation from a Dense Hot Plasma

A sufficiently dense, hot plasma radiates as a blackbody. These blackbody photons can be inverse Compton scattered by relativistic electrons to produce X-rays, the so-called blackbody-Compton model (Beall et al. 1978). In the discussion that follows, we assume for computational simplicity that the relativistic electrons which scatter the thermal photons are thoroughly mixed with an optically thick plasma, or photosphere, at a temperature of  $10^4$ K.

The assumption of thorough mixing of the photosphere and the relativistic electrons is not a critical one. Falk and Arnett (1977) suggest that the expanding photosphere may fragment into optically thick "blobs" due to Rayleigh-Taylor instabilities. If a similar situation occurs in a dense, expanding plasma, the energy density of the thermal photons within the interstices may be roughly that of the energy density of the unfragmented photosphere. The Razin effect will suppress synchrotron radiation within the interstices, since frequencies are suppressed which are less than  $\nu_R = 20(N_e/B)$  Hz (Razin 1960). This can be in the gigahertz range for typical values of magnetic field, B, and electron number density,  $N_e$ . Free-free absorption requires higher densities, and is more likely to occur as the radio flux passes through the dense photosphere. For simplicity, we will assume a spherically symmetric, optically thick plasma

with a uniform magnetic field, thoroughly mixed with a distribution of relativistic electrons having a power-law spectrum. The number density of the relativistic electrons is assumed to be a function of the radius,  $r$ , of the plasma.

As the plasma expands, the rapid decrease in the optical depth allows recombination of the photosphere, reducing the free-free opacity at radio frequencies. Following Falk and Arnett (1977), we note that the luminosity,  $L$ , of an expanding photosphere decreases exponentially with a characteristic time,  $t_d$ , such that  $L=L \exp(-t/t_d)$ . Here,  $t_d$  is the diffusion timescale based on a random walk approximation for a photon inside the plasma. As the plasma expands, its density will decrease. Thus, the opacity,  $\kappa$ , of the material will decrease with time. This will allow the photosphere to begin to recombine, which reduces the amount of material subsequent photons must move through in order to escape the plasma. We may estimate the average diffusion time  $\langle t_d \rangle$  between times  $t_1$  and  $t_2$  as

$$7.13 \quad \langle t_d \rangle = \frac{1}{t_2 - t_1} \int_{t_1}^{t_2} \frac{3\kappa(t)M(t)}{4\pi cR(t)} dt$$

where  $\kappa(t)$  is the mean opacity,  $M(t)$  is the mass interior to the photospheric radius  $R_{ph}$ ,  $R(t)$  is the radius of the spherical plasma, and  $c$  is the velocity of light. If  $t_d$  is assumed to decrease linearly as the photosphere expands from

$R(t_1)$  to  $R(t_2)$ , then the average mass  $M$  is roughly half the original value,  $M(t_1)$ . We assume that the opacity within the photosphere has some average value,  $\kappa$ , and that its dependence on time can be neglected. We may now integrate equation 7.13 to find

$$7.14 \quad \langle t_d \rangle = \frac{3\bar{\kappa}M}{8\pi c} \cdot \frac{1}{R-R_0} \ln \left( \frac{R}{R_0} \right)$$

(Falk and Arnett 1977).

From the diffusion timescale, we may define a diffusion radius,  $R_d$ , such that

$$7.15 \quad R_d = c \langle t_d \rangle = \frac{3\bar{\kappa}M}{8\pi} \left( \frac{1}{R-R_0} \right) \ln \left( \frac{R}{R_0} \right)$$

The luminosity of the expanding, spherically symmetric plasma as a function of the plasma radius  $R$  then becomes

$$7.16 \quad L = L_0 e^{-R/R_d}, \text{ where } L_0 = 4\pi R^2 \sigma T^4 (1 - e^{-\tau_{opt}})$$

In equation 7.16,  $\sigma$  is the Stefan-Boltzmann constant,  $T$  is the mean temperature, and  $\tau_{opt} = \tau_0 (R_0/R)^2$  is the optical depth resulting from electron scattering. We may define an effective photospheric radius,  $R_{ph}$ , by combining equation 7.16 and

$$7.17 \quad L = 4\pi R_{ph}^2 \sigma T^4$$

to yield

$$7.18 \quad R_{ph} = R(1 - e^{-\tau_{opt}})^{1/2} \cdot e^{-\frac{R}{2R_d}}$$

We may estimate the value of the ratio,  $R/2R_d$ , in equation 7.16 by expanding the expression the expression for  $R_d$  (equation 7.15) as a series. After some manipulation, we find that

$$7.19 \quad R_{ph} = R(1 - e^{-\tau_{opt}})^{1/2} \cdot e^{-\left(\frac{R}{R_0}\right)^2 / \tau_{opt}}$$

It can be seen that after some initial linear expansion,  $R_d$  will rapidly approach zero. As the photospheric radius decreases, a "recombination wave" will move inward, reducing the electron number density,  $N_e$ , and consequently the free-free absorption and Razin-Tsytoich suppression. We assume that the optical depths in the source is on the order of 10, so that for reasonable photospheric densities, the recombination timescale ( $t=10^{12}/N_e$  seconds) is very much shorter than the expansion timescale of the source. It is likely, therefore, that the decrease in the electron number density  $N_e$  beyond  $R_{ph}$  is due primarily to recombination, and not to expansion. Thus, in the presence of a magnetic field, relativistic particles found beyond  $R_{ph}$  will emit synchrotron radiation that does not undergo significant free-free absorption or Razin-Tsytoich suppression.

To determine the synchrotron radiation from such an environment, we note that in the plane-parallel approximation, the intensity of synchrotron radiation as a function of  $r$ , the position vector inside the plasma, is

$$7.20 \quad I_{\nu}(r) = \frac{j_{\nu}}{\alpha_{\nu}} [1 - e^{-\tau_{\nu}(r)}], \text{ where } \tau_{\nu}(r) = 2\alpha_{\nu}(R^2 - R_{ph}^2)^{1/2}$$

Here,  $I_{\nu}$  is the synchrotron intensity at frequency  $\nu$ ,  $j_{\nu} = j_{\nu}(r)$  is the synchrotron emissivity per unit volume, and  $\alpha_{\nu}$  is the absorption coefficient per unit length for free-free absorption. We have not explicitly considered synchrotron self-absorption in equation 7.20. Since the radio observations of Cen A defined both a power-law and a self-absorbed portion of the radio spectrum, we can model the temporal variability of the (unabsorbed) power-law portion of the spectrum. The Razin-Tsytoovich effect is included in the calculations implicitly, since the integration is always taken from  $R_{ph}$  to  $R$ . The synchrotron radiation at  $r < R_{ph}$  is thus assumed to be suppressed.

We make the plausible assumption that the relativistic electrons are not distributed uniformly throughout the photosphere, but are concentrated in a shell at a certain radius. Such a scenario is the likely consequence of shock acceleration of the relativistic particles or of injection of relativistic particles over some finite interval of time

into the plasma. We may model this shell-like structure with a density distribution of the form  $N(\gamma) = N_0(\gamma) (1/1 + ((r-a)/\xi R)^2) = N_0(\gamma) f(r)$ , where  $N_0(\gamma)$  is the relativistic electron number density at  $r=a$ , and  $\xi$  is a parameter which allows us to vary the relative concentration of the radiating electrons about  $r=a$ . The synchrotron emissivity per unit volume then becomes

$$7.21 \quad j_\nu(r) \equiv j_\nu(r=a) \cdot f(r) = j_{\nu_0} \cdot f(r)$$

and the synchrotron luminosity  $L_\nu$  is

$$7.22 \quad L_\nu = 8\pi^2 \int_{R_{ph}}^R \left(\frac{j_{\nu_0}}{\alpha_\nu}\right) \cdot f(r) \cdot [1 - e^{-\tau_\nu(r)}] \cdot r \cdot dr$$

If we assume  $\alpha_\nu$  is roughly constant for  $R_{ph} < r < R$ , equation 7.22 becomes

$$7.23 \quad L_\nu = 8\pi^2 \frac{j_{\nu_0}}{\alpha_\nu} \int_{R_{ph}}^R f(r) [1 - e^{-\alpha_\nu(R^2 - r^2)^{1/2}}] \cdot r \cdot dr$$

Because of the dependence of the electron number density  $N_0$  upon the photospheric radius  $R_{ph}$ , the "radio depth" will always be approximately equal to  $\alpha_\nu(R - R_{ph})$ . That is, the effective radio depth can never be greater than the optical depth. With these cautions in mind, equation 7.23

can be integrated by computer. The results of these integrations are plotted in figure 7.1 for varying values of  $\tau_0$  and  $\xi$  as  $R/R_0$  increases.

To model the temporal variability of the X-ray flux  $F(\nu_c)$ , we must determine the behavior of  $F(\nu_c)$  as a function of  $R$ . We first note that  $\lambda \propto R^{-n+2}$ , and that  $\Omega = 1 - \exp(-\tau_{opt})$ , where  $\tau_{opt} = \tau_0 (R_0/R)^2$ . Parameterizing equation 7.7 in terms of  $R$ , we then have

$$7.24 \quad F(\nu_c) = F_0(\nu_c) [1 - e^{-\tau_0 (R_0/R)^2}] \cdot \left(\frac{R_0}{R}\right) (T/T_0)^{3.5}$$

for  $q=0.5$  ( $n=2.0$ ). For an adiabatically expanding source ( $\tau \propto R^{-1}$ ). The X-ray flux as a monotonically decreasing function of plasma radius  $R$  is then given as

$$7.25 \quad F(\nu_c) = F_0(\nu_c) [1 - e^{-\tau_0 (R_0/R)^2}] \cdot \left(\frac{R_0}{R}\right)^4$$

It is possible, however, that the flaring observed in Cen A is representative of an explosive release of energy. Such an event could cause shock heating of the photosphere in a manner similar to that predicted by Falk and Arnett

(1977) for supernova explosions. After the increase from an initial quiescent temperature and corresponding rise in the X-ray flux, the shock heating is overcome by adiabatic expansion, and the X-ray flux decreases. The initial explosive energy release seems likely to be associated with the production of relativistic particles. The X-ray flux from an adiabatically expanding plasma is plotted in figure 7.2 as a solid line, along with the 2-6 keV X-ray data. In the plots, we have allowed the time of the expansion to start early in 1974. Varying the parameters in the theory changes the times of the radio peaks. In general, however, the single or multiple radio flares are produced for a wide range of the parameters. Thus, the flaring seems to be a ubiquitous occurrence for an expanding, optically thick plasma which contains relativistic electrons.

#### 7.1.2.5: Radio and X-ray Radiation from an Optically Thin Plasma within a Dense Association of Stars.

It is possible that the principal contribution to the energy density in thermal photons comes from stars in the galactic nucleus. For starlight to have an energy density greater than that of the plasma containing the relativistic particles, the plasma must be transparent to optical photons. For this optically thin case, the plasma will have a number density (particles  $\text{cm}^{-3}$ ) considerably less than that previously assumed. In such an environment, the

previous assumption of an optically thick photosphere with a uniform number density of electrons certainly does not apply. We assume that the number density of the plasma decreases radially. In this case, free-free absorption or suppression by the Razin-Tsytoich effect will limit the emission of synchrotron radiation to the volume beyond a certain radius, which we call  $r_R$ .

The Razin-Tsytoich effect suppresses synchrotron radiation below a frequency  $\nu_R = 20 (N_e/B)$ , where  $N_e$  is the electron number density of the plasma, and  $B$  is the value of the magnetic field in gauss. To calculate the radius  $r_R$ , we may assume a density distribution for the plasma and invert the function to obtain the value of  $r_R$  as a function of  $N_e$  and  $E$ . Thus, for

$$N_e(t) = N_{e_0}(t) \left[ \frac{1}{1 + (\frac{r}{R})^2} \right]$$

7.26

$$r_R = \zeta R \left[ \frac{20 N_{e_0}(t)}{\nu_{\text{obs}} B(t)} - 1 \right]^{1/2}$$

where  $\nu_{\text{obs}}$  is the observing frequency,  $N_e(t) = N_e(t=0) (R_0/R)^3$  is the density at  $r=0$  as a function of the radius  $R$  of the spherical plasma,  $R_0$  is the initial radius of the plasma,  $B$  is the magnetic field in gauss ( $B = B_0 (R_0/R)^2$ ), and  $\zeta$  is the parameter which represents the degree of central concentration of the optically thin plasma. Parameterizing equation 7.26 in terms of  $R$ , we find

$$7.27 \quad \frac{r_R}{R_0} = \zeta \frac{R}{R_0} \left[ \frac{20 N_0}{v_{\text{obs}} B_0} \left( \frac{R_0}{R} \right) - 1 \right]^{1/2}$$

For any physical situation,  $r_R$  is initially positive, and is set to zero if the value in the brackets becomes negative.

Equation 7.23 thus becomes

$$7.28 \quad L_\nu = 8\pi^2 \cdot \frac{j_{\nu 0}}{\alpha_\nu} \int_{r_R}^R f(r) [1 - e^{-\tau(r)}] \cdot r \cdot dr$$

where  $\alpha_\nu \gg 0$  because of the smaller electron density. The rather weak dependence of  $r_R$  on  $R$  does not "uncover" the plasma's relativistic electron distribution with sufficient alacrity to overcome the adiabatic expansion. Therefore, expansions of an optically thin plasma must be characterized by a monotonic decrease. There is also no expected correlation between the radio and X-ray data in this case, since the expansion of the plasma does not affect the energy density of the thermal photons.

### 7.1.3: Discussion

The lack of evidence for significant hardening in the X-ray power-law spectral index from mid 1974 through 1976 suggests that particle acceleration did not take place during that period. If this is the case, the double radio

flare can only be explained by the compact (optically thick) blackbody-Compton model. Additionally, the compact model provides an explanation for the manner in which the radio and X-ray fluxes track one another until the relative minimum in July 1975, and then separate.

The most common astrophysical environment that radiates as a hot ( $10^4$ K) blackbody is the photosphere of a star. The explosive nature of the recent flares in Cen A is, indeed, suggestive of supernova explosions. For the supernova hypothesis to be correct, however, young supernova must contain significant numbers of relativistic particles. The evidence is to the contrary.

Recent work by Marscher and Brown (1978) and Beall (1979) strongly suggests that relativistic particles are not contained in significant numbers in supernovae until a time as least 70 years after the initial explosion. It seems unlikely, therefore, that the direct source of the radio and X-ray variability we observe in Cen A (and other active galactic nuclei) is caused by supernova explosions. The multiple supernova model of Colgate (1967) seems unlikely, because it also suggests an optically thin case. Two other possibilities have been proposed.

Fabian et al. (1976) have suggested that quasi-spherical accretion onto a massive black hole would produce a photosphere with a radius  $r=10^{15}$  cm and a minimum temperature  $T=10^4$ K. Alternatively, Ozernoy (1972) has suggested that a "supermassive body" might be responsible for the energy output of active galactic nuclei. It is also possible that a combination of these two physical environments exists.

We wish to make a final comment about the possibility of neutrino production in an environment such as we have described. The combination of relativistic particles and a dense photosphere suggests the possibility that a significant flux of neutrinos may be produced by the decay of pions which are created from proton-proton interactions of the relativistic particles with the ambient material. Though we leave a detailed calculation of this flux to the future, it is possible that the neutrinos could be produced by active galactic nuclei in sufficient numbers to be detectable by currently available techniques of neutrino astronomy.

#### 7.1.4: Conclusions

The radio and X-ray variability from the nucleus of Cen A is suggestive of a dense ( $\sim 10^{10}$  particles  $\text{cm}^{-3}$ ), hot plasma which initially radiates as a  $10^4\text{K}$  blackbody. The radio variability is consistent with a partially opaque, expanding plasma. Of the three most thoroughly investigated models, multiple supernovae, a massive black hole, or a "supermassive body," only the latter two seem plausible. It is noted that the two are not mutually exclusive objects.

Upper limits on the energy in the recent outbursts are of the same order of magnitude as the energy release in supernovae explosions. Finally, upper limits for the energy in relativistic particles in the entire nucleus indicate that there may be sufficient energy to form another pair of radio lobes similar to the two already present.

#### 7.2: 3C273

##### 7.2.1: General Discussion

Qualitatively, the spectra of 3C273 and NGC 5128 are similar (see figures 3.7 and 4.3). The notable difference is the peak at 100 microns for Cen A, which is presumably due to thermal emission from dust. Because of the high luminosity of the non-thermal component in 3C273, such a feature, if present, may not be visible. It seems unlikely

that dust emission is the cause of the variable, power-law infrared source. At radio and far-infrared frequencies, the data available suggest that the spectrum of 3C273 from 1 to 100,000 GHz can be modelled as a single synchrotron source. A possible spectrum (dashed line) has been drawn through the data in figure 4.3. The turnover in the spectrum at approximately  $2 \times 10^{12}$  Hz is suggestive of synchrotron or inverse Compton losses for the power-law distribution of relativistic particles. This cutoff frequency gives the relationship between the magnetic field and the time in seconds since the injection of the particles into the source region. Pacholczyk (1970, equation 7.55) notes that

$$7.29 \quad \nu_t = 9.97 \times 10^{23} \frac{1}{B^3 t^2}$$

where  $t$  is the time in seconds since injection,  $B$  is the magnetic field in gauss, and  $\nu_t$  is the cutoff frequency in Hz. For 3C273,  $\nu_t$  is approximately  $1.8 \times 10^{12}$  Hz, giving

$$7.30 \quad t^2 B^3 = 5.6 \times 10^{11}$$

The radio flux decrease below 1 GHz with a power-law index approximately equal to 0.3. This is suggestive of a low energy cutoff in the distribution of relativistic particles. If this is the case, the relationship between the low frequency cutoff,  $\nu_l$ , the magnetic field B, and the electron energy,  $\gamma$ , (the ratio of the total electron energy over the rest mass- $E/mc^2$ ) is given by Pacholczyk (1970) as

$$7.31 \quad \nu_l \approx 4.11 \times 10^6 B \gamma^2$$

For a distribution of electrons stationary in time, a similar equation holds for the upper limit of a synchrotron spectrum.

The composite spectrum of 3C273, as well as recent observations by the IUE spacecraft (Boksenburg et al. 1978) suggest that a power-law continuum underlies the observed optical and ultraviolet flux. One possible spectrum has been drawn as a dashed line in figure 4.3. Though the data do not unequivocally yield the relative contributions of thermal, line, and continuum emissions, the general agreement between the values of the power-law spectral index in the far infrared, the ultraviolet, and at X-ray energies suggests that there may be some phenomenological connection

between the production mechanisms in these separate parts of the electromagnetic spectrum. This interpretation is also consistent with the interpretation by Pounds (1978) that the radio and X-ray fluxes tracked one another during the Ariel V observations. Assuming that the X-rays are produced by inverse Compton scattering of an ambient distribution of photons, we can model the radio and X-ray flux as we did for Centaurus A (see section 7.1). We reserve the discussion of the possible origin of the optical and ultraviolet continuum for later in this chapter.

#### 7.2.2: A Model for the Radio and X-ray Flux from 3C273

We suggest a model for the radio and X-ray flux for 3C273 where relativistic electrons produce the synchrotron spectrum which extended from radio wavelengths into the far infrared (see figure 4.3). The same relativistic electrons inverse Compton scatter ambient photons to produce the X-ray flux. In this model we assume that the electrons which radiate by synchrotron emission in the far infrared are mostly responsible for the inverse Compton scattering of ambient photons which produce the X-ray radiation. We can thus model the far infrared and X-ray data in a manner similar to that used for Cen A. Following that discussion, we find that  $F(\nu_c)/F(\nu_g) = 10^{-7}$ ,  $q=1$ , and (from equation 7.1)

$$7.32 \quad 4.96 \times 10^{13} = \Omega T^4 B^{-2}$$

For  $\Omega=1$ , and  $T=10^4 K$ ,  $B=14.2$  gauss. From equation 7.29, the cutoff in the synchrotron spectrum of  $2 \times 10^{12}$  Hz yields a lifetime for the synchrotron of  $1.4 \times 10^6$  seconds. Assuming a temperature of  $T=10^3 K$  implies  $B=1.4 \times 10^{-1}$  gauss. The time since injection of a power-law distribution of relativistic particles then becomes  $t=1.4 \times 10^7$  seconds. For the source to exhibit significant variability at frequencies greater than  $\nu_t$ , the timescale for synchrotron losses must be short compared to the frequency with which new particles are injected (or exposed) in the source region. Also, adiabatic expansion of the source and turbulent accelerations of relativistic particles on timescales short compared to the synchrotron (or inverse Compton) loss times can cause changes in the intensity of the synchrotron spectrum.

A lower bound to the range of  $\gamma$ 's in the source can be established by assuming the low-frequency radio cutoff represents a lower limit to the energy of the radiating particles. Equation 7.31 with  $T=10^4 K$  and  $B=14.2$  gauss, gives a lower limit for the electron energy of  $\gamma=10$ . The corresponding upper limit obtained by letting  $\nu_l = \nu_t$  in equation 7.31 has a value of  $\gamma=10^3$ . The break in the inverse Compton spectrum would be expected to occur at approximately  $10^{12}$  Hz. Assuming a temperature of  $10^3 K$ , the range of electron energies from  $\gamma=10^3$  to  $\gamma=10^4$ .

### 7.2.3: The Energy Contained in Relativistic Particles in 3C273

Given the range in the values of  $\gamma$ , we may estimate the total energy in relativistic particles in the source region. From figure 4.3, we find that  $F(\nu_0) = 10^{-30} \text{ ergs cm}^{-2} \text{ s}^{-1} \text{ Hz}^{-1}$  at  $\nu = 10^{10} \text{ Hz}$ . Combining this with equation 7.7, we find that

$$7.33 \quad 2.04 \times 10^{71} = A R^3 T^4$$

for  $\Omega=1$  and  $D=2.63 \times 10^{27} \text{ cm}$  (876 Mpc). If we assume  $T=10^4 \text{ K}$  and a range of  $\gamma$ 's from  $10^1$  to  $10^3$ , the total energy in relativistic particles is  $10^{51}$  ergs, and the number density of the radiating particles is  $10^5$  (assuming a source radius of 30 lt. days). For  $T=10^3 \text{ K}$  and  $\gamma$ 's ranging  $10^3$  to  $10^5$ , the total energy is  $10^{54}$  ergs, and the number density of radiating particles is  $10^8$ . The total energies are a factor of 1000 greater than the values calculated for Cen A using similar parameters.

### 7.2.4: A Discussion of the Optical and Ultraviolet Continuum.

The models of Celgate, Colvin, and Petschek (1975) and Katz (1976) can adequately account for the optical and ultraviolet continuum in 3C273. It is interesting to

consider, however, the possibility that a significant synchrotron-Compton flux can arise from a source such as 3C273. Assuming that the thermal-Compton model discussed in the previous section is responsible for the X-ray radiation, it seems reasonable to ask what form the synchrotron-Compton flux would take. Following Tucker (1976) we may construct the ratio of synchrotron-Compton flux to synchrotron flux  $F(\nu_{sc})/F(\nu_s)$  as

$$7.34 \quad \frac{F(\nu_{sc})}{F(\nu_s)} = \left[ \frac{1}{p} - \frac{2}{p+2} + \frac{1}{p+1} - \frac{2}{(p+1)^2} \right] \left( \frac{2.49 \times 10^{-25}}{1.67 \times 10^{-21}} \right) \nu_{sc}^{-q}$$

$$\cdot \frac{2^{n+2} A \left( \frac{D}{R} \right)^2 \int N(\gamma) \gamma^{n-1} d\gamma}{A a(n) B^{q+1} \left( \frac{6.27 \times 10^{10}}{\nu_s} \right)^q}$$

where  $p=q+1, n=2q+1, a(n)$  is derived from the synchrotron spectrum and is a function of the electron number spectrum's slope,  $B$  is the magnetic field,  $D$  is the distance to the source,  $R$  is the source radius, and  $q$  is the power-law spectral index of the synchrotron flux. In equation 7.34,  $A$  is determined from observations of the synchrotron flux and is obtained from the equation  $F(\nu_s) = A \nu^{-q}$ . For 3C273,  $A = 1 \times 10^{-10}$ ,  $F(\nu_{sc})/F(\nu_s) = 3 \times 10^{-3}$ , and  $(\nu_{sc}/\nu_s)^{-0.5} = 3.75 \times 10^{-3}$ . For  $n=2$  ( $q=0.5$ ),  $a(2) = 0.103$ , and equation 7.34 becomes

$$7.35 \quad 8.88 \times 10^{21} = R^2 B^{1.5}$$

The blackbody-Compton model previously discussed as a source of X-ray photons provides a second equation for the source, assuming that the radiations we see originate within the same volume. A further constraint can be placed on such a model by noting that the radio observations require that the synchrotron self-absorption turn-over frequency be less than  $10^{10}$  Hz. For 3C273, equation 7.4 yields the constraint that

$$7.36 \quad v_m^5 \leq 7.51 \times 10^{81} BR^{-4}$$

If we assume equation 7.36 is an equality, the three equations completely determine the value of  $\Omega T^4$  to be  $1.82 \times 10^3$ . If the dilution factor  $\Omega=1$ ,  $T=6.53K$ , which is rather close to the  $3^{\circ}K$  background radiation. If  $T=10^4K$ ,  $\Omega=10^{-13}$ , which is a dilution factor suggestive of starlight radiation in a galaxy. If the radio, optical, ultraviolet, and X-ray radiation all originate from a common source region, the preceding calculations suggest that the source environment is optically thin. This would seem plausible if the bulk motion of the radiating plasma were relativistic. In such a circumstance, the radiating particles could quickly leave the region in which they were accelerated. Some evidence for bulk relativistic motion of the radiating

particles is present in the optical jet associated with 3C273. The presence of observational evidence for only one jet may be due to the fact that another jet radiating preferentially in a different direction will not be seen. The actual physical environment in 3C273 may not be determined until concurrent radio, infrared, optical, ultraviolet, and X-ray measurements are performed which can set limits on the relative variability of the various portions of the electromagnetic spectrum. We have not attempted to model the gamma-ray emission of 3C273 as 2nd order Compton scattering.

## 7.3: NGC 4151

### 7.3.1: General Discussion

In common with most Seyfert galaxies, the composite spectrum of NGC 4151 (see figure 5.5) shows a relatively weak, constant radio source associated with the nuclear region. The radio flux is likely to be synchrotron radiation from an extended source. In view of the apparent lack of concurrent variability between the radio and X-ray radiation as discussed in chapter 5, it is likely that the relativistic electrons producing the observed radio flux are not directly associated with the X-ray producing region.

Oke and Sargent (1968) have suggested on the basis of optical and infrared measurements of NGC 4151 that the nucleus consists of two physically distinct regions: the first region has a number density of  $N=5 \times 10^3$  particles  $\text{cm}^{-3}$  and a temperature of  $2 \times 10^4 \text{K}$ . The mass of this region was estimated to be  $2 \times 10^5 M_{\odot}$  on the basis of emission line luminosities. According to Oke and Sargent, the first region fills approximately 2.5 percent of the total source volume, and is in the form of filaments in relative motion with respect to one another. The second region has an effective temperature  $T=10^6 \text{K}$ . The assumed density of 100 particles  $\text{cm}^{-3}$  would allow the hotter gas to be in pressure equilibrium with the  $2 \times 10^4$  gas. In the same paper, Oke and Sargent propose that the infrared spectrum (see figure 5.5) is due to synchrotron radiation, and that the turnover in the far-infrared is due to Razin-Tsytovich suppression.

In view of the flattening of the spectrum of NGC 4151 from the infrared into the optical region, it is possible that the optical and ultraviolet portion of the spectrum represent the contribution of an underlying power-law spectrum to the observed radiation. This conclusion is supported by recent observations of the IUE spacecraft (Boksenburg et al. 1978), which show a power-law spectrum.

There is some controversy over whether a power-law synchrotron spectrum can radiate at optical and ultraviolet frequencies. According to Hoyle, Burbidge, and Sargent (1966), a bright, compact synchrotron source which could radiate an optical and ultraviolet spectrum would suffer inverse-Compton losses that would limit the source lifetime to less than a second. They further note that such a source would show inverse-Compton emission at a much greater level than the synchrotron emission. Woltjer (1966) notes that the "inverse-Compton catastrophe" just mentioned can be overcome if the electron motion is anisotropic and does not make an angle with the magnetic field of greater than  $10^\circ$ . Katz (1975) suggests that it is possible to produce a power-law spectrum in the optical and ultraviolet region by upscattering of low energy photons by non-relativistic electrons. Colgate, Colven, and Petschek (1975) propose that the optical flux from quasars can be produced by upscattering of photons by oscillations of a turbulent plasma. They associate the turbulent plasma with colliding

supernova shock fronts. Unfortunately, the data do not place significant constraints on any of these models.

In a recent paper, Prichet (1977) notes that the physical environments in the nuclear bulges of morphologically distinct galaxies possess "quite similar" populations of stars. It seems plausible that the stellar distribution in a galactic nucleus contributes significantly to whatever non-thermal source may exist there. The contribution may take the form of supernovae, accretion material, formation of coalescing black holes, stellar winds, formation of supermassive stars, etc. This suggests that we look for models for the nuclear regions of the galaxies which incorporate similar features.

The line emission in the optical and ultraviolet, and the power-law continuum seem to be frequently observed in extragalactic sources (Boksenburg et al. 1978). This implies that the line emission and the continuum are produced by some associated mechanism. Otherwise, we would expect to see from source to source only a continuum or only line emission. If the region in which the line emission occurs surrounds the region in which the relativistic particles are accelerated, this condition is fulfilled. Optical synchrotron radiation may be produced in the line emitting region or in the accelerating region, assuming that the bulk motion of the relativistic electrons is anisotropic (Woltjer 1966). In this view, inverse-Compton scattering of

the optical, synchrotron photons or ambient, thermal photons may produce the X-ray flux. It is also possible that the optical and ultraviolet continuum is produced by inverse-Compton scattering of synchrotron radiation which extends into the far infrared data. Of course, this spectrum is unobservable to us. The observations which may unequivocally limit the possible models have not yet been made.

### 7.3.2: A Model for the X-ray Flux from NGC 4151

We model the X-ray radiation as inverse-Compton scattering of an ambient distribution of thermal photons by relativistic electrons in the source region. Assuming that the source has the same approximate distribution of relativistic electrons as that calculated for the other galactic nuclei, equation 7.7 becomes

$$7.37 \quad F(\nu_c) = (3.28 \times 10^{-86}) \Omega_A R^3 T^{3.5} \nu^{-.5}$$

In equation 7.37, we have taken  $D=5.7 \times 10^{25}$  cm (19Mpc). The X-ray data at  $10^{18}$  Hz yield a value of  $F(\nu_c) = 3 \times 10^{-28}$  ergs  $\text{cm}^{-2} \text{s}^{-1} \text{Hz}^{-1}$ . Therefore, equation 7.37 becomes

$$7.38 \quad 9.15 \times 10^{66} = \Omega_A R^3 T^{3.5}$$

If we assume  $\Omega=1$ ,  $T=10^3 K$ , and  $R=1$  lt. day, then  $A=5.27 \times 10^{10}$ , where  $A$  is the normalization constant for the number spectrum of the power-law distribution of relativistic electrons. For  $T=10^4 K$ , and  $R=1$  lt.day,  $A=5.27 \times 10^6$ . The value of  $A$  is proportional to the number density of relativistic electrons, and can thus be compared to the values obtained when using the model on other sources. In Cen A, for example,  $AR^3 T^{3.5} = 6.34 \times 10^6$ . Thus, the energy in relativistic particles in the nucleus of NGC 4151 is approximately 15 times greater than that for Centaurus A, assuming similar models for the source.

#### 7.4: The Galactic Center

##### 7.4.1: General discussion

The general character of the radiation from the nucleus of the Milky Way Galaxy is remarkably similar to that observed in NGC 4151. The principal difference is the absolute intensity of the radiation. This can be seen by comparing figures 5.5 and 6.5. There is a relatively sharp peak in the infrared emission at  $10^{13}$  GHz in the Galactic Center. The relatively broadened feature in NGC 4151 may possibly be due to the greater heating of gas and dust in NGC 4151 by the non-thermal source.

#### 7.4.2: A Model for the X-ray Emission from GCX

The qualitative similarity between the spectra for GCX and NGC 4151 may imply some morphological similarity. This will be discussed in more detail in Chapter 8. We may model the X-ray emission from the Galactic Nucleus as a thermal-Compton process in a manner akin to that previously discussed for NGC 4151. Assuming  $q=0.5$ , we find that equation 7.24 becomes

$$7.39 \quad F(\nu_c) = (1.18 \times 10^{-79}) \Omega A R^3 T^{3.5} \nu^{-.5}$$

Using the observed value of the X-ray flux for the 1976 observation, equation 7.39 becomes

$$7.40 \quad \Omega A R^3 T^{3.5} = 8.45 \times 10^{64}$$

For  $T=10^3 K$ , and  $R=1$  lt. day,  $A=1.54 \times 10^8$ . Assuming that  $T=10^4 K$ ,  $A=4.86 \times 10^4$ . These values represent a decrease from those obtained for NGC 4151 by a factor of  $10^3$ .

## CHAPTER 8: DISCUSSION

### 8.1: The Thermal Source in a Galactic Nucleus

A source with a radius of  $10^{15}$  to  $10^{17}$  cm which emits blackbody radiation with an effective temperature of  $10^3$  to  $10^4$  K will have an extremely high luminosity. The luminosity,  $L$ , in ergs  $s^{-1}$ , of such an object is given as (equation 7.17)

$$L = 4\pi R^2 \Omega \sigma T^4$$

where  $\sigma$  is the Stefan-Boltzmann constant,  $R$  is the source radius,  $T$  is the effective temperature, and  $\Omega$  is the dilution factor to account for a greybody approximation. Using figures 3.7, 4.3, 5.5, and 6.5 for Cen A, 3C273, NGC 4151, and GCX, respectively, we have estimated the optical and infrared luminosities of the sources. Felten and Gould (1977) and Felten (1978) have suggested that we may use these luminosities along with equation 7.17 to place constraints on the physical size and temperature of plasma, assuming  $\Omega=1$ .

The infrared and optical luminosities for those sources not obscured by dust are approximately equal.

The infrared or optical luminosities in units of  $\text{ergs s}^{-1}$  are as follows:

Cen A----- $10^{42}$

3C273----- $10^{46}$

NGC 4151--- $10^{44}$

GCX----- $10^{40}$

In these estimates, we note that for some of the sources (Cen A, GCX, and possibly NGC 4151) the radiation from the assumed blackbody source in the center of the emitting region may be re-radiated by dust surrounding the primary source.

Equation 7.17 can now be used to place limits on the blackbody radiators used previously as sources of ambient photons inverse Compton scattered to produce X-ray radiation. Thus, for Cen A,  $R^3 \Omega T^4 < 2.81 \times 10^{45}$ . The assumption that  $T = 10^4 \text{K}$  implies a source radius  $R < 5.3 \times 10^{14} \text{cm}$ . For  $T < 10^3 \text{K}$ ,  $R < 5.3 \times 10^{16} \text{cm}$ . We may determine another relationship between the source radius and the temperature using equations 7.3 and 7.4. Combining this result with equation 7.17, and with the infrared flux measured by Harper (1977) we derive an upper limit on the temperature of the blackbody radiator of  $3 \times 10^3 \text{K}$ . The infrared and optical luminosities for other sources do not significantly constrain the parameters for models of the emitting regions.

Even for Cen A, we note that the constraint is significant only if the luminosity of the spherical plasma

is constant over time. For an expanding plasma which we consider here, the time-averaged luminosity is the important parameter, since re-radiation of the optical photons by the intervening dust will smooth any fluctuations that are present. Thus, for the nucleus of Cen A, recurrent injection of dynamically expanding plasmons is not constrained by the limits derived for the source by the infrared observations.

## 8.2: The Composite Spectra of the Sources Observed

We now compare the order-of-magnitude luminosities (in  $\text{ergs s}^{-1}$ ) of the radio, infrared, optical, and X-ray data for the four sources. Using figures 3.7, 4.3, 5.5, and 6.5, we note that:

Source	Luminosity			
	Radio	Infrared	Optical	X-ray
Cen A	$10^{41}$	$10^{42}$	$10^{41}$	$10^{41}$
3C273	$10^{45}-10^{46}$	$10^{46}$	$10^{46}$	$10^{45}$
NGC 4151	$10^{38}$	$10^{43}$	$10^{43}-10^{44}$	$10^{43}$
GCX	$10^{34}$	$10^{40}$	$10^{37}$	$10^{38}$

We note that the composite spectrum of Cen A and of 3C273 have roughly uniform luminosities over the entire electromagnetic spectrum. This is not the case for NGC 4151 and GCX which have radio luminosities significantly weaker than the flux at other wavelengths. Additionally, the radio sources in the nucleus of Cen A and in 3C273 are markedly variable.

Based on these considerations, we suggest that the elliptical galaxy, NGC 5128 (Cen A), and the quasar, 3C273, be paired as having similar source morphologies. This is contrary to the commonly assumed association between Seyfert galaxies and quasars. The data also show similarities between the composite spectra of the Seyfert galaxy, NGC 4151, and the Galactic Center (GCX).

As previously mentioned, Prichett (1977) has reported that the nuclear bulges of morphologically distinct galaxies possess similar distributions of stars. If the general character of the nuclear environment is determined by the bulk properties of the nuclear region, the similarities which we note between the composite spectra presented here are not surprising.

### 8.3: General Remarks

From the data available, it is not possible to determine, unequivocally, a model for the production of electromagnetic radiation in galactic nuclei. It is possible, however, to develop a consistent model for the nuclear regions of the four sources which have been observed. In the model discussed in Chapter 7, relativistic particles inverse Compton scatter photons to produce the X-ray radiation.

The data for Cen A are consistent with a thermal-Compton model in which the ambient distribution of photons is principally that emitted by a hot, expanding plasma. In

this view, the expanding plasma becomes optically thin (see Chapter 7 for a further discussion) during 1975.

Applying the model developed for Centaurus A to the other sources discussed yields a consistent picture for the X-ray production. The ultraviolet, optical, and near-infrared continuum may be adequately explained by upscattering of optical photons by non-relativistic electrons in the source (Katz 1977). Alternatively, it is possible to model the infrared-optical-ultraviolet continuum as synchrotron-Compton emission. If the synchrotron-Compton radiation comes from the same region as the X-ray radiation, the temperature of the blackbody photon distribution can be determined uniquely. For 3C273, this temperature is on the order of 6K. This value of the effective temperature suggests that the principal source of photons may come from a combination of starlight and the background 3K blackbody radiation. If this is indeed the case, the relativistic particles producing the observed radiation must have left the dense region in which they were accelerated.

For a common ground to exist between the source environments in Cen A, 3C273, NGC 4151, and GCX, there must be some mechanism which suppresses or absorbs the radio emission from the nucleus of NGC 4151 and the Milky Way.

#### 8.4: Fossible Sources of Relativistic Particles

##### Produced in a Galactic Nucleus

There are several processes which may occur in the dense environment of a galactic nucleus that could lead to the acceleration of particles to relativistic energies. Reviews of the likely source mechanisms are presented in Ozernoy (1974) and Rees (1977). The sources of relativistic particles may include shock fronts from multiple supernovae, accretion onto a massive black hole, and super-massive stars (variously called spinars, magnetoplasmic bodies, etc.). Recently, Bell (1978), and Blanford and Ostriker (1978) have postulated that relativistic particles can be accelerated by plasma waves in supernovae shock fronts as the shocks interact with the interstellar medium. This process, or turbulent acceleration as suggested by Pacholczyk and Scott (1976), may also account for the production of relativistic particles in a galactic nucleus.

#### 8.5: A Possible Distinction Between the Physical

##### Environments in Radio-Quiet and Radio-Bright

##### Galactic Nuclei

The lack of radio emission in some galactic nuclei may be due to suppression by various processes or simply to the lack of a sufficiently strong magnetic field to cause significant synchrotron radiation. Directed motion of the relativistic particles along "ordered" magnetic field lines is also a possible explanation for weak radio emission.

It is interesting to speculate that the distinction between radio-bright galactic nuclei and those that are relatively quiescent may be due to some large-scale property of the nuclear system, such as angular momentum. Such a distinction is suggested, in part, by the relatively weak radio emission associated with most Seyfert galaxies and the galactic center region of the Milky Way.

If the nucleus of a galaxy has significant net angular momentum, the system is likely to collapse into a disc. The disc, when formed, may be stable against further collapse. For an elliptical galaxy, which is likely to have less net angular momentum in its nuclear region, the collapsing material may not produce an appreciably flattened disc. If this is the case, the stability of the system against further collapse is likely to depend on many factors, including the rate of coalescence, the composition of the material, the luminosity of the associated stars, etc. In such an environment, it is possible that the turbulence associated with the contraction (or accretion) of the material may generate magnetic fields by a dynamo process. In such a disordered environment, the magnetic field is also likely to be highly disordered. This is contrary to the situation in most spiral galaxies, where the bulk motion of the accreting (or contracting) material is assumed to define some preferred angular momentum vector.

## CONCLUSIONS

There is a considerable similarity between the emission of quasar, 3C273, and the elliptical galaxy, Centaurus A (NGC 5128), and between the Seyfert galaxy, NGC 4151, and the nucleus of the Milky Way. The principal distinction is the difference in absolute luminosity between sources. The two spiral galaxies studied (NGC 4151 and the Milky Way) have a relatively low ratio of radio to non-radio luminosities when compared to similar ratios for the spectra of Cen A and 3C273.

Studies of the variability of NGC 5128 (Cen A) and NGC 4151 indicate a connection between the radio and X-ray radiation only in Cen A, based on the in-phase variability of the radio and X-ray fluxes on timescales of days to years. In NGC 4151, such a correlation between the radio and X-ray fluxes does not occur. This is concluded both from observations of X-ray variability during times when no change in the radio flux is detected, and from the fact that the radio spectrum shows no low-frequency cutoff. The lack of such a cutoff indicates that the radio emission comes from an extended region, and may not be associated with the compact X-ray source which varies on timescales of days. Correlation between the variability of the optical/ultraviolet and X-ray fluxes is predicted by the model, but lack of coverage prevents this correlation from being demonstrated.

The radio data suggest that there are two distinct classes of radio sources in the sample of four sources observed. However, in view of the similarity between other portions of the composite spectra of the four sources, the difference at radio frequencies may be due to a detail of the emission mechanism and may not be fundamental to the source regions which produce the relativistic particles. The similarities between the physical environments in the nuclei of "morphologically distinct" galaxies has already been pointed out by Prichett (1977). Weedman and Stein (1977) note the similarities between the properties of Seyfert nuclei and quasars. The extrapolation of Seyfert luminosity-verses-distance plots to include quasars is also well known (Weedman 1977).

In view of these similarities and the similarities between the composite spectra of the four sources studied here, it is possible that the nuclear regions of all galaxies contain an active region which differs from others only in magnitude. In this view, radio-bright and radio-quiet quasars may represent emission during past epochs of the nuclei of elliptical and Seyfert galaxies, respectively.

It is appropriate to make a final comment about the technique of "multiple-wavelength" astronomy. Though a considerable amount of effort is required to arrange the concurrent observations, the technique is invaluable in

placing constraints on models for sources which radiate over a large portion of the electromagnetic spectrum. Clearly, it may not be necessary to observe all individual sources concurrently in every frequency band of the electromagnetic spectrum. If a source does not exhibit variability in one portion of the electromagnetic spectrum, concurrent observations in that frequency range are not crucial. Because of this, we suggest that Seyfert galaxies and radio-quiet quasars may most profitably be studied by concurrent observations at infrared, optical, ultraviolet, X-ray, and gamma-ray frequencies, while elliptical galaxies and radio-bright quasars require observations at radio, X-ray, and gamma-ray frequencies. For elliptical galaxies and radio-bright quasars, the utility of concurrent infrared, optical, and ultraviolet observations will depend on a lack of obscuring dust in the nuclear region.

Additional systematic observations of the sources discussed (as well as other representatives of their classes) will undoubtedly provide a further basis for understanding the most luminous objects in our universe.

## APPENDIX A

### A.1: Mechanisms of energy loss for X-rays:

A beam of photons passing through an attenuating medium will decrease in intensity in a way that is proportional to the absorption coefficient of the material and the intensity of the beam. This can be expressed as

$$A.1 \quad \frac{dN}{N} = -\mu dx$$

where  $N$  is the number of photons, and  $\mu$  is the mass absorption coefficient (in  $\text{cm}^{-1}\text{g}^{-1}$ ) times the density ( $\text{g cm}^{-3}$ ) of the material. The solution to this equation is

$$A.2 \quad N(x) = N_0 e^{-\mu x}$$

For composite materials, the mass absorption coefficient is the sum of the individual mass absorption coefficients weighted by the fraction of the total mass of each element. X-ray photons interact with matter by three principal processes: Photoelectric effect, Compton scattering, and Pair Production. We will briefly discuss each of these in turn.

#### A.1: The Photoelectric effect:

The energy of a photon incident on an atom may be completely absorbed by the atom, leaving the atom in an

excited or ionized state. The spectrometer crystal is cesium iodide, and the minimum energy required to ionize these elements is less than 15 eV. Even the most tightly bound electrons (i.e. electrons in the K-shell) can be ejected by 30 keV photons. Immediately above the ionization energy for each shell, the attenuation coefficient falls off as  $E^{-g}$ , where  $g$  has a range of 1 to 3. Atoms in the crystal may retain some of the energy and emit Auger electrons by radiativeless de-excitation. The atoms may also fill shells at higher levels and subsequently emit photons with a maximum energy of 30 keV. These transitions are usually L to K.

Photons produced by transitions into the K-shell have energies slightly less than 30 keV. The crystal is more transparent to these photons. As a result, the emitted photons may escape the crystal. The probability of detection of a K-escape event is given by Riegler (1969) as 27 percent at 30 keV, and 5 percent at 100 keV for an infinitely thick absorber. In all other cases, the energy absorbed by the detector crystal is proportional to the incident X-ray energy.

#### A.2: Compton scattering:

For energies much greater than those necessary to ionize the atom, the photon wavelength becomes very much less than the diameter of the atom. At these energies, Compton

scattering becomes an important mechanism for the attenuation of the incident X-rays (it is somewhat ironic that the inverse Compton mechanism is responsible for the production of the X-rays we see from certain sources-see chapter 4). The total energy given to the electron by a single Compton collision in the electron rest frame is

$$A.3 \quad \epsilon_1 = \frac{\epsilon}{1 + \frac{\epsilon}{m_e c^2} (1 - \cos \theta)}$$

where  $\epsilon$  is the initial photon energy, and  $m_e c^2$  is the rest energy of the electron. The maximum energy is gained by the electron when  $\theta = 180^\circ$ . For a photon with an energy of 100 keV, the recoil electron can have a maximum energy of 28 keV. For a photon energy of 1 MeV, the recoil electron's maximum energy is 800 keV. Therefore, a monochromatic beam of X-rays directed into the crystal will produce electrons with energies up to these limits. This maximum is called the Compton edge.

### A.3: Pair production:

As the photon energy increases, the cross sections for photoelectric absorption and Compton scattering decrease. As the photon energy increases above 1.02 MeV (twice the rest energy of an electron), pair production becomes possible and at higher energies this process becomes the dominant energy loss mechanism. In pair production, which

can take place only in an electric or magnetic field, the total gamma-ray energy is converted into a positron and an electron and their shared kinetic energy. In normal matter, the pair production takes place in the electric field close to the nucleus of the atoms. For cesium iodide, pair production becomes the dominant mechanism when the photon energy exceeds 6 MeV.

After the positron-electron pair is produced, they may lose energy by bremsstrahlung. Bound-free electronic transitions are also possible. Additionally, the positron will eventually annihilate, producing two 0.511 MeV photons, which may escape the crystal or interact in the aforementioned fashions. The energy deposited in the crystal by Compton interactions is complex.

#### A.4: Production of scintillation light:

The presence of sodium ions in the cesium iodide crystals, along with the normal imperfections, produce energy levels between the valence band and the conduction band. The energy levels between the conduction and valence bands are likely to be populated in a crystal exposed to X-ray radiation. The resultant transitions to the ground states are accompanied by photon emission. The total light intensity thus produced is proportional to the amount of energy deposited in the crystal by the incident X-rays.

The scintillation light is collected by photomultiplier tubes, whose outputs are proportional to the scintillation light in the crystal. The amplitude of the output pulse from the photomultiplier is thus proportional to the energy deposited in the crystal by the incident X-ray photon.

## APPENDIX B

### Expressing a Position on the Celestial Sphere as a Vector in the Local Coordinate System

We now wish to find a method of expressing a position on the sky (that is, a vector in the celestial coordinate system) as a vector in the local coordinate system just defined. This may be done using rotation matrices (Goldstein 1965, Chapter 4).

Given the RA and Dec of a source, we construct a unit vector which is co-linear with the position vector of the source in Celestial Coordinates. This unit vector may arbitrarily be chosen as the Z-axis of a source coordinate system as described previously for the local coordinate system. For purposes of consistency, we also choose an X-axis for the source to be local east, and a Y-axis to be local north. In this coordinate system, the position vector of the source is  $(0,0,1)$ .

To align the source X-axis with that of the celestial sphere, we rotate about the source X-axis by an angle  $-(90-\delta_s)$ , where  $\delta_s$  is the source declination. We then rotate about the new Z-axis by an angle  $(\alpha_s - \alpha_l)$  to place the two Y-axes in the same plane. The third rotation about the new X-axis by  $(90-\delta_l)$  yields a vector for the source in terms of the local coordinate system.

In principle, the procedure is quite simple. In analytical form, the combination of three rotation matrices

is remarkably cumbersome. Fortunately, the rotations can be performed by the computers used to analyze the data. It should be noted that any vector expressed in terms of right ascension and declination can be transformed in the preceding manner to a vector of a local coordinate system. Symbolically, the rotations are expressed as follows (Goldstein 1950):

$$V_{\ell} = [R_x(90-\delta_{\ell}) \cdot R_z(\alpha_s - \alpha_{\ell}) \cdot R_x(-90 + \delta_s)] \cdot V_s$$

B.4

where

$$R_x = \begin{pmatrix} 1 & 0 & 0 \\ 0 & \cos \theta & \sin \theta \\ 0 & -\sin \theta & \cos \theta \end{pmatrix} \quad \text{and} \quad R_z = \begin{pmatrix} \cos \theta & \sin \theta & 0 \\ -\sin \theta & \cos \theta & 0 \\ 0 & 0 & 1 \end{pmatrix}$$

The position vector of the source is taken to be the x and y component of the original vector  $V_s$  as transformed into the local coordinate system. The technique does not preserve arc length. However, for skymaps  $20^{\circ} \times 20^{\circ}$  in extent, the error induced by this approximation is  $< 0.5\%$ .

## APPENDIX C

### The Distribution of Stars in a Galactic Nucleus

Population I distributions of stars in a galaxy have a large aggregate angular momentum. Because of this, the Population I stars do not readily lose angular momentum by gravitational interactions. It is probable, therefore, that the distribution of stars in the region close to the center of a galaxy mimics the distribution of Population II stars, and is spherically symmetric. If the galaxy is elliptical, then the majority of stars share in this spherically symmetric distribution.

Using this spherically symmetric distribution of stars in a galactic nucleus, we may calculate the dilution factor  $\Omega$ , the ratio of the area of the sky subtended by stars to the total area of the sky. The dilution factor is the fraction by which the energy density for starlight photons is reduced over that within a blackbody at the same temperature as the stars. For a shell of stars of average radius  $r_*$  and number density  $\rho(r)$  (stars  $\text{cm}^{-3}$ ) at a distance  $r$  from the observer, the ratio  $d\Omega$  becomes

$$\text{C.1} \quad d\Omega = \pi r_*^2 \rho(r) dr$$

Assuming a gaussian distribution of stars,  $\rho(r) = \rho_0 \exp(-r^2/2R^2)$ , where  $\rho$  is the central density of stars and  $R$  is the radius within which the number density of stars decreases to 60 percent of the central density. The probability that the discs of stars overlap one another is small. Integrating the resultant equation from zero to infinity yields;

$$C.2 \quad \Omega = \pi \sqrt{\frac{\pi}{2}} r_*^2 \rho_0 R_s$$

This dilution factor is less than one for any physical situation. The energy density of the photons from the gaussian distribution of stars is then equal to  $\Omega a T^4$  at the center of the galaxy, where  $a$  is the first radiation constant, and  $T$  is the average surface temperature of the stars in the distribution.

We may modify equation C.2 in the following way. The total number of stars in the galactic nucleus (or any gaussian distribution of stars) is

$$C.3 \quad N = \int 4\pi r^2 \rho(r) dr = \sqrt{\frac{\pi}{2}} 4\pi R_s^3 \rho_0$$

By combining this with equation C.2, we find that

C.4

$$\Omega = \frac{r_*^2 N}{4R_s^2}$$

To gain some intuition of the magnitudes involved for various galactic nuclei, we may use Centaurus A as an example. Recent observations of a flux of approximately 150 Jy at 100 microns (Harper 1978) can be used to place an upper limit on  $N$ , the total number of stars in the nucleus of Cen A. If all the stars are of solar luminosity, then the maximum number of stars is  $10^{10}$ . For red giants, whose luminosity is  $100L_\odot$ , the maximum number of stars is  $10^8$ . If supergiant stars are responsible for the blackbody photons inverse-Compton scattered to produce the observed X-ray radiation, then the luminosity argument implies that there are a maximum of  $10^6$  of these stars in Cen A's nucleus. Assuming a luminosity class of stars also implies an average stellar radius. We thus obtain a relationship between the radius of the stellar distribution  $R$  and the dilution factor  $\Omega$ . For the blackbody-Compton mechanism to be the dominant inverse-Compton loss mechanism, the energy density  $U = 0.04T^4$  for the blackbody radiation must be greater than the energy density of the synchrotron radiation. This is discussed in detail in Chapter 7. If, for example, the dilution factor  $\Omega = 10^{-5}$ ,  $r_* = 10^{12} \text{cm}$ , and  $N = 10^6$ , then  $R$  must be roughly  $3 \times 10^{17} \text{cm}$ . Whether such a dense cluster of stars can be stable against dynamical collapse needs to be investigated.

In the paper by Spitzer and Hart (1971), it is suggested that globular clusters with several mass components of stars would stratify in a time

$$C.5 \quad t \approx \frac{.9R_h^{\frac{3}{2}} N^{\frac{1}{2}}}{M_s^{\frac{1}{2}} \log(.4N)} \times 10^6 \text{ years}$$

where  $R_h$  is the radius of the distribution in parsecs, and  $M_s$  is the mass of the stars in the distribution. The most massive stars would have the most centrally condensed distribution. After the initial condensation, the dense nucleus may experience a more protracted evolution due to the lack of lighter stars to carry away any more angular momentum from the central system. Although the calculations of Spitzer and Hart were done for less massive distributions of stars (in globular clusters), their work suggests that for the nucleus of Centaurus A, a centrally condensed distribution of massive stars will form in a timescale of  $10^5$  years. Thereafter, the limiting timescale for further collapse may be the nuclear lifetime of the stars, since mass loss by individual stars may, at that point, be the primary means of loss of angular momentum. In view of the  $R^{-2}$  dependence of the

dilution factor upon the stellar distribution, this central, massive population is the only one we will use in estimating the dilution factor used in Chapter 7.

## BIBLIOGRAPHY

- Andrew, B.H., MacLeod, J.M., Harvey, G.A., and Mehd, W.J., 1978, A.J., 83, 863.
- Auriemma, G., Angeloni, L., Belli, B.M., Bernadi, A., Cardini, D., Costa, E., Emanuele, A., Giovannelli, P., and Ubertini, P., 1978, Ap.J. (Letters), 221, L7.
- Baity, W.A., Jones, T.W., Wheaton, W.A., and Peterson, L.E., 1975, Ap.J. (Letters), 199, L5.
- Balick, B. and Brown, R.L., 1974, Ap.J., 194, 265.
- Balick, B. and Sanders, R.H., 1974, Ap.J., 191, 325.
- Beall, J.E., 1979, Ap. J. (to be published).
- Beall, J.H., Rose, W.K., Graf, W., Frice, K.M., Dent, W.A., Hobbs, R.W., Conklin, E.K., Ulich, B.L., Dennis, B.R., Crannell, C.J., Dolan, J.F., Frost, K.J., and Orwig, L.E., 1978, Ap.J., 219, 738.
- Becklin, E.E., Frogel, J.A., Kleinmann, D.E., Neugebauer, G., Ney, E.F., and Strecker, D.W., 1971, Ap.J. (Letters), 190, L15.
- Becklin, E.E., Mathews, K., Neugebauer, G., and Willner, S.P., 1976, Ap.J., 219, 121.
- Becklin, E.E. and Neugebauer, G., 1968, Ap.J., 151, 145.  
, 1975, Ap.J. (Letters), 200, L71.
- Bell, R., 1978, M.N.R.A.S.
- Bennett, K., Penengo, P., Rochester, G.K., Sanderson, T.R., Sood, E.K., 1972, Nature, 238, 31.
- Boldt, E., Doong, H., Serlemitsos, F., and Riegler, G., 1968, Canadian Journal of Physics, 44, 444.

Birks, J.E., 1964, (the MacMillan Company: New York).  
 Bowyer, S.C., Lampton, M., Mack, J., de Mendonca, F., 1970,  
 Ap. J. (Letters), 161, L1.  
 Bracewell, R.N., Colvin, R.S., D'Addario, L.F., Grebenkemper,  
 C.J., Price, K.M., and Thompson, A.R., 1973, Proc. IEEE, 61, 1249.  
 Burbidge, G.A., Burbidge, E.M., and Sandage, A.P., 1963,  
 Rev. Mod. Phys., 35, 947.  
 McCracken, K.G., Thomas, R.W., 1968, Nature, 219, 1124.  
 Chandrasekhar, S., 1964, Phys. Rev. Letters, 12, 114.  
 Coe, M.J., 1978, private communication.  
 Cclgate, S.A., 1967, Ap. J., 150, 163.  
 Cella, G., Fanti, C., Fanti, R., Gioia, I., Lari, C.,  
 Lequeux, J., Lucas, R., Ulrich, M.-H., 1975, Astr. and Ap.,  
 38, 205.  
 Condon, J. and Dressel, L., 1978, private communication.  
 Crane P., 1978, Ph.D. Thesis, MIT.  
 Cruddace, R.G., Fritz, G., Shulman, S., Friedman, H., McKee, J.,  
 Johnson, M., 1978, Ap.J. (Letters), 222, L95.  
 Davidsen, A.F., Hartig, G.F., Pastie, W.G., 1977, Nature, 269, 203.  
 Davies, R.D., Walsh, D., Erowne, I.W.A., Edwards, M.A., Noble, R.G.,  
 1976, Nature, 261, 476.  
 Eyles, C.J., Skinner, G.K., Willmore, A.P., Rosenberg, F.D.,  
 1975, Nature, 257, 291.  
 Davison, P.J.N., Culhane, J.L., Mitchell, R.J., and Fabian, A.C.,  
 1975, Ap. J. (Letters), 196, L23.  
 de Bruyn, A.G. and Willis, A.G., 1974, Astron. and Ap., 33, 351.  
 Dennis, B.R., Frost, K.J., Lencho, R.J., and Orwig, L.E., 1977,

- Space Sci, Instrumentation, 3,325.
- Dennis, B.R., Maurer, G.S., Cutler, E.P., Crannell, C.J.,  
Dclar, J.F., Frost, K.J., and Orwig, L.E., 1979, NASA Technical  
Memorandum 79559.
- Dent, W. and Hobbs, R., 1973, A.J., 78, 163.
- Dent, W.A. and Kapitzky, J.E., 1976, A.J., 81, 1053.
- Dclan, J.F., 1972, Ap. and Sp. Sci., 17, 472.
- Dclan, J.F., Crannell, C.J., Dennis, B.R., Frost, K.J., Orwig, L.E.,  
1978, preprint, NASA Technical Memorandum No. 79626.
- Dolan, J.F., Crannell, C.J., Dennis, B.R., Orwig, L.E., Maurer, G.S.,  
and Frost, K.J., 1977, Ap.J., 217, 809.
- Eyer, C.S., Coe, M.J. Engel, R.A., Quenby, J.T., 1978, preprint.
- Fakian, A.C., Maccagni, D., Rees, J.J., and Stoeger, W.R., 1976,  
Nature, 260,683.
- Falk, W.W., and Arnett, D.W., 1977, Ap. J. Supplement, 33, 515.
- Felten, J.E., 1978, private communication.
- Felten, J.E., and Gould, R., 1977, private communication.
- Felten, J.E., and Morrison, E., 1966, Ap. J., 146, 686.
- Fichtel, C., Kniffen, D., Thompson, D., 1976, private communication.
- Fisher, F.C., Jordan, W.C., Meyeroff, A.J., Acton, L.W., and  
Boethig, D.T., 1968, Ap.J., 151, 1.
- Fogarty, W.G. and Schuch, N.J., 1975, Nature, 254, 124.
- Fowler, W.A., 1964, Rev. Mod. Phys., 36, 545.
- Friedman, H., Byram, E.T., and Chubb, T.A., 1967, Science, 156, 374.
- Gatley, I., Becklin, E.E., Werner, M.W., Harper, D.A., 1978,  
Ap.J., 220, 822.
- Ginzburg, V. and Syrovatskii, S., 1965, Ann. Rev. Astr. Ap., 3,297.

- Grasdalen, G.L., 1976, Ap. J. (Letters), 208, L11.
- Grasdalen, G.L., and Joyce, F.R., 1976, Ap.J., 208, 317.
- Grindlay, J.E., Helsken, H.F., Hanbury-Brown, R., Davis, J. and  
Allen, L.E., 1975a, Ap.J. (Letters), 197, L9.
- Grindlay, J.E., Schnopper, M., Schreier, E.J., Gursky, H.,  
and Farsingault, D.R., 1975b, Ap. J. (Letters), 201, L133.
- Gursky, H., Gorenstein, P., and Giacconi, R., 1967, Ap.J. (Letters),  
150, L75.
- Gursky, H., Kellogg, E.M., Leong, C., Tananbaum, H.,  
Giacconi, R., 1971, Ap.J. (Letters), 165, L43.
- Hall, B.D., Meegan, C.A., Walraven, G.D., Djuth, F.T.,  
Harper, 1978, private communication.
- Haynes, R.C., 1976, Ap.J., 210, 631.
- Haynes, R.C., Ellis, D.V., Fishman, G.J., Glenn, S.W.,  
and Kurfess, J.D., 1969, Ap.J. (Letters), 155, L31.
- Haynes, R.C., Walraven, G.D., Meegan, C.A., Hall, B.D.,  
Djuth, F.T., and Shelton, D.J., 1975, Ap.J., 201, 593.
- Hjellming, R.M., 1973, An Introduction to the NRAO Interferometer  
(Greenbank, W.Va.: National Radio Astronomy Observatory).
- Hobbs, B.W., 1978, private communication.
- Hobbs, B., and Dent, W., A.J., 82, 21.
- Hcyle, F., and Fowler, W.A., 1963, M.N.R.A.S., 125, 169.
- Ives, J.C., Sanford, P.W., and Penston, M.V., 1976, Ap.J.  
(Letters), 207, L159.
- Jeans, J. H., 1929, Astronomy and Cosmogony, P.352 (Cambridge U. Press).
- Jernigan, J.G., Apparao, K.M.V., Bradt, H.V., Doxsey, R.E.,  
Dower, R.G., McClintock, J.E., 1978, Nature, 272, 701.

Kaufmann, P. and Beall, J.H., 1979, to be published in Astr. and Ap.  
Kaufmann, P., Scalise, Jr., E., Raffaelli, J.C., and  
Marques des Santos, F., 1978, preprint.  
Kellermann, K.I., and Pauliny-Toth, I.I.K., 1968, Ann. Rev.  
Astr. and Ap., 6, 417.  
Kellogg, E., Gursky, H., Leong, C., Schreier, E., Tananbaum, H.,  
Giacconi, R., 1971, Ap. J. (Letters), 165, L49.  
Kellogg, E., Gursky, H., Murray, S., Tananbaum, H., and  
Giacconi, R., 1971, Ap.J. (Letters), 169, L99.  
Kemp, J.C., Rieke, G.H., Lebofsky, M.J., Coyne, G.V.,  
1977, Ap.J. (Letters), 215, L107.  
Kleinmann, D.E., and Wright, E.I., 1974, Ap. J. (Letters), 191, L19.  
Kunkel, W.E. and Bradt, H.V., 1971, Ap. J. (Letters), 170, L7.  
Lampton, M., Margon, B., Bowyer, C.S., Mahoney, W., and  
Lawrence, A., Pye, J.P., and Elvis, M., 1977, M.N.R.A.S., 181, 93P.  
Leventhal, M., MacCallum, C.J., and Stang, P.D., 1978,  
Ap.J. (Letters), 225, L11.  
Lewin, W.H.G., Clark, G.W., Gerassimenko, M., and Smith, W.B.,  
1969, Nature, 223, 1142.  
Lewin, W.H.G., Ricker, G.R., and McClintock, J.E., 1971,  
Ap.J. (Letters), 169, L17.  
Lynds, C.E., 1968, Astron. J., 73, 888.  
and Anderson, K., 1972, Ap. J. (Letters), 171, L45.  
Lyuty, Y.M. and Pronik, V.I., 1975, Variable Stars and  
Stellar Evolution, I.A.U. Symposium, 59, 591.  
Marscher, A.P., and Brown, R.L., 1978, Ap.J., 220, 474.  
Mayer, W., Bradt, H.V., and Bappaport, S., 1970, Ap.J. (Letters),

159, L115.

Morgan, W.W., 1958, PASP, 70, 364.

Morrison, P., 1969, Ap. J. (Letters), 157, L73.

Mushotzky, R.F., 1977, Ph.D. Thesis, UCSD.

Mushotzky, R.F., Baity, W.A., Wheaton, W.A., and Peterson,  
L.E., 1976, Ap. J. (Letters), 206, L45.

Mushotzky, R.F., Holt, S.S., and Serlemitsos, P.J., 1978,  
Ap.J. (Letters), 225, L115.

Mushotzky, R.F., Serlemitsos, P.J., Becker, R.H., Boldt, E.A.,  
and Holt, S.S., 1978, Ap. J., 220, 790.

Cke, J.E. and Shields, G.A., 1976, Ap. J., 107, 713.

Ozernoy, L.M., 1966, Ap. J., 43, 300.

Czernoy, L.M., 1974, Galaxies and Relativistic Astrophysics, ed.  
B. Barbanis and J.D. Hadjidemetriou, (New York: Springer-Verlag),  
p.65.

Fachluczky, A.G. and Scott, J.S., 1976, Ap. J., 210, 311.

Penston, M.V., Penston, M.J., Neugebauer, G., Tritton, K.P.,  
Becklin, E.E., and Visvanathan, N., 1971, M.N.R.A.S., 153, 29.

Penston, M.V., Penston, M.J., Selmes, R.A., Becklin, E.E.,  
and Neugebauer, G., 1974, M.N.R.A.S., 169, 357.

Petschek, A.G., Colgate, S.A., and Colvin, J.D., 1976, Ap. J., 209, 356.

Pipher, J., 1977, private communication.

Pounds, K.A., 1977, Proc. of the Eighth Symposium on Relativistic  
Astrophysics, New York Acad. of Sciences, 302, 361.

Price, K.M. and Stull, M.A., 1973, Nature, 245, 83.

Rees, M.I., 1977, Proc. of the Eighth Texas Symposium on Relativistic  
Astrophysics, New York Acad. of Sciences, 302, 613.

- Ricker, G.R., McClintock, J.E., Gerassimenko, M., Lewin, W.H.G.,  
1973, Ap.J., 184, 237.
- Riegler, G., 1969, Ph.D. Thesis, University of Maryland.
- Rieke, G., 1977, private communication.
- Rieke, G., 1978, private communication.
- Rieke, G.H. and Low, F.J., 1972, Ap. J. (Letters), 176, L95.
- Rieke, G.H. and Low, F.J., 1973, Ap.J., 184, 415.
- Salpeter, E.E., 1964, Ap. J., 140, 796.
- Sanford, F.W., 1977, Proc. of the Eighth Texas Symposium on  
Relativistic Astrophysics, New York Acad. of Sciences, 302, 387.
- Schmidt, G.D., Peterson, E.M., and Weaver, E.A., 1978, Ap.J.  
(Letters), 220, L31.
- Schoenfelder, V., Graser, U., Dougherty, J., 1977, Ap.J., 217, 306.
- Serlemitscs, P.J., Becker, R., Boldt, E.A., Holt, S.S., Pravdo, S.,  
Rechtschild, R., and Swank, J.H., 1975, Symposium on X-ray  
Binaries, NASA SP-389, 77.
- Seyfert, C.K., 1943, Ap. J., 97, 28.
- Slish, V.I., 1963, Nature, 199, 682.
- Spitzer, I. and Saslaw, W.C., 1966, Ap. J., 143, 400.
- Stark, J.F., Davison, P.J.N., and Culhane, J.L., 1976, M.N.R.A.S.,
- Stern, L., 1975, private communication.
- Stockton, A., 1978, Nature, 274, 342.  
174, 35F.
- Stull, M.A. and Price, K.M., 1975, Nature, 255, 467.
- Swanenburg, B.N., Bennett, K., Bignami, G.F., Caraveo, P., Hermsen, W.  
Kanbach, G., Masnou, J.L., Mayer-Fasselwander, H.A., Paul, J.A.,  
Sacco, B., Scarsi, L., and Wills, R.D., 1978, Nature, 275, 298.

Tapia, S., 1977, private communication.  
 Thomas, R.M., Davison, F.J.N., Clancy, M.C., and Buselli, G.,  
 1975, M.N.R.A.S., 170, 569.  
 Toor, A. and Seward, F.D., 1974, A.J., 79, 995.  
 Tucker, W.H., 1976, Radiation Processes in Astrophysics (Cambridge:  
 MIT Press).  
 Tucker, W.H., Kellogg, E., Gursky, H., Giacconi, R. and Tananbaum,  
 H., 1973, Ap. J., 180, 715.  
 Ulich, E.L., 1974, Icarus, 21, 254.  
 Ulich, E.L., 1977, private communication.  
 Ulmer, M., 1977, Ap.J. (Letters), 218, L1.  
 van den Bergh, S., 1976, Ap. J., 208, 673.  
 van der Laan, H., 1966, Nature, 211, 1131.  
 Waak, J.A. and Hobbs, R.W., 1977, preprint.  
 Wade, C.M., Hjellming, B.M., Kellermann, K.I. and Wardle, J.F.C.,  
 Weedman, D.W., 1977, Ann. Rev. Astr. and Ap., 15.  
 1971, Ap. J. (Letters), 170, L11.  
 Winkler, F.F. and White, A.E., 1975, Ap. J. (Letters), 199, L139.  
 Williams, P.J.S., 1963, Nature, 200, 56.  
 Wilson, A.M., Carpenter, G.F., Eyles, C.J., Skinner, G.K.,  
 and Willmore, A.F., 1977, Ap.J. (Letters), 215, L111.  
 Woltjer, L., 1964, Nature, 201, 807.  
 Wu, C.H., 1977, Ap. J. (Letters), 217, L117.  
 Wu, C.C. and Weekman, D.W., 1978, Ap.J., 223, 798.  
 Zel'Dovich, Y.B., 1964, Proc. Acad. Sci. USSR, 155, 67.  
 Zel'Dovich, Y.B. and Novikov, I.D., 1971, Relativistic Astrophysics  
 (University of Chicago Press: Chicago).

TABLE 3.1

## Radio Flux Density of the Nucleus of Cen A (NGC 5128)

<u>10.7 GHz</u>		
07-11-73	5.97	.41
07-12-73	5.53	.37
07-13-73	6.17	.29
07-14-73	6.00	.25
07-15-73	5.72	.26
07-18-73	6.32	.24
08-08-73	4.00	.19
05-23-74	8.38	.13
01-21-75	8.02	.11
01-22-75	7.58	.11
06-25-75	7.85	.14
07-23-75	6.05	.18
01-18-76	9.48	.15
05-31-76	8.28	.09
07-14-76	6.63	.11
07-21-76	7.60	.11
07-30-76	7.44	.11
07-31-76	7.12	.08
08-01-76	7.47	.12
08-02-76	6.60	.19
08-03-76	6.17	.11
08-04-76	6.25	.17
08-05-76	6.25	.20
08-09-76	5.49	.14
08-10-76	4.88	.20
09-01-76	5.92	.12
09-02-76	5.29	.19
<u>31.4 GHz</u>		
05-21-75	17.09	.35
10-07-75	19.52	.47
12-08-75	20.52	.39
03-09-76	17.68	.25
06-02-76	16.29	.26
<u>85.2 GHz</u>		
12-08-75	11.72	.50
<u>90 GHz</u>		
05-17-76	10.5	.3
07-30,31-76	8.6	.7
08-29-76	8.9	.7
11-20-76	9.5	.6
02-15-77	9.4	.2

TABLE 5.1

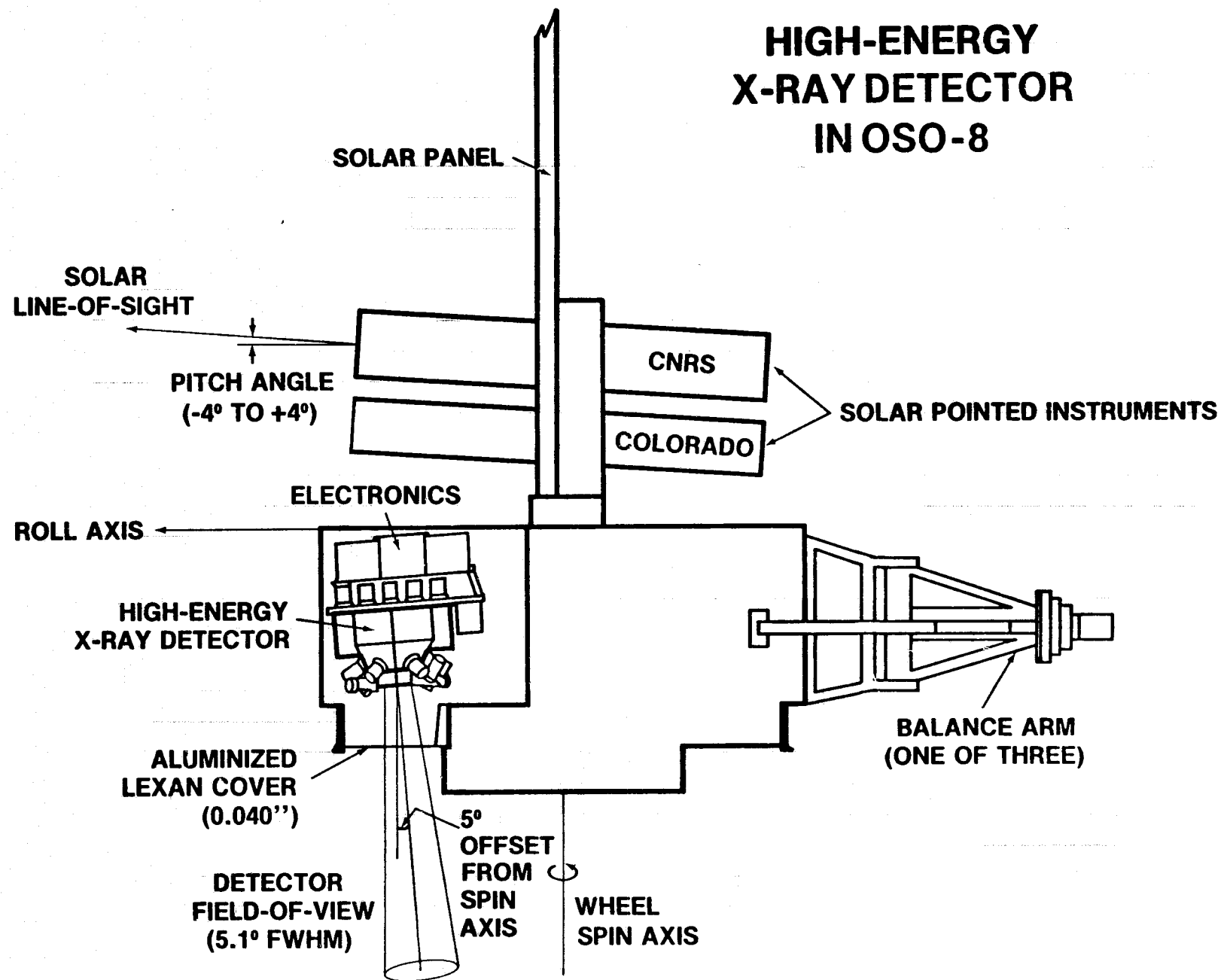
## Radio Flux Density of the Nucleus of NGC 4151

<u>2.695 GHz</u>		
Date	S (mJy)	Standard Deviation (mJy)
05-31-77	169.3	12.3
06-03-77	171.8	8.0

<u>8.085 GHz</u>		
Date	S (mJy)	Standard Deviation (mJy)
05-31-77	62.8	11.7
06-03-77	60.7	6.4

# HIGH-ENERGY X-RAY DETECTOR IN OSO-8



136

Figure 2.1

# OSO-8 20keV-5MeV. X-RAY DETECTOR

PARAMETERS OF DETECTORS	
SENSITIVE AREA	27.5cm <sup>2</sup>
MAXIMUM ACCEPTANCE ANGLE	5.9°
F.W.H.M.	5.1°
AREA X SOLID ANGLE FACTOR	0.25cm <sup>2</sup> sr
MINIMUM SHIELD THICKNESS	2"

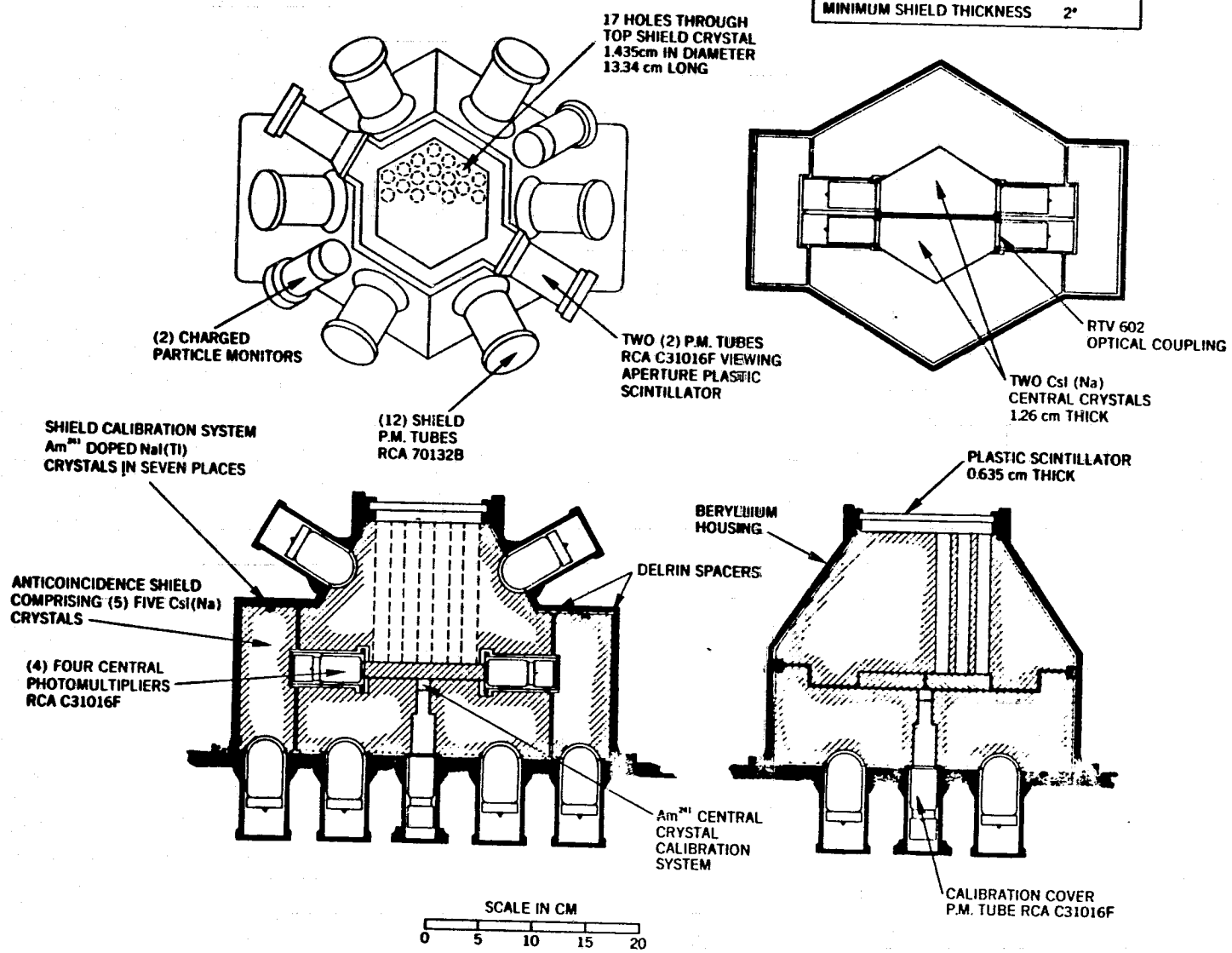


FIGURE 2.2

137

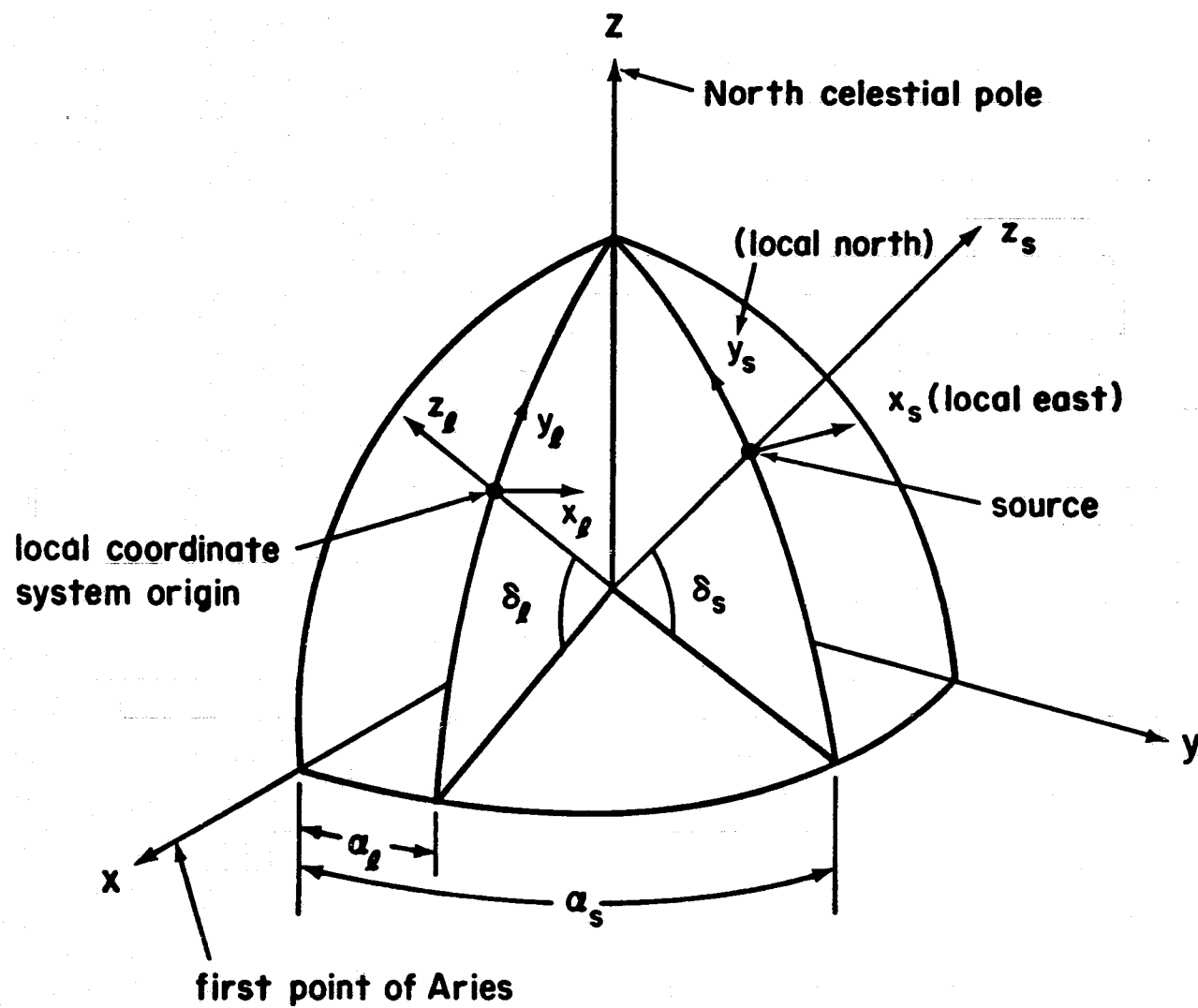


Figure 2.3

Figure 2.4

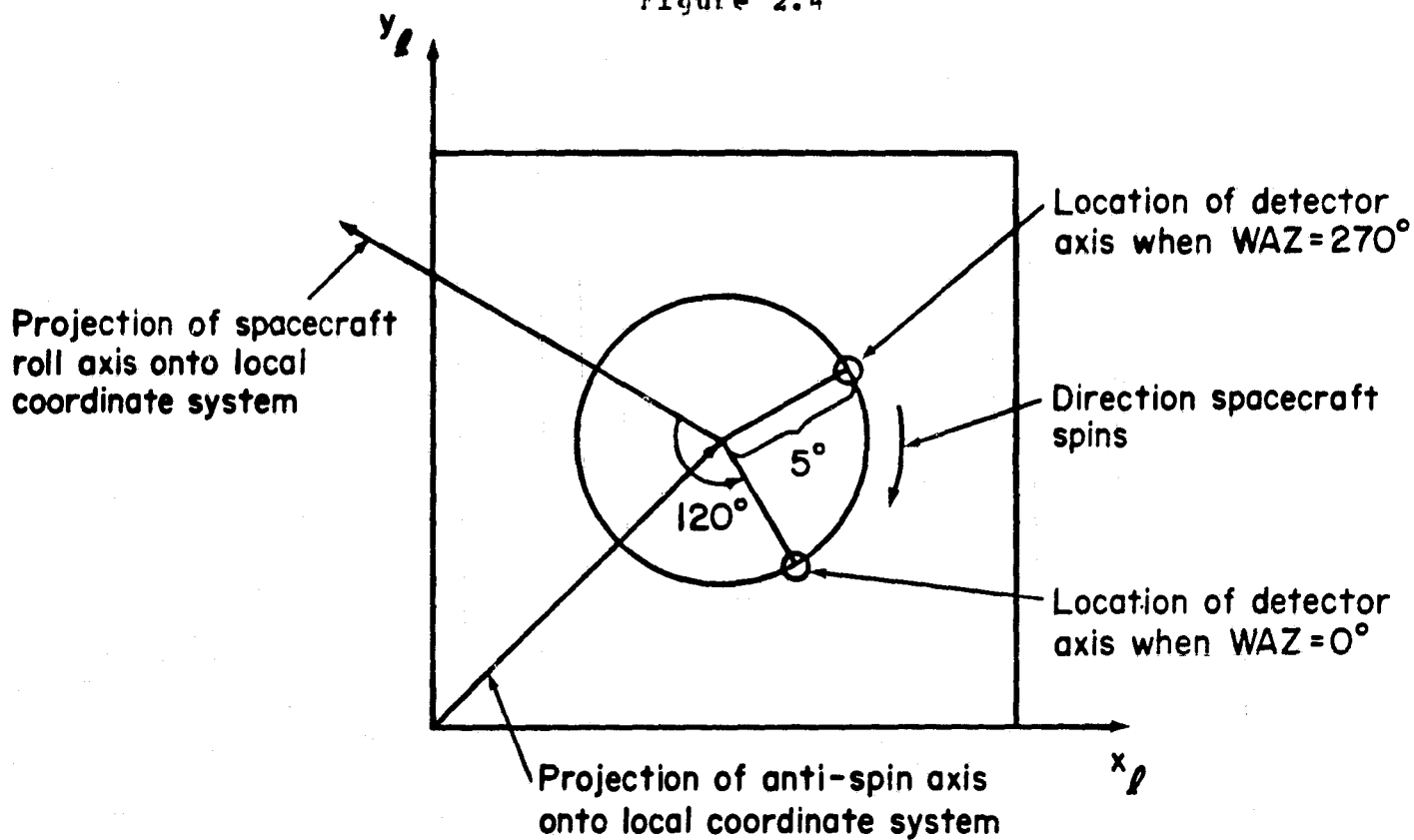


Figure 2.5

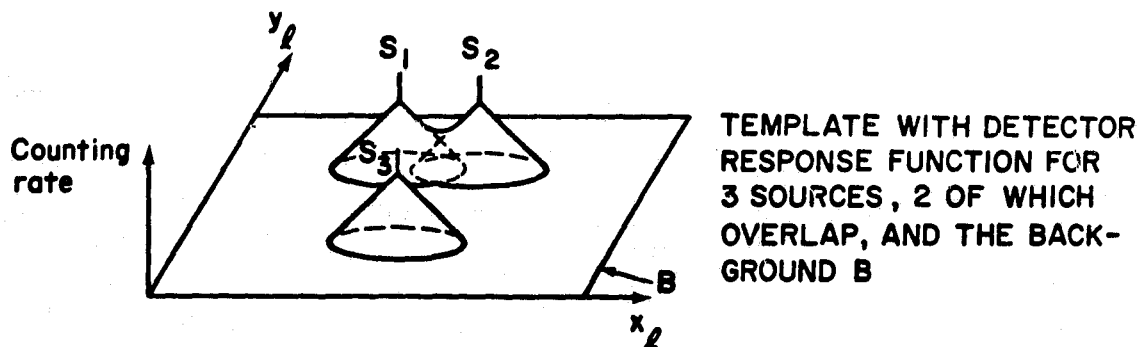


Figure 2.6

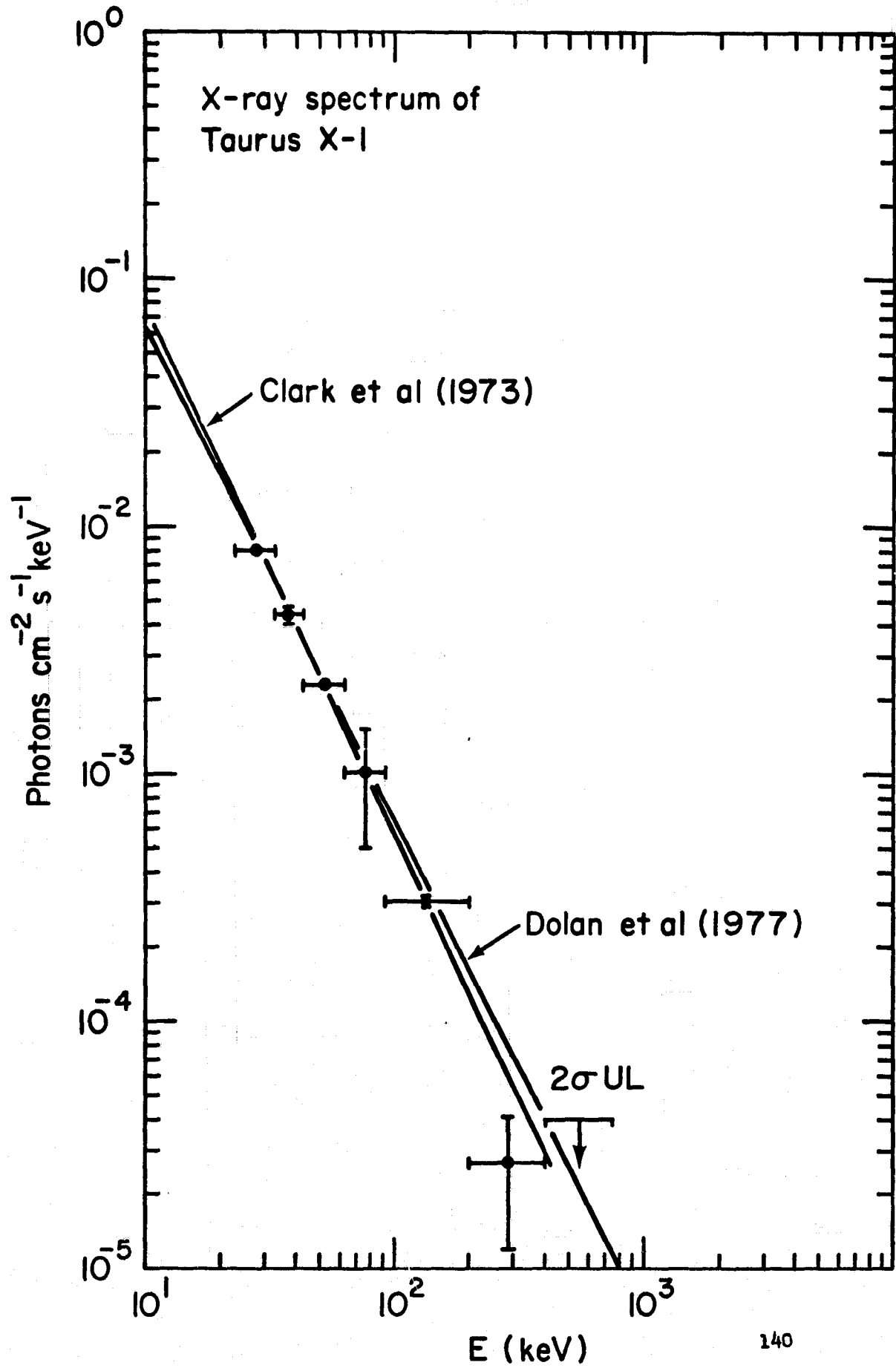


Figure 2.7

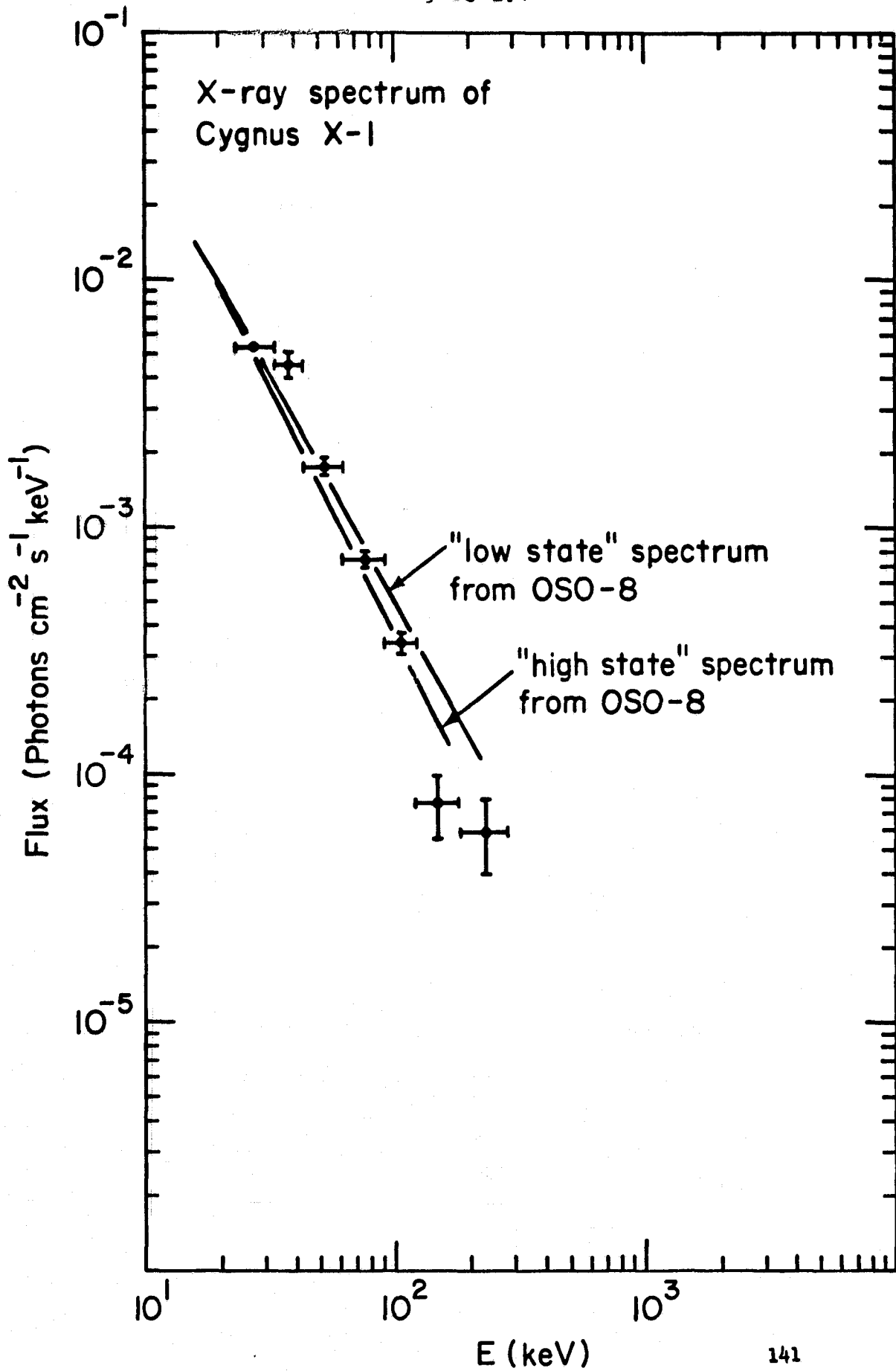
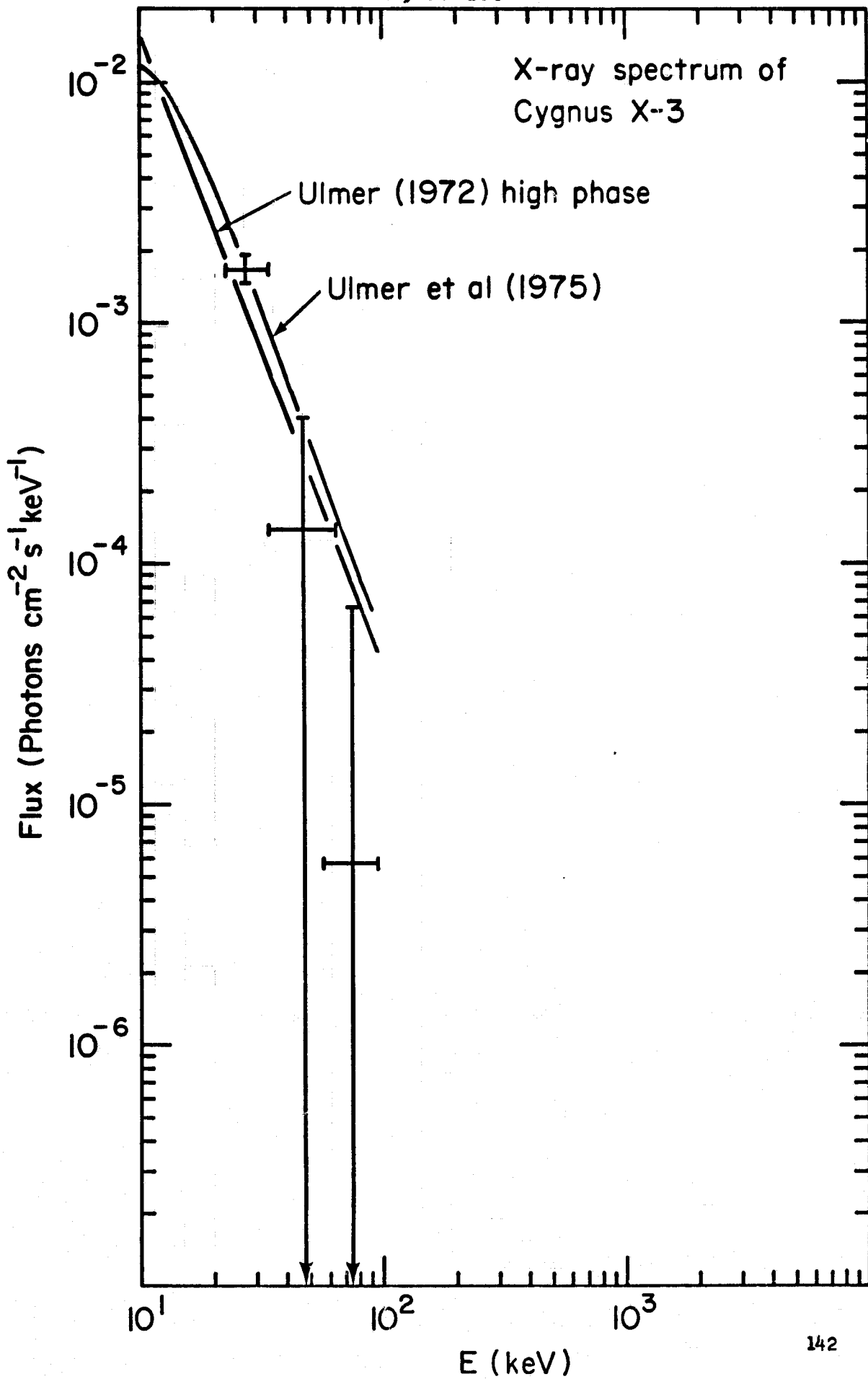


Figure 2.8



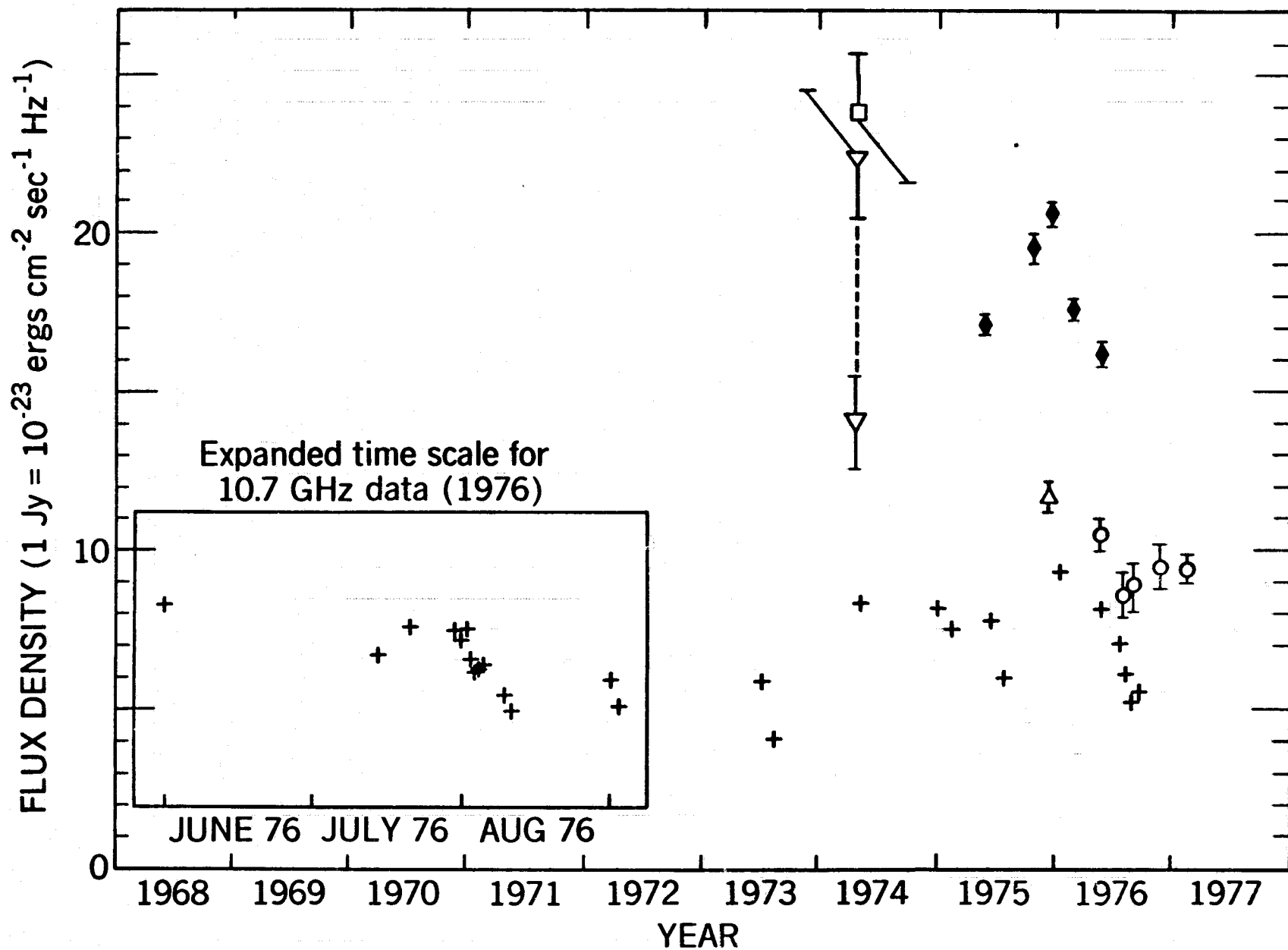


Figure 3.1

Graf and Price (10.7 GHz) = +; Dent and Hobbs (31.4 GHz) = ◆, (85.2 GHz) = △;  
Kellermann (31.5 GHz) = □, (89 GHz) = ○; Conklin and Ulich (90 GHz) = ◊.

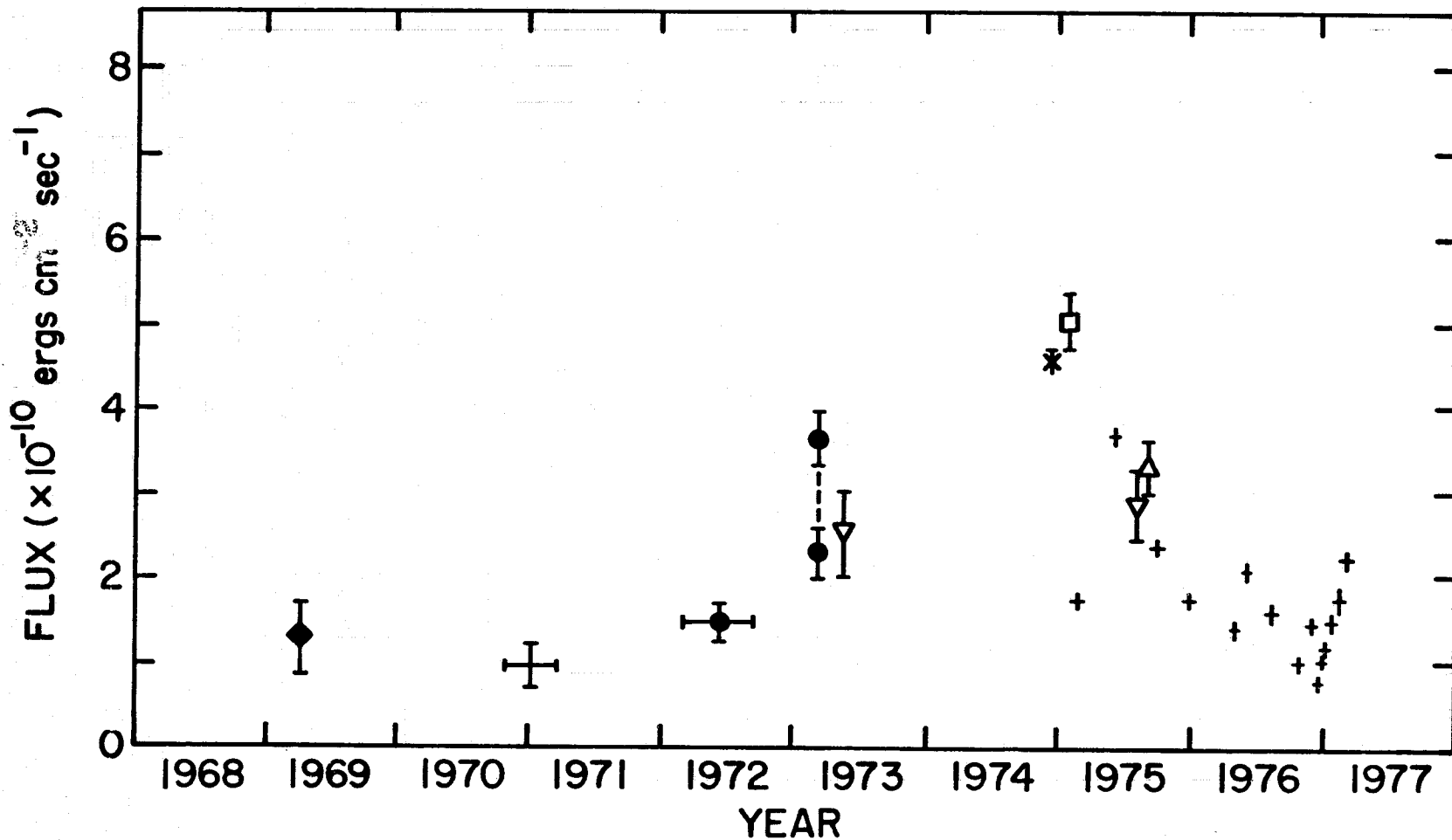
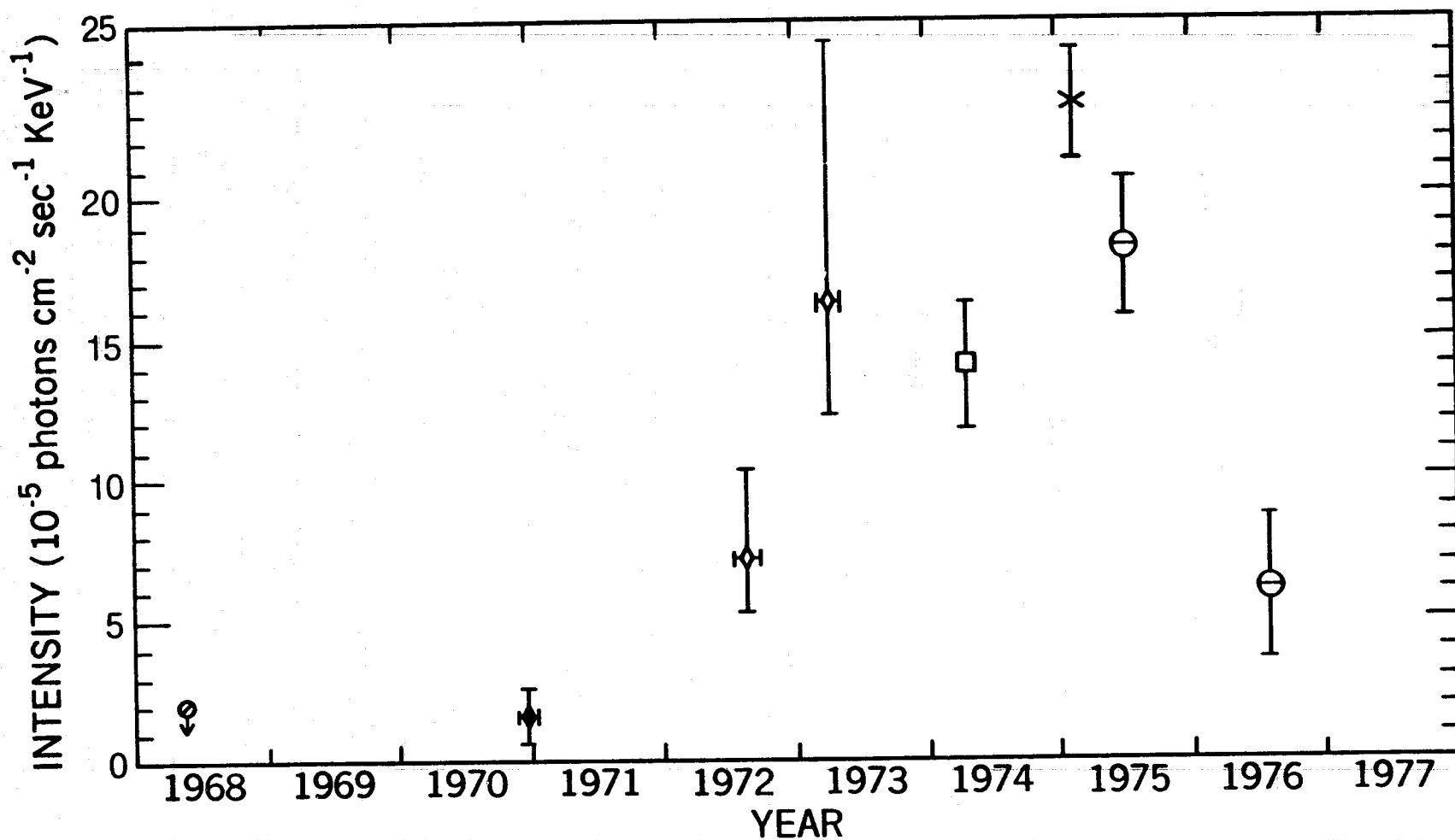
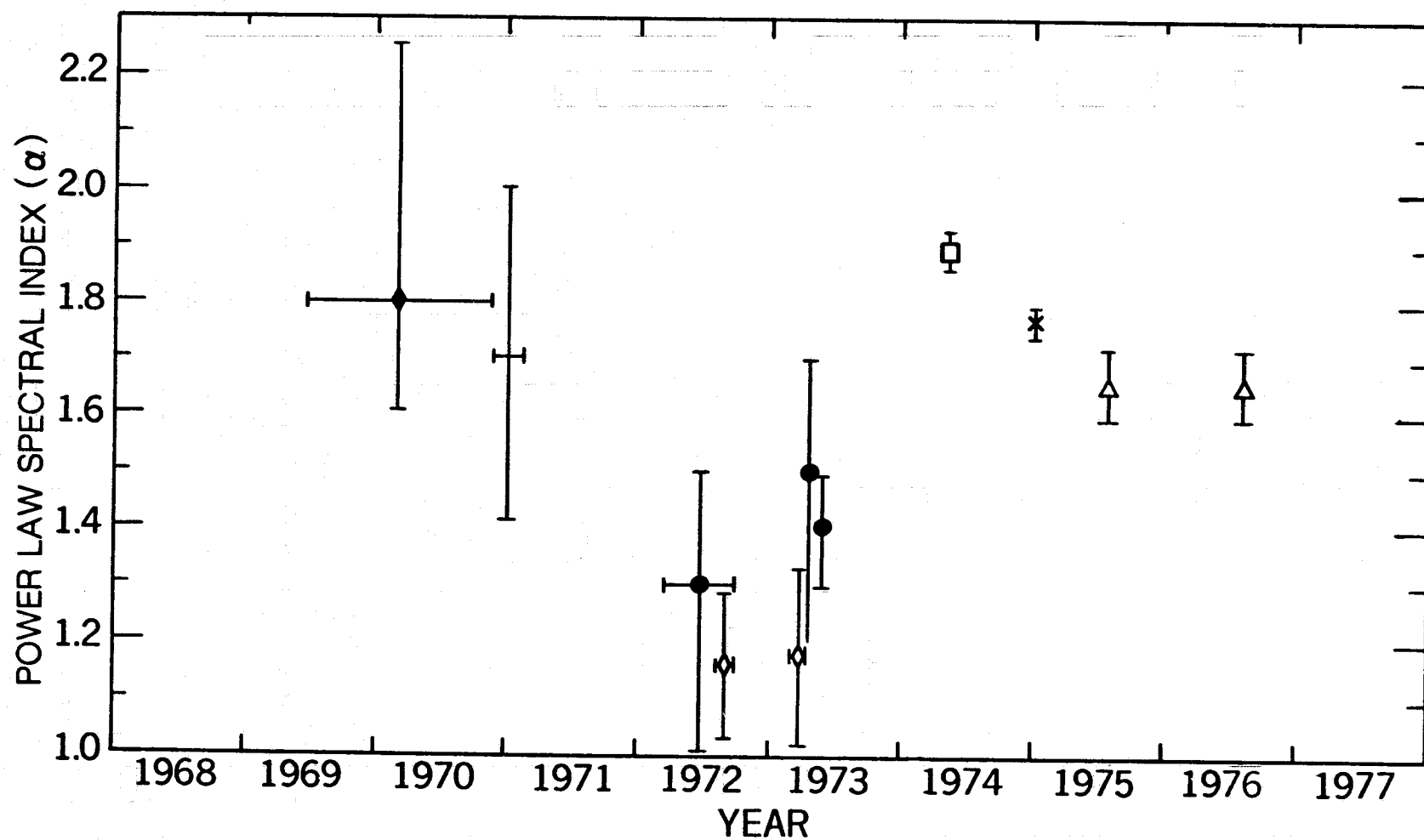


Figure 3.2

Lampton et al. (Rocket) =  $\blacklozenge$ ; Tucker et al. (Uhuru) =  $\boxplus$ ; Winkler and White (OSO-7/MIT) =  $\blacklozenge$ ; Davison et al., Stark et al. (Ariel V) =  $\boxtimes$   
 Grindlay et al. (ANS) =  $\boxplus$ ; Stark et al. (Copernicus) =  $\nabla$ ; Serlemitsos et al. (OSO-8) =  $\boxtimes$ ; Lawrence et al. (Ariel V; Copernicus) =  $+$



Haymes et al. (Balloon) =  $\circ$ ; Lampton et al. (Balloon) =  $\blacklozenge$ ; Mushotzky et al. (OSO - 7) =  $\blacklozenge$ ;  
 Hall et al. (Balloon) =  $\square$ ; Stark et al. (Ariel V, Extrapolation) =  $\times$ ; Beall et al. (OSO - 8) =  $\circ$ .



Lampton et al. =  $\blacklozenge$ ; Tucker et al. =  $\pm$ ; Winkler and White =  $\bullet$ ; Mushotzky et al. =  $\square$ ;  
Hall et al. =  $\square$ ; Stark et al. =  $\ast$ ; Mushotzky and Serlemitsos =  $\triangle$ .

Figure 3.5

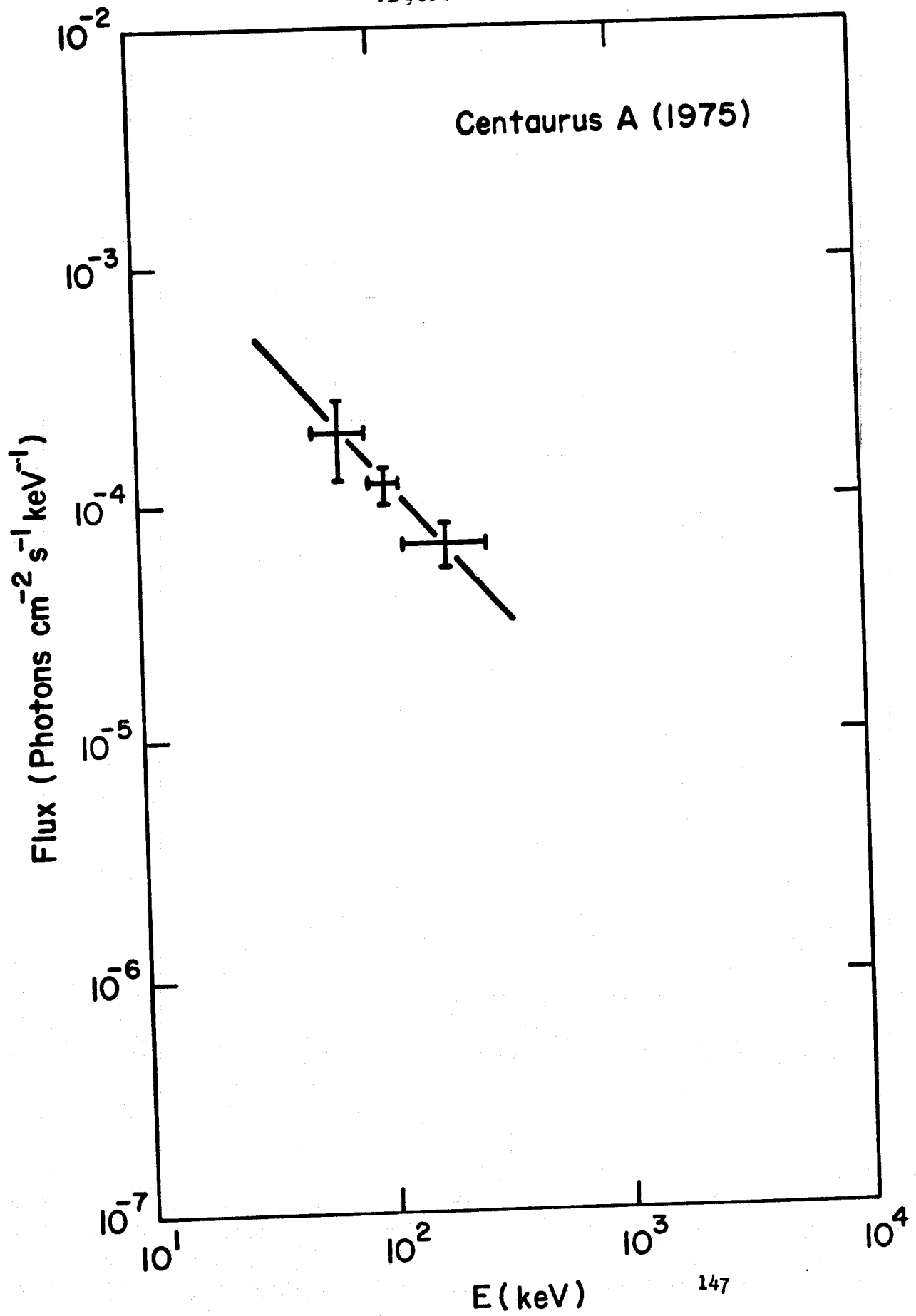
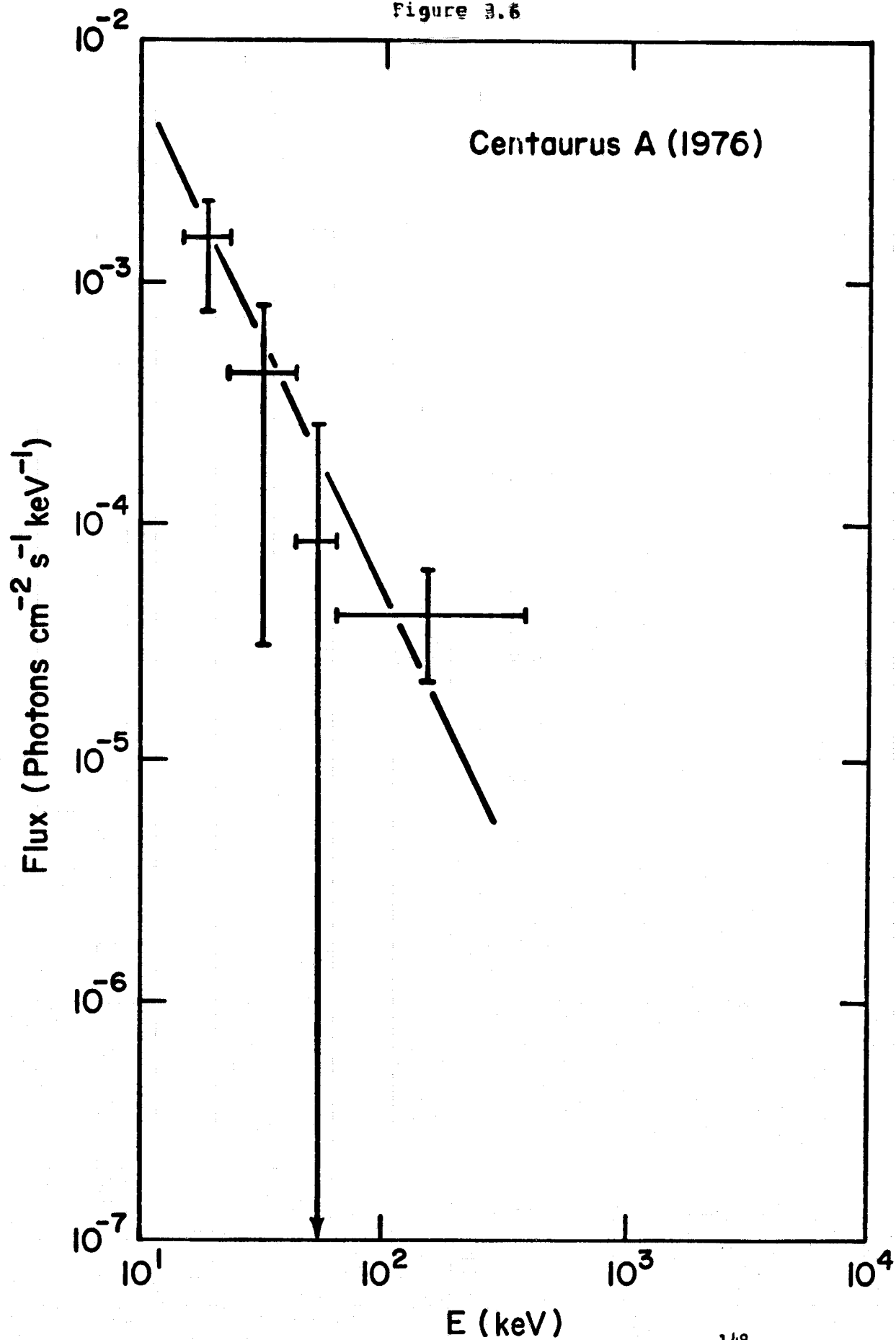


Figure 3.6



# Composite Spectrum of Cen A (NGC 5128)

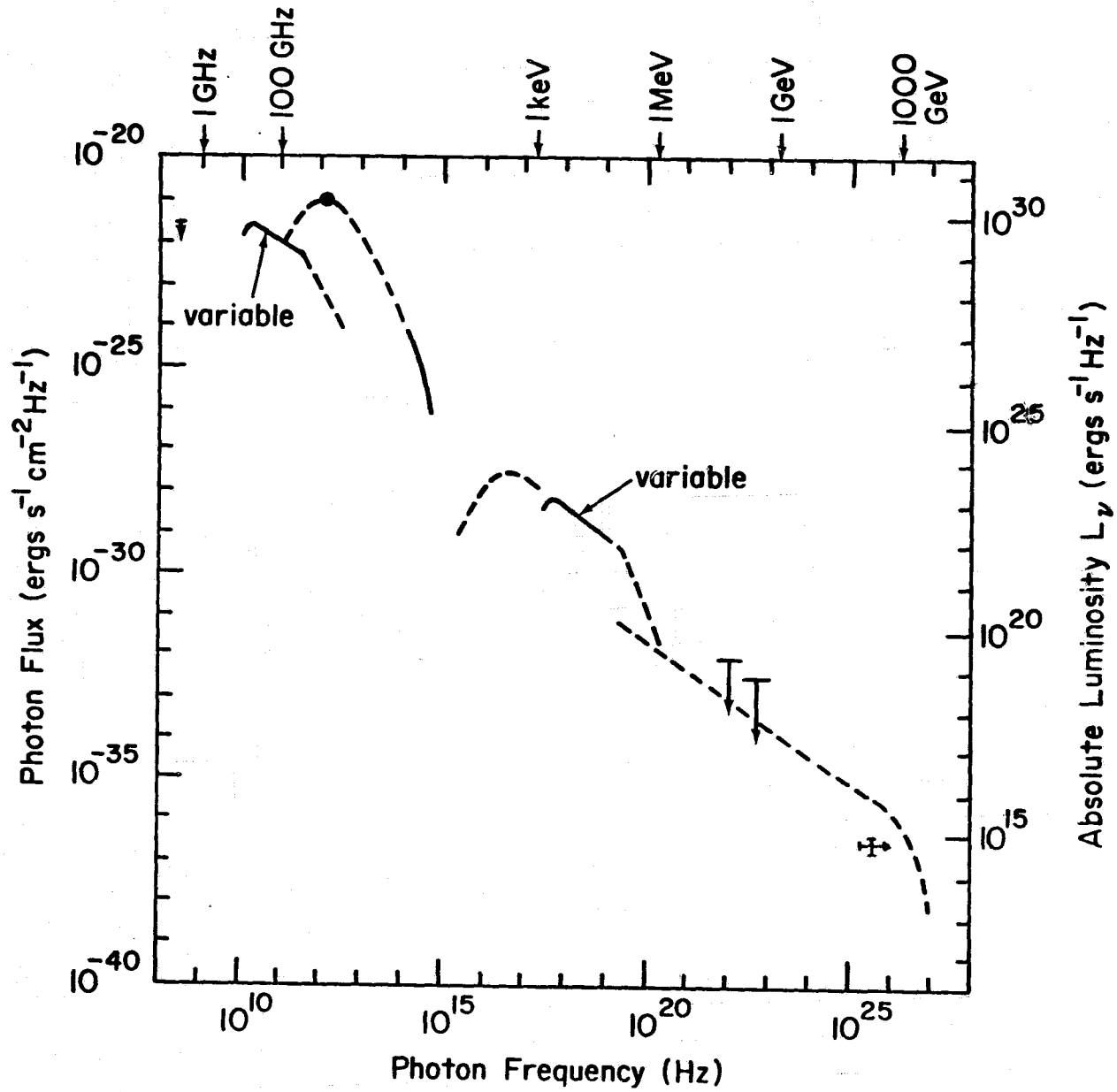


Figure 3.7

Figure 4.1

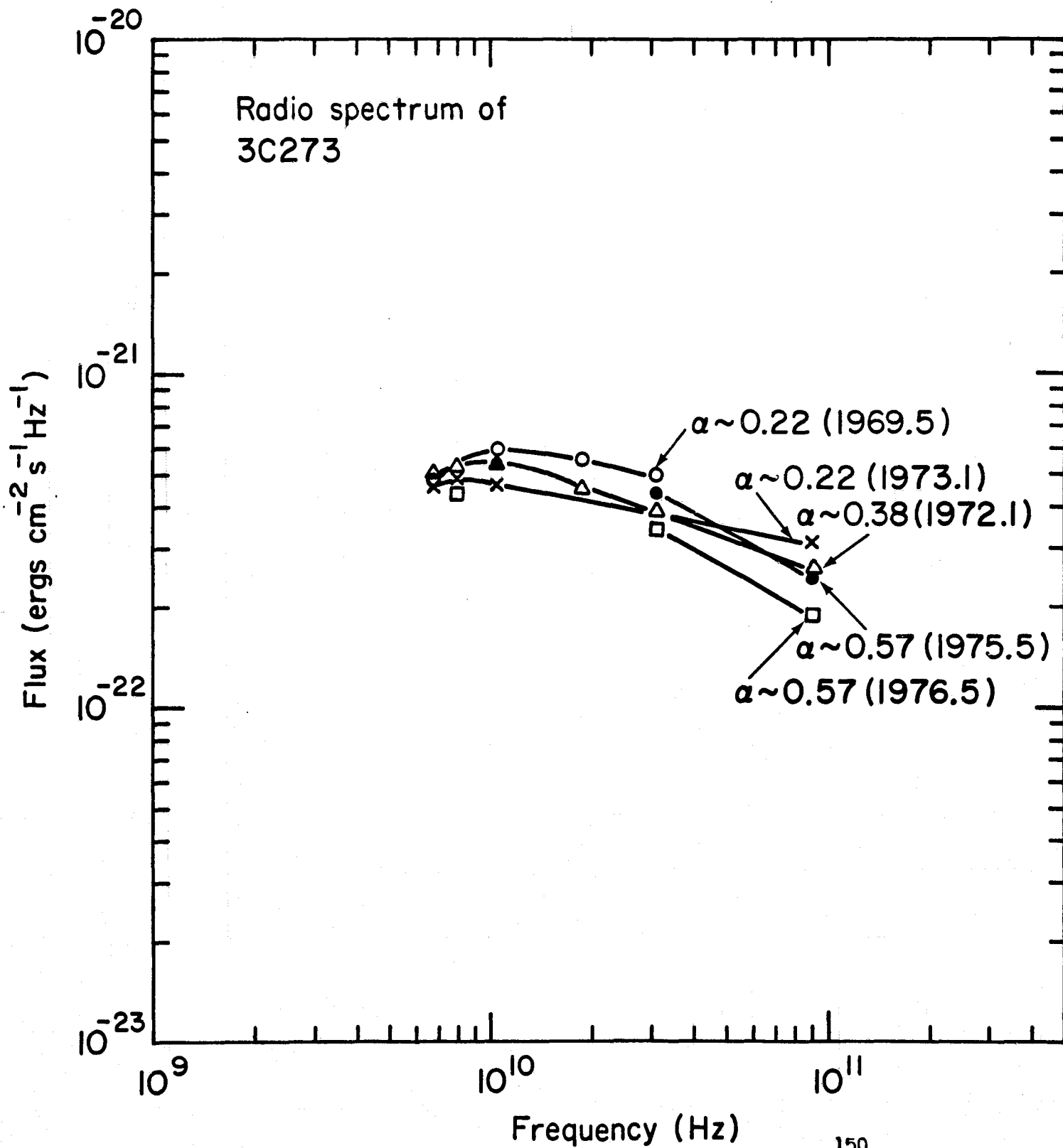


Figure 4.2

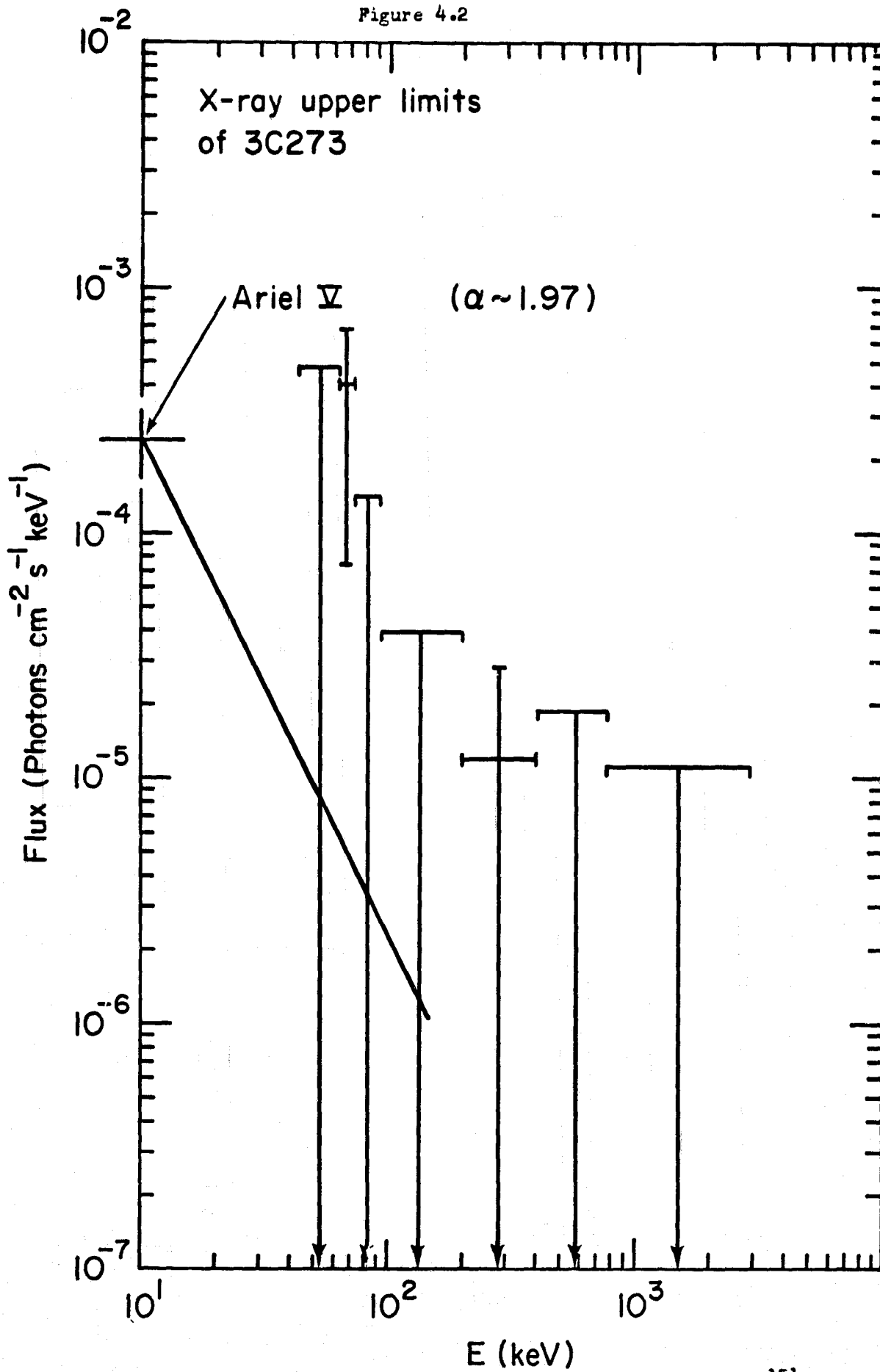
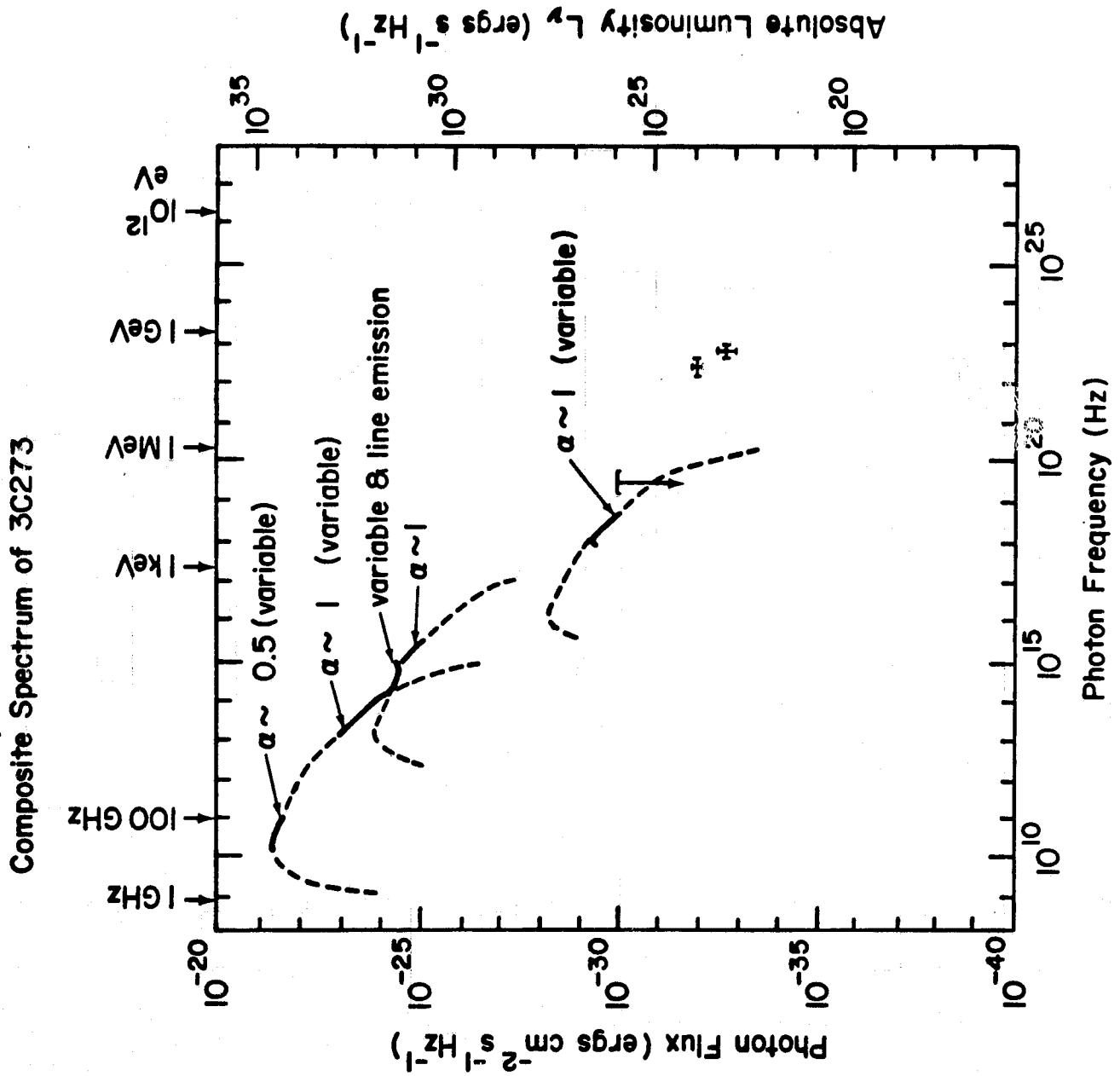


Figure 4.3



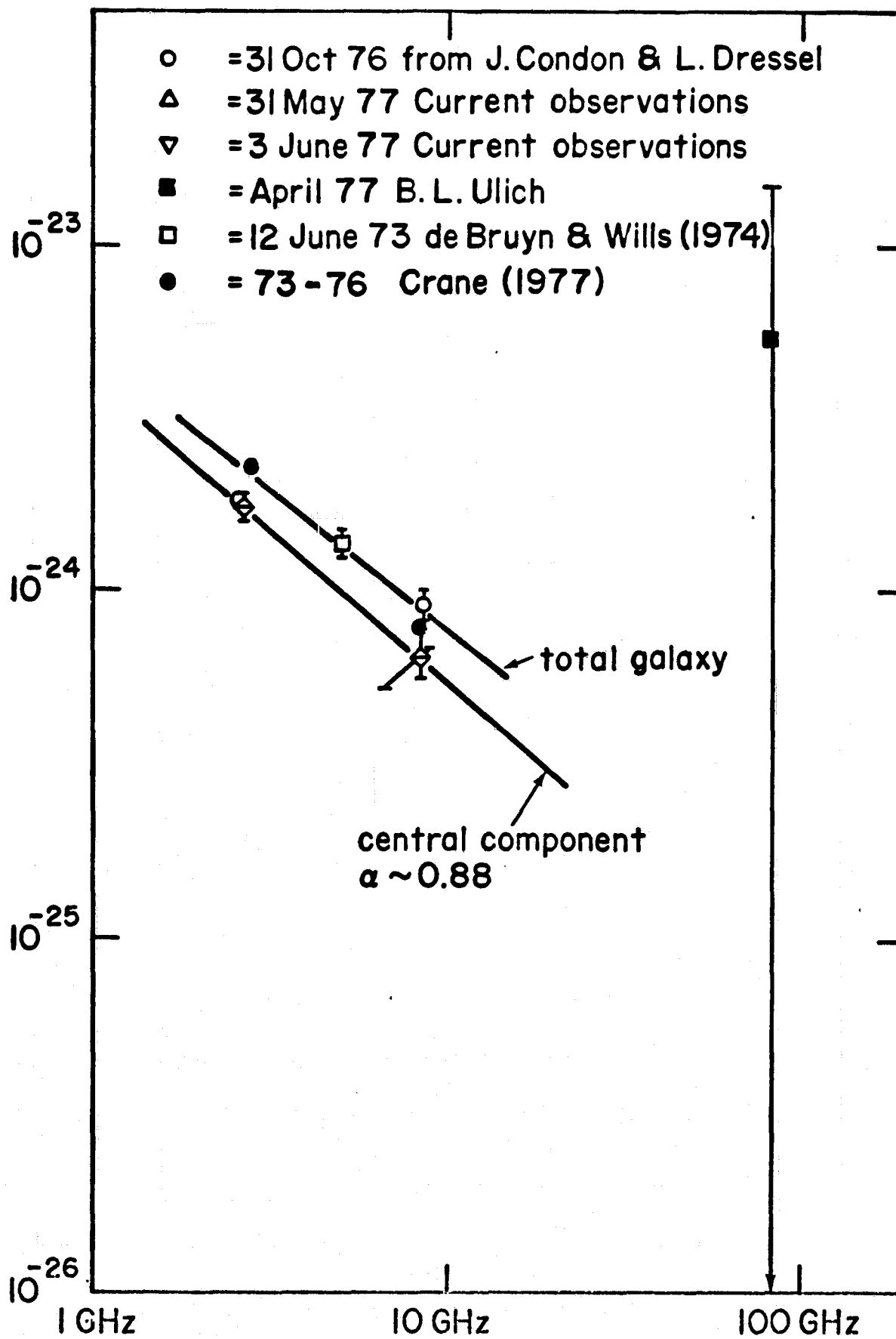


Figure 5.2

NGC 4151  
Infrared & UVB data

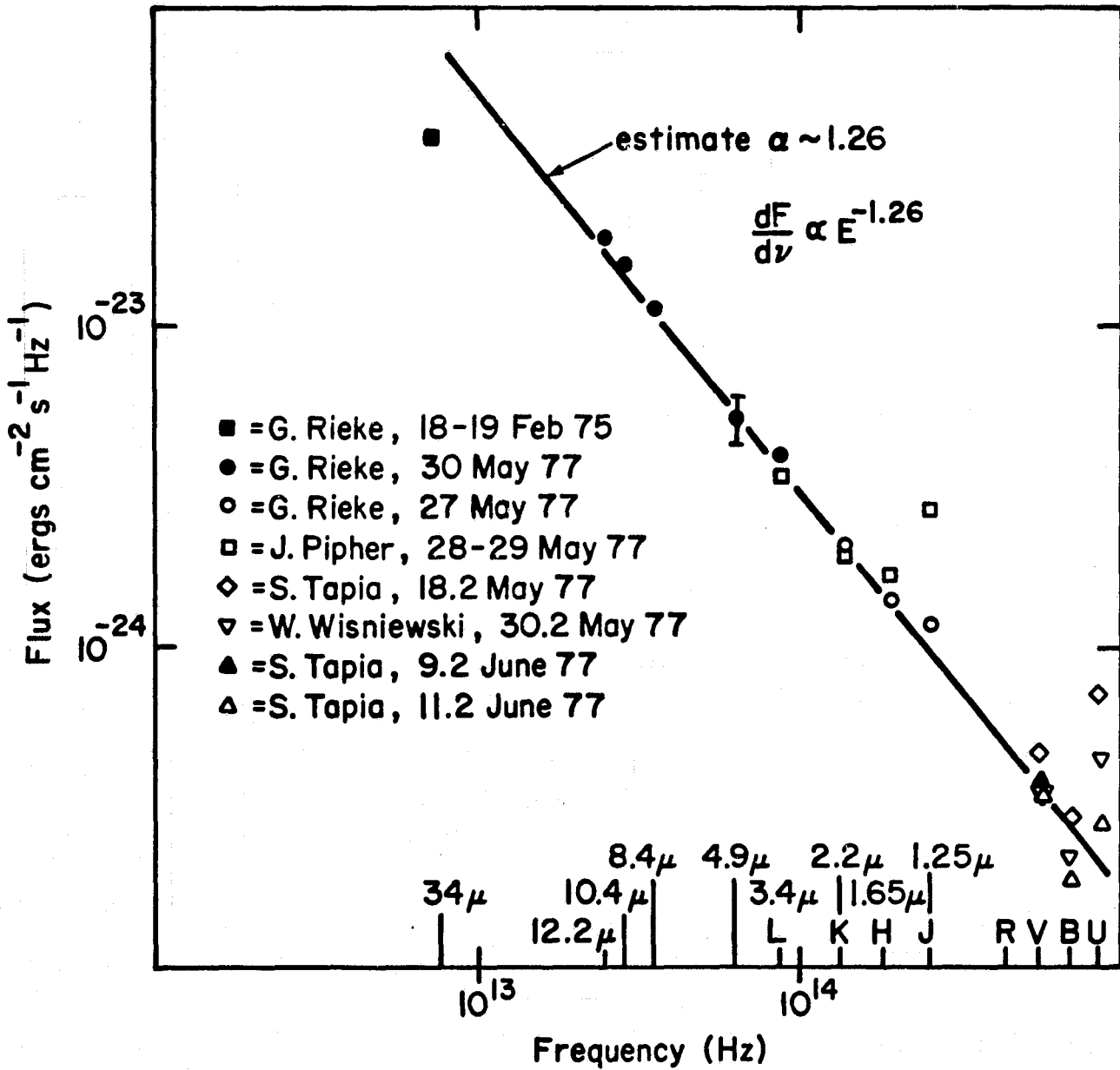
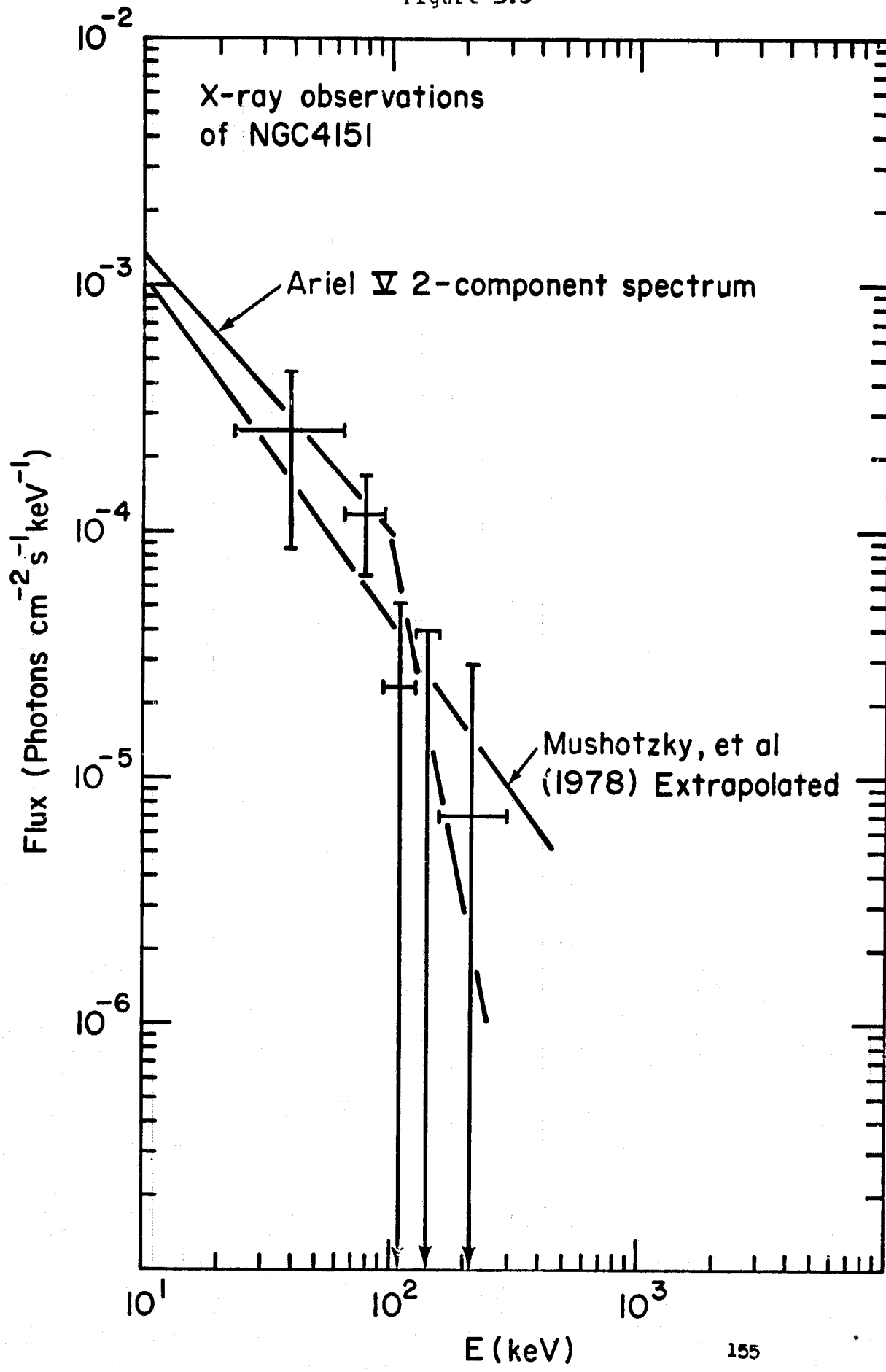


Figure 5.3



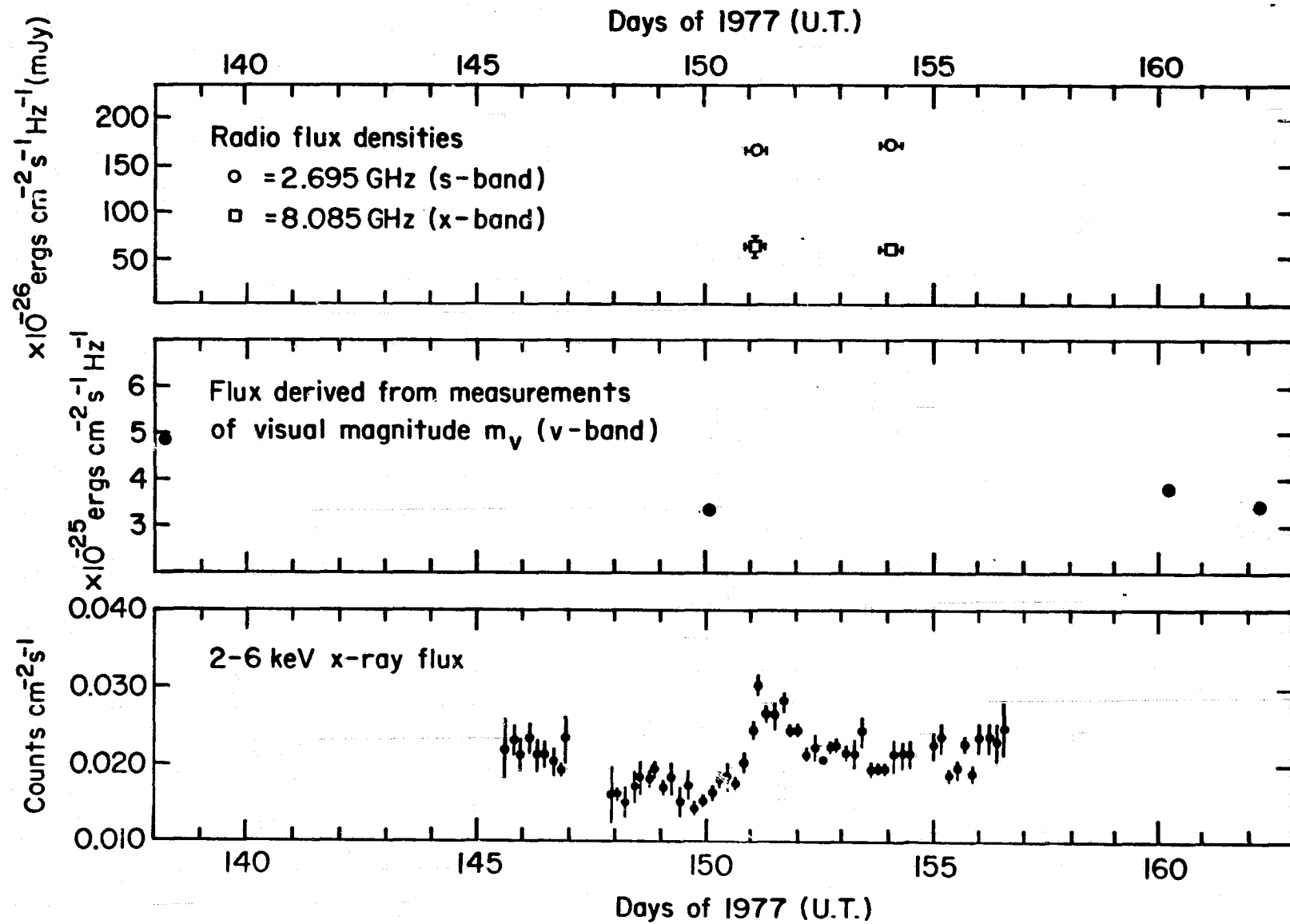
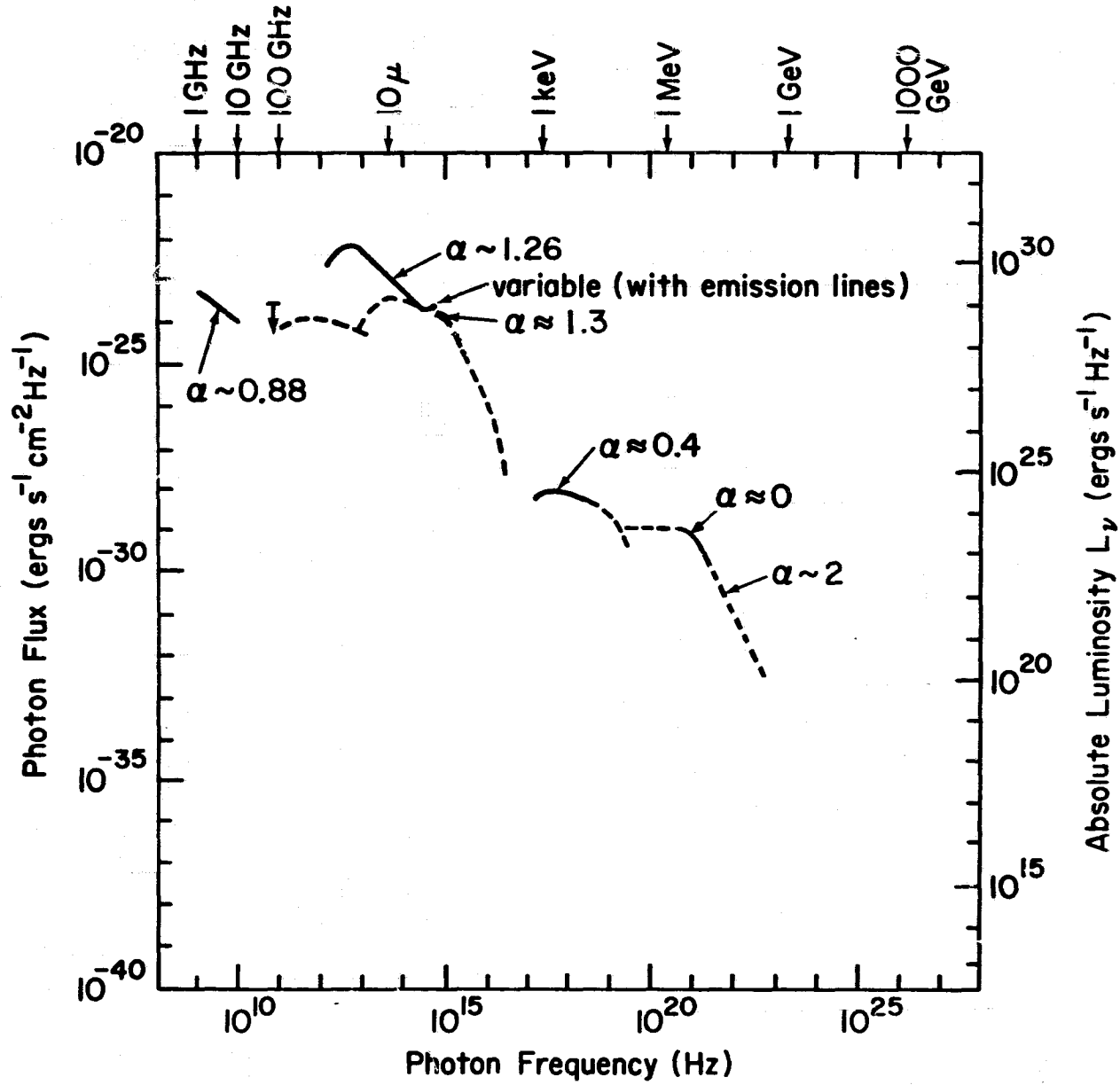


Figure 5.4

Composite Spectrum of  
NGC 4151



157

Figure 5.5

Figure 6.1

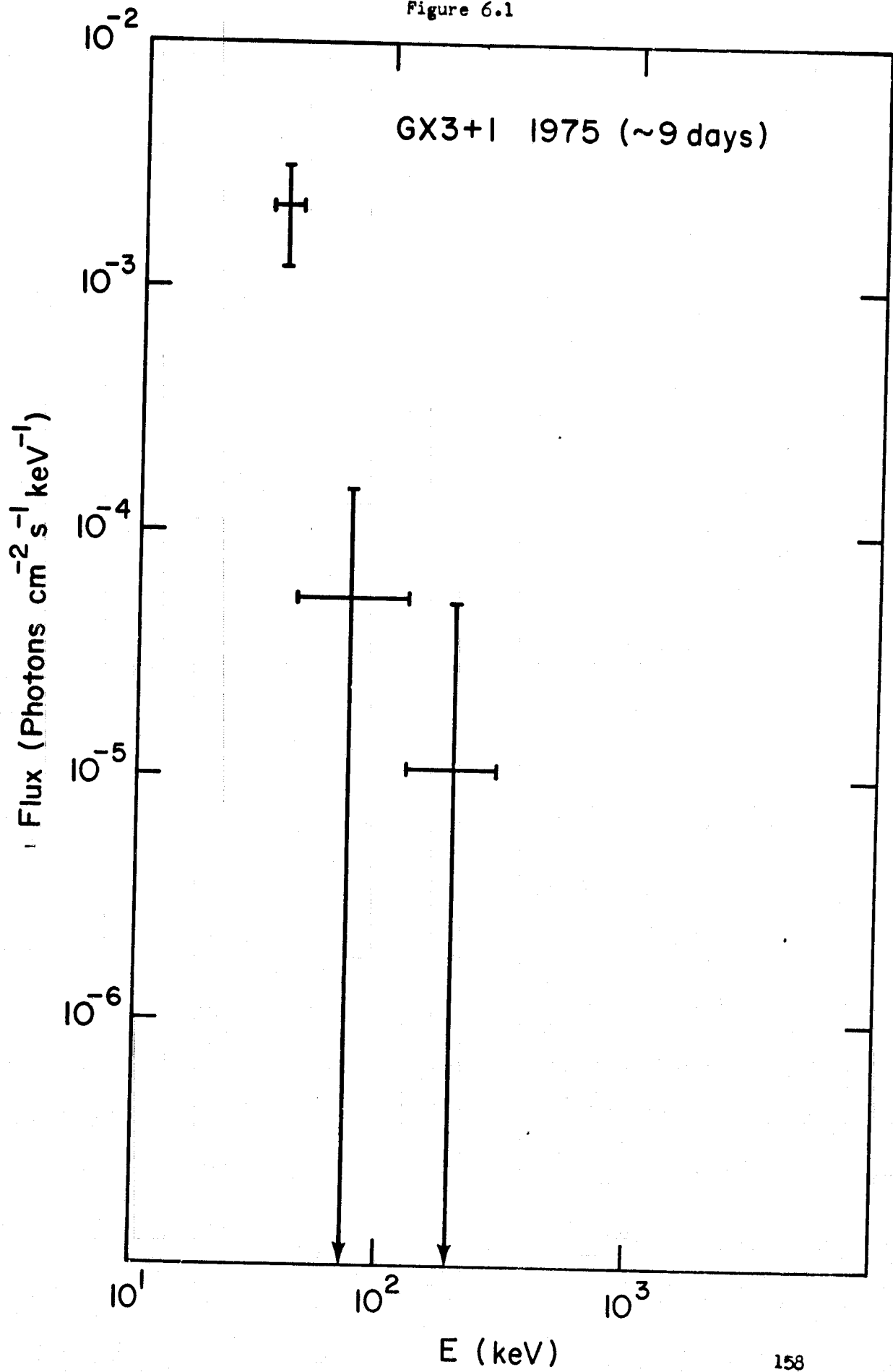


Figure 6.2

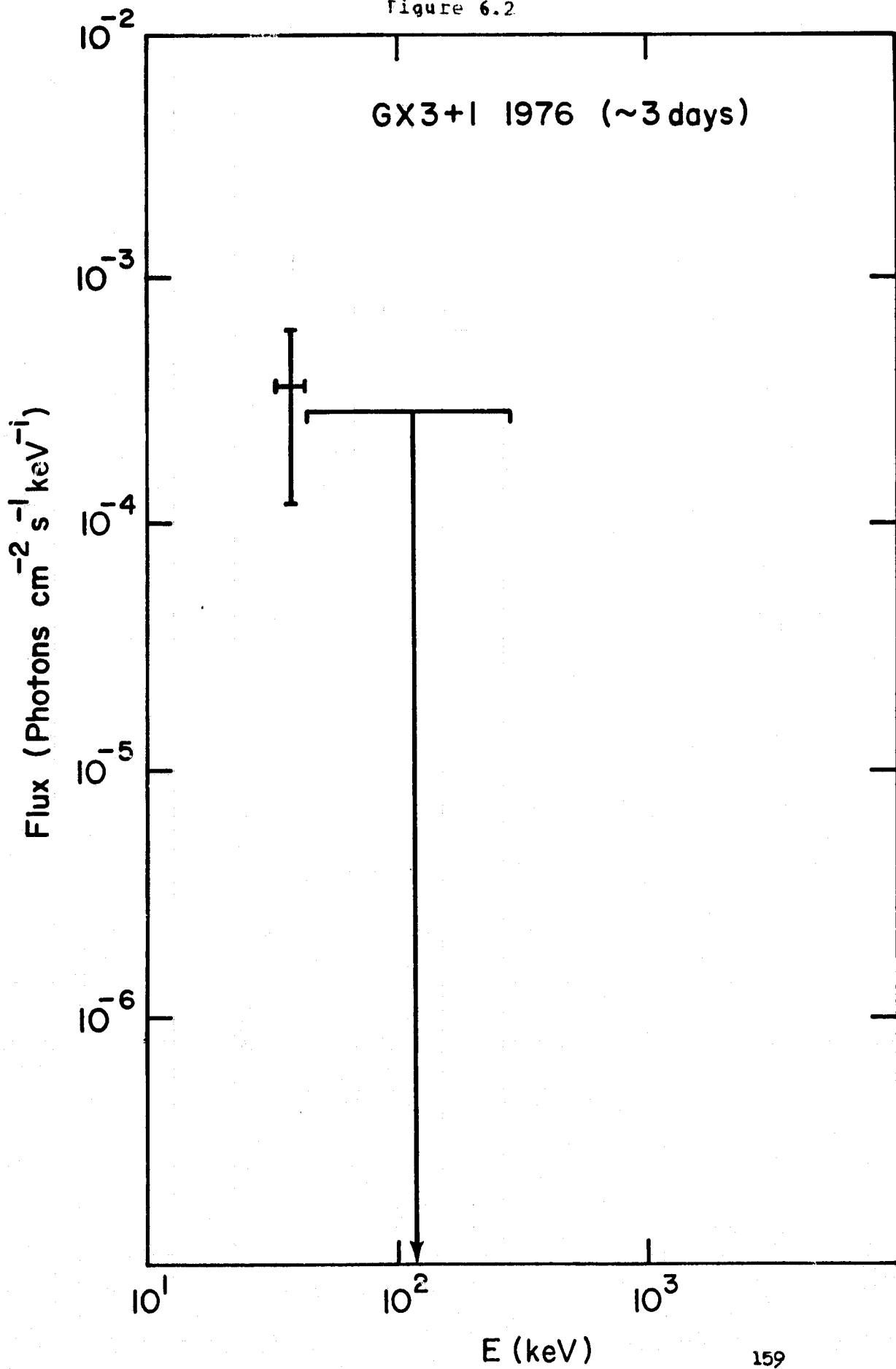


Figure 6.3

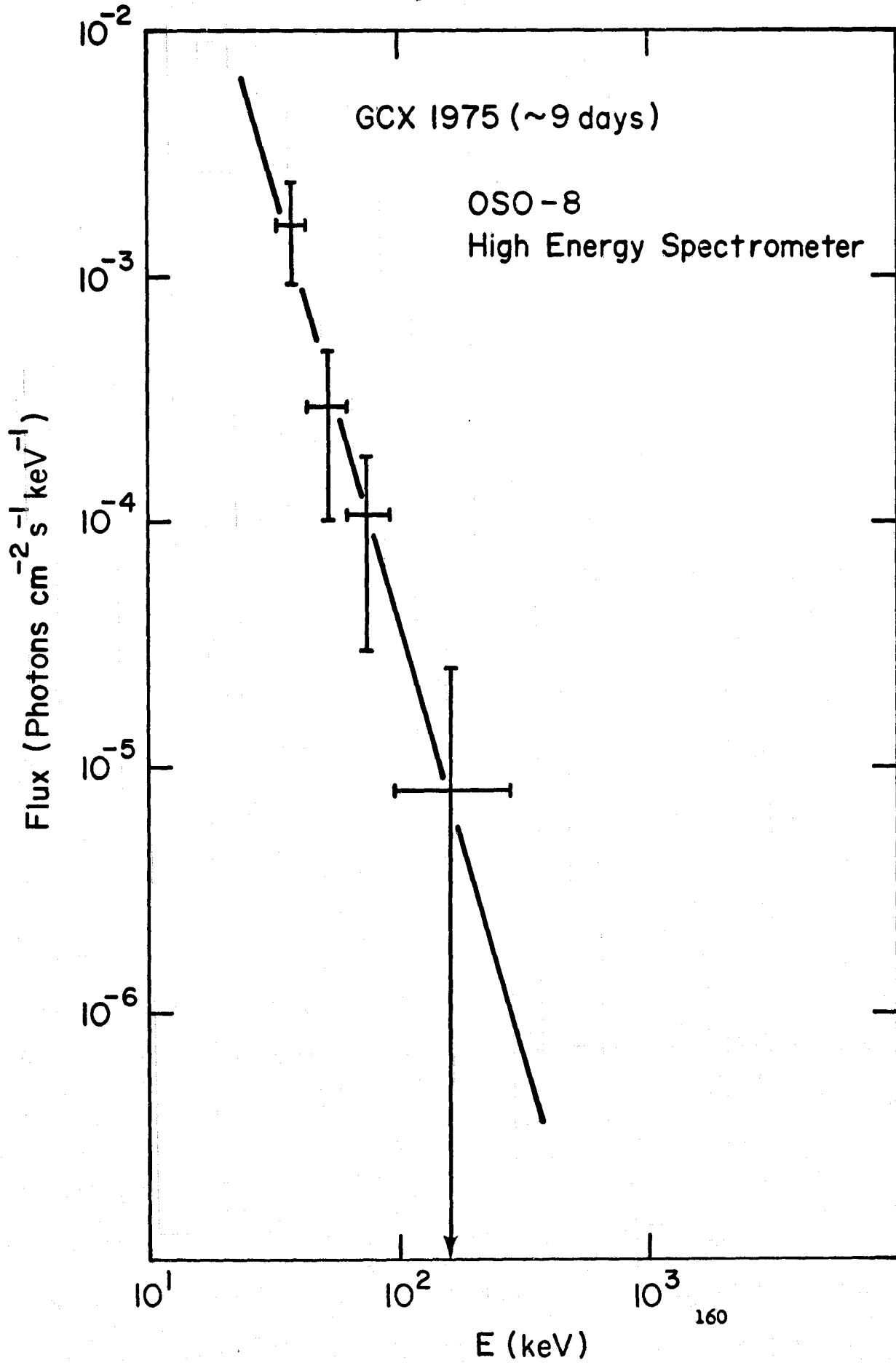


Figure 6.4

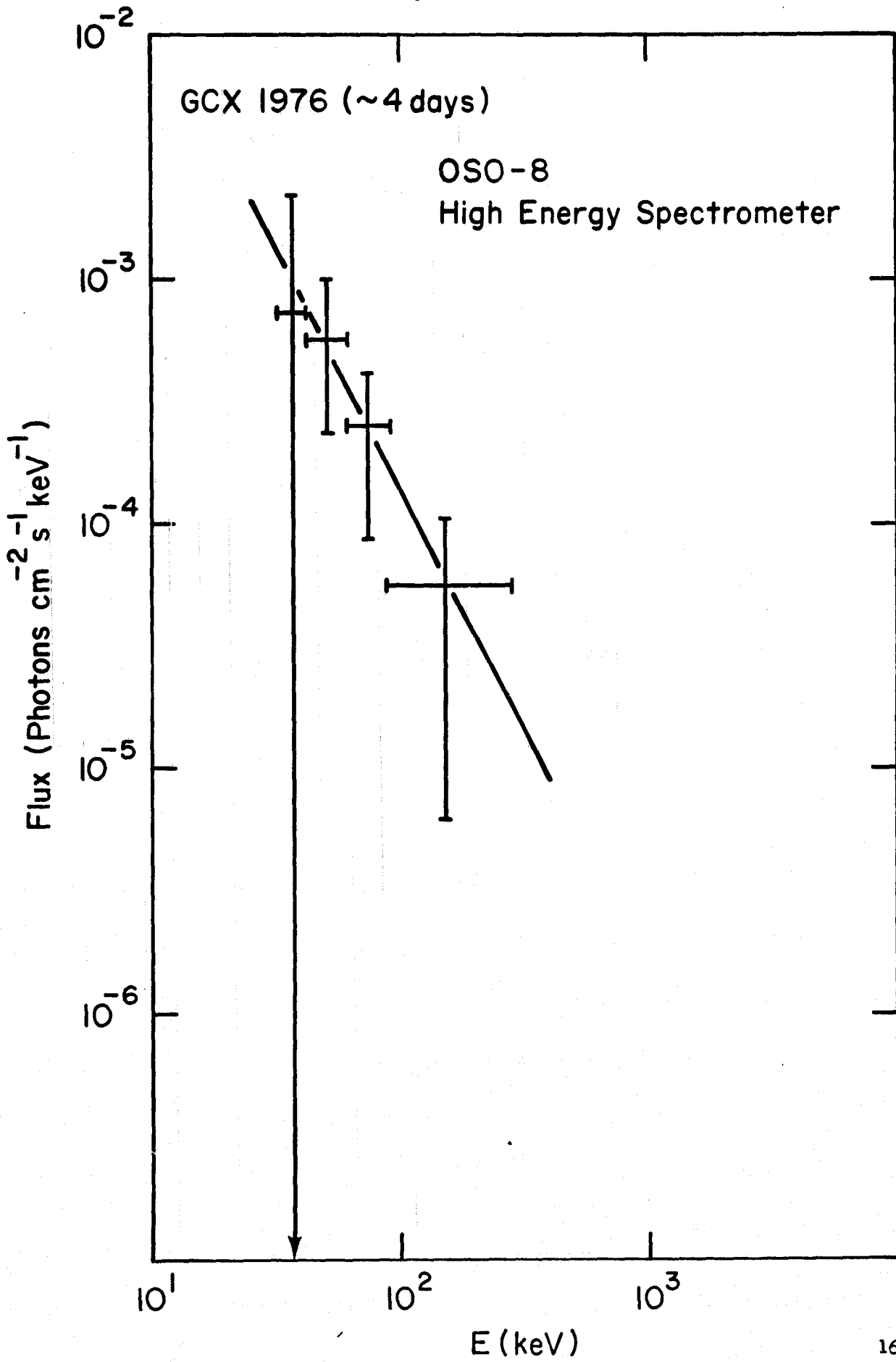
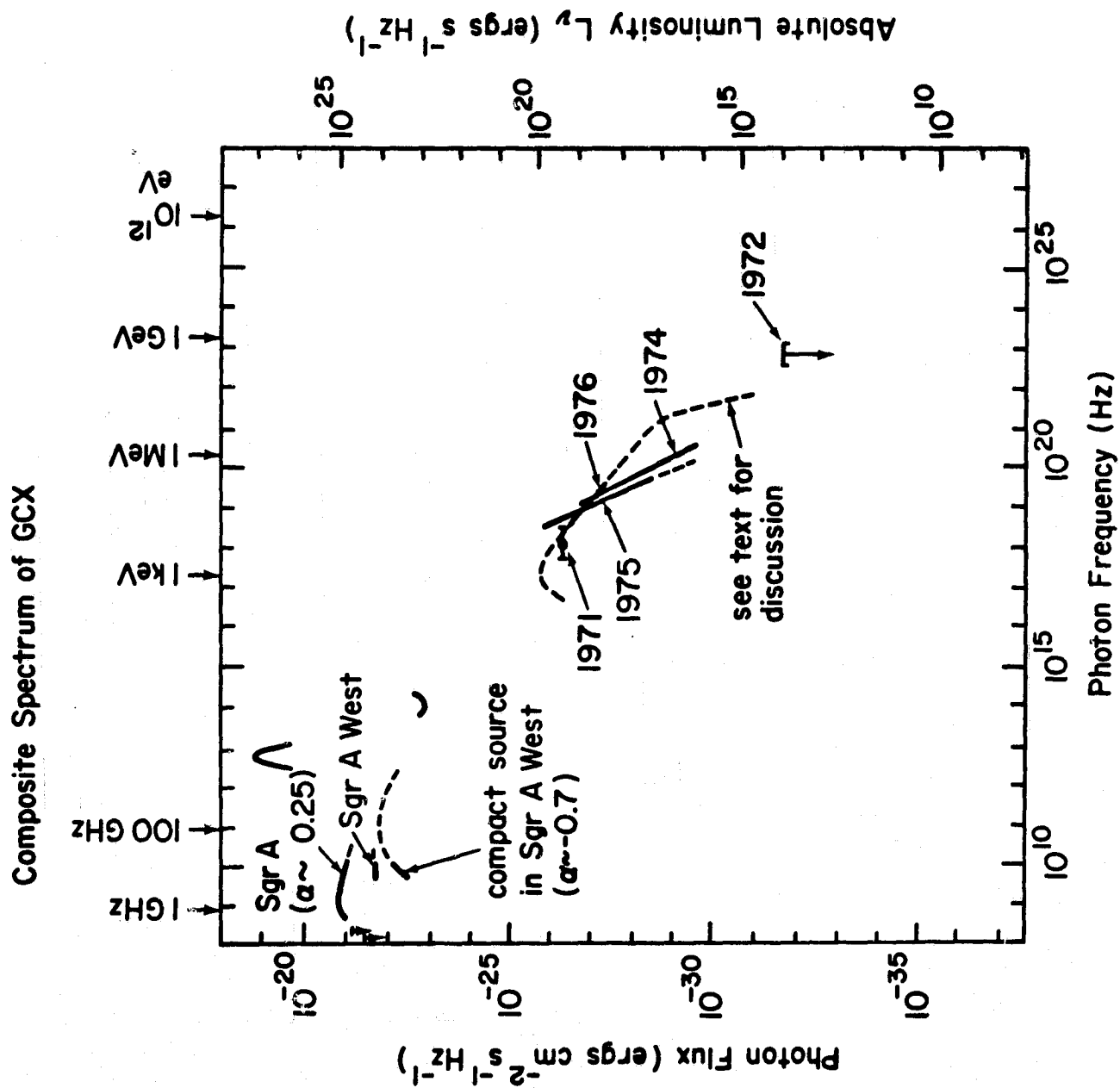


Figure 6.5



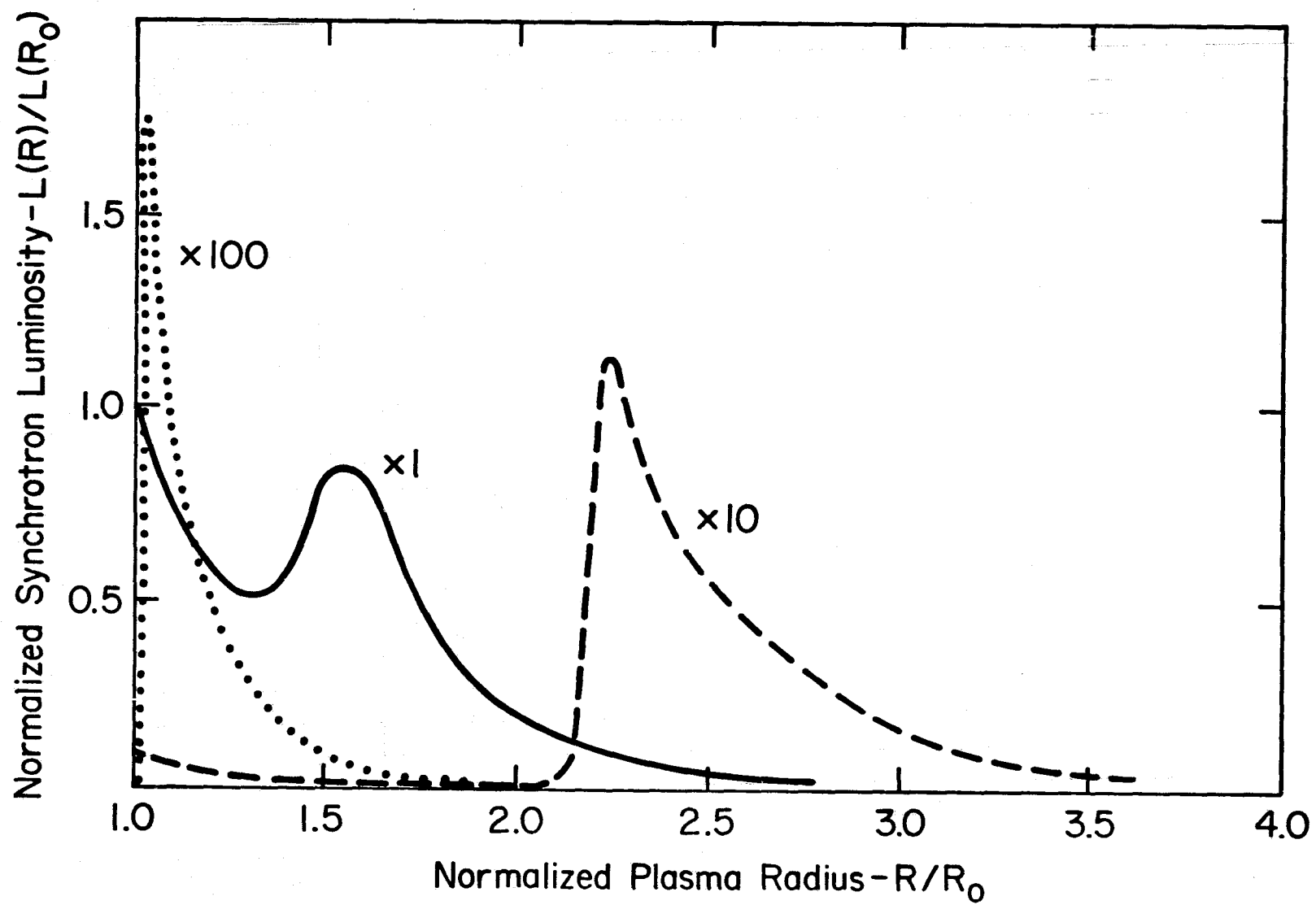


Figure 7.1

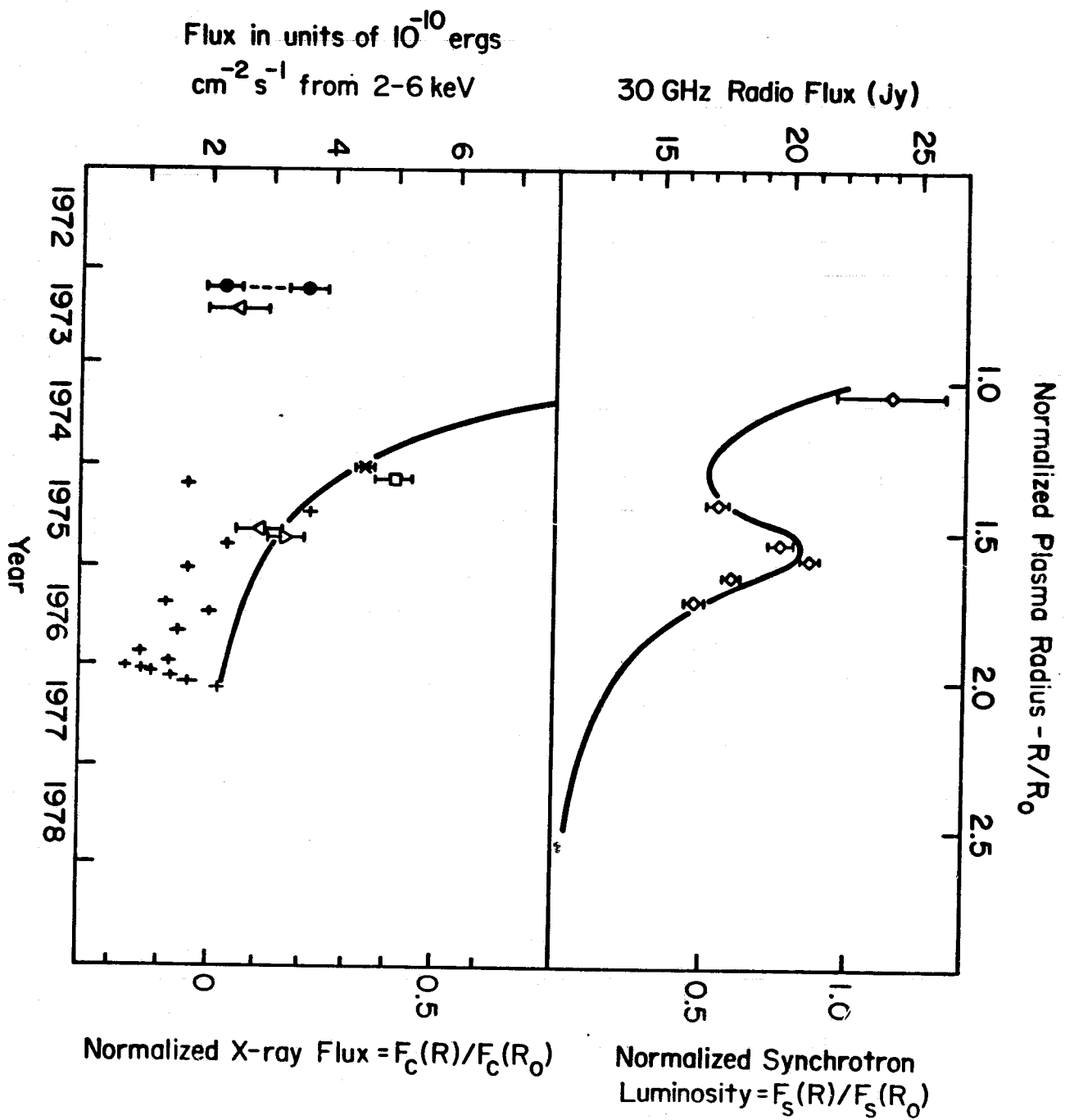


Figure 7.2

## BIBLIOGRAPHIC DATA SHEET

1. Report No.	2. Government Accession No.	3. Recipient's Catalog No.	
4. Title and Subtitle  On the Physical Environment in Galactic Nuclei		5. Report Date	
		6. Performing Organization Code 684	
7. Author(s) J.H. Beall		8. Performing Organization Report No.	
9. Performing Organization Name and Address Laboratory for Astronomy and Solar Physics Goddard Space Flight Center Greenbelt, MD. 20770		10. Work Unit No.	
		11. Contract or Grant No. NGL 21-002-033	
12. Sponsoring Agency Name and Address		13. Type of Report and Period Covered	
		14. Sponsoring Agency Code	
15. Supplementary Notes			
<p>16. Abstract Galactic nuclei and quasars emit radiation over the entire electromagnetic spectrum. This suggests that concurrent observations over a wide frequency range may provide useful information in determining appropriate models for the physical environment in which the radiation is produced. In conjunction with observations by the High Energy Spectrometer on OSO-8, four sources have been studied in this manner: the nucleus of the elliptical galaxy, Centaurus A (NGC 5128); the quasar, 3C273; the Seyfert galaxy, NGC 4151; and the nucleus of the Milky Way (GOX). Concurrent observations are used to construct the composite spectra (from radio to X-ray) for Cen A and NGC 4151, while the composite spectra of 3C273 and GOX are derived from the OSO-8 data and from other observers. Additionally, a skymap technique has been developed and is used to analyze the 1975 and 1976 observations of the galactic center region. The data are consistent with a significant, hard X-ray source at the radio and infrared position of the nucleus of the Milky Way.</p> <p>A theoretical analysis of the temporal variability of the Cen A data is undertaken and its implications discussed. Additionally, we note that the similarities between the composite spectra of the observed sources suggest that radio-bright and radio-quiet quasars may represent the emission from galactic nuclei with elliptical and Seyfert-like morphologies, respectively.</p>			
17. Key Words (Selected by Author(s)) Galactic nuclei, quasars, X-ray sources, Extragalactic Astronomy.		18. Distribution Statement	
19. Security Classif. (of this report) unclassified	20. Security Classif. (of this page) unclassified	21. No. of Pages 188	22. Price*